STUDY OF PICKUPS AND KICKERS IN PARTICLE ACCELERATORS

By

MUKESH KUMAR

Enrolment No. PHYS03201304006

Raja Ramanna Centre for Advanced Technology, Indore

A thesis submitted to the

Board of Studies in Physical Sciences

In partial fulfillment of requirements

for the Degree of

DOCTOR OF PHILOSOPHY

of

HOMI BHABHA NATIONAL INSTITUTE

October, 2018

Homi Bhabha National Institute[1]

Recommendations of the Viva Voce Committee

As members of the Viva Voce Committee, we certify that we have read the dissertation prepared by Mukesh Kumar entitled " Study of pickups and kickers in particle accelerators " and recommend that it may be accepted as fulfilling the thesis requirement for the award of Degree of Doctor of Philosophy.

Chairman - Prof. A. Banerjee	**Date:** 14/03/2019
Guide / Convener - Prof. V.K. Senecha	**Date:** 14/03/2019
Member 1- Prof. A. Chakrabarti	**Date:** 14.3.19
Member 2- Prof. V.Kumar	**Date:** 14.3.19
Member 3- Prof. Satya Bulusu	**Date:** 14.3.19
Member 4- Prof. M.P. Singh	**Date:** 14.3.19
Member 5- Prof. H. Ghosh	**Date:** 14.03.19
External Examiner- Prof. Puneet Jain	**Date:-** 14.3.19

Final approval and acceptance of this thesis is contingent upon the candidate's submission of the final copies of the thesis to HBNI.

I/We hereby certify that I/we have read this thesis prepared under my/our direction and recommend that it may be accepted as fulfilling the thesis requirement.

Date: 14-03-2019

Place: Indore

Co-guide (if applicable)

Guide : Dr. V. K. Senecha

[1] This page is to be included only for final submission after successful completion of viva voce.

STATEMENT BY AUTHOR

This dissertation has been submitted in partial fulfillment of requirements for an advanced degree at Homi Bhabha National Institute (HBNI) and is deposited in the Library to be made available to borrowers under rules of the HBNI.

Brief quotations from this dissertation are allowable without special permission, provided that accurate acknowledgement of source is made. Requests for permission for extended quotation from or reproduction of this manuscript in whole or in part may be granted by the Competent Authority of HBNI when in his or her judgment the proposed use of the material is in the interests of scholarship. In all other instances, however, permission must be obtained from the author.

Mukesh Kumar

DECLARATION

I, hereby declare that the investigation presented in the thesis has been carried out by me. The work is original and has not been submitted earlier as a whole or in part for a degree / diploma at this or any other Institution / University.

Mukesh Kumar

List of Publications arising from the thesis

Journal

1. "New expression for the current induced in a strip for the fringe field effect in a circular cross-section stripline", Mukesh Kumar, Journal of Korean physical Society (**2012**) Vol. **60**, Issue 9, pp. 1469-1472.
2. "Analytical expression for position sensitivity of linear response beam position monitor having inter-electrode cross talk", Mukesh Kumar, A. Ojha, A.D. Garg , T.A. Puntambekar and V.K. Senecha, Nuclear Instruments and Methods in Physics Research A, (**2017**) **844**, pp. 90-95.
3. "Improved design and in-situ measurements of new beam position monitors for Indus-2", Mukesh Kumar, L.K. Babbar, A.C. Holikatti, S. Yadav, Y. Tyagi, T.A. Puntambekar and V.K. Senecha, Journal of Instrumentation (**2018**) **13**(01), P01003.
4. "Modified coaxial wire method for measurement of transfer impedance of beam position monitors", Mukesh Kumar, L.K. Babbar, R.K.Deo, T.A. Puntambekar and V.K. Senecha, Physical Review Accelerators and Beams (**2018**) **21**, 052801 pp.1-11.

Conferences

1. "Physics design of beam position indicator for insertion device section in Indus-2", Mukesh Kumar, L.K. Babbar, S. Yadav, T. A. Puntambekar and C. P. Navathe, DAE- BRNS Indian Particle Accelerator Conference (InPAC-**2013**), VECC, Kolkata, India(2013).
2. "Mechanical design, development and installation of vacuum compatible beam position indicators for insertion device in Indus-2", L.K. Babbar, Mukesh Kumar, D.P. Yadav, B.N. Upadhyay, R. Sridhar and T.A. Puntambekar, DAE- BRNS Indian Particle Accelerator Conference (InPAC-2015), TIFR, Mumbai, India (**2015**).

Mukesh Kumar

DEDICATIONS

To my parents

Late Smt. Bhagwati Sharma *&* ***Shri Om Prakash Sharma****,*

And my wife

Bhawana Sharma

This humble work is a sign of their blessings and love.

ACKNOWLEDGEMENTS

With great pleasure and sense of gratitude, I take this opportunity to express my sincere thanks to my guide Prof. V. K. Senecha (Prof. Homi Bhabha National Institute and Head, Proton Linac Development Division, RRCAT), for his invaluable guidance, advice, mentoring and research support for my Ph.D study.

It gives me immense pleasure to express my gratitude and thanks to Shri T. A. Puntambekar (Head, Beam Diagnostics and Coolant Systems Division, RRCAT) for providing me opportunity, valuable guidance and active support at each stage of work.

Besides my guide and advisor, I would like to thank my thesis committee: Dr. A. Banerjee, Dr. A. Chakrabarti, Dr. V.S. Pandit, Dr. V. Kumar, Dr. M.P Singh, Dr. H. Ghosh and Dr. S. Bulusu for their insightful comments and encouragement which helped me to widen my research from various perspectives.

I would like to take this opportunity to express my sincere gratitude to Dr. P.D. Gupta, (Former Director, RRCAT), who encouraged me to register myself for the Ph.D. program. I would also like to thank Dr. P.A. Naik, Director, RRCAT, who has been a continuous source of encouragement during my Ph.D. work.

I would like to extend my sincere thanks to Shri P. Shrivastava (Associate Director, Proton Accelerator Group and Head, Pulsed High Power Microwave Division, RRCAT) and Shri D. Baxy (Pulsed High Power Microwave Division, RRCAT) for providing CST Studio Suite to carry out simulation for my Ph. D. work.

Last but not the least, I sincerely wish to express my gratefulness to Shri R.K. Deo (RF Systems Division) and all the team members of Beam Diagnostics Section, RRCAT, Indore, for the stimulating discussions.

My family and friends deserves the special mention for their unconditional support, care and blessings without which it would not have been possible for me to complete this research work.

CONTENTS

SYNOPSIS

Pickup and kicker are important devices essentially used for beam diagnostics purpose in particle accelerators. These devices not only help during commissioning but they also ensure uninterrupted and smooth operation of the accelerators. Pickups and kickers have numbers of applications like orbit measurement, tune measurement, instability detection, various feedback systems, beam position monitoring, energy measurement (time of flight experiments) etc. in synchrotrons, transfer lines and linear accelerators.

A large number of devices used for probing beam of charged particles in an accelerator for beam diagnostic applications can be broadly classified as pickups and kickers. The electromagnetic field associated with a beam of charge particles moving inside vacuum chamber interacts with its surrounding medium. Pickup is a device that interacts with electromagnetic fields associated with beam and generates signal. On the other hand, kicker is a device which works just opposite to the pickup. The kicker, driven by an external source, generates electromagnetic fields inside the vacuum chamber. This field excited by kicker interacts with beam and changes its momentum. The change in longitudinal momentum is termed as energy change and change in transverse momentum is related to transverse kick received by the beam. In principle, a device which is used as a pickup can also be used as a kicker when excited externally. For practical applications, the design of the pickups and kickers is generally different depending upon the intended application, sensitivity, dynamic range etc. The parameters which serve as figure of merit of a pickup are transfer impedance and position sensitivity. Their counterparts in kicker are longitudinal and transverse shunt impedances.

There are different types of pickups and kickers like capacitive pickups, magnetic pickups, striplines, RF cavities etc. that have been used as diagnostic devices in particle accelerators. The work presented in this thesis deals with capacitive pickups (shoe-box and button electrode configuration) and striplines commonly used as pickups and kickers for various beam diagnostics applications in particle accelerators. The chief motivation for pursuing the thesis work is because of the following two objectives.

(i). Study of stripline and shoe box beam diagnostic devices for design and development of beam position monitors (BPM) and kickers for future projects like up-gradation of Indus accelerator and High Intensity Proton linear Accelerator (HIPA) for Indian Spallation Neutron Source (ISNS).

(ii). Design of button electrode BPMs for insertion devices and replacement of old BPMs of Indus-2 with new BPMs having improved performance, and development of modified setup (easy to implement) of coaxial wire method to measure transfer impedance of these BPMs.

In view of the first objective of the thesis, the fringe field in coaxial stripline is studied; modified expressions for effective width for strip (electrode) and other parameters of stripline are derived. The effect of inter-electrode cross talk on difference over sum signal of two-electrode BPM is also studied and modified expression of position sensitivity in shoe box BPM is derived. The modified expressions produce results which are more close to the simulation results as compared to earlier expressions available in the literature. Although, computer simulation software (eg. CST Studio Suite) provides tools to design and analyze devices like stripline and capacitive pickups, but theoretical understanding on these devices is essential to interpret simulated and measured results. The modified expressions derived for stripline and capacitive BPMs provide analytical tools to calculate different parameters in stripline and shoe box monitors. These expressions provide significant insight in design as well as interpretation of simulation and experimental results for these devices.

In view of the second objective of the thesis, two different types of button electrode BPMs are designed for the insertion devices and replacement of the old BPMs in Indus-2 with new BPMs. The new BPMs have improved quality like higher transfer impedance, equal position sensitivity in both transverse planes, resonance free structure over wide frequency range and fast decaying wake-fields as compared to the old BPMs. A modified setup of coaxial wire method is also designed and developed to measure transfer impedances of these BPMs. In modified coaxial wire method, the impedance matching elements have been eliminated and the effect of mismatch is analyzed to obtain modified expression for transfer impedance of the capacitive BPM. The setup of modified coaxial wire method is easy to implement and immune to any change in impedance of coaxial structure arising due to change in wire diameter or any other factor as compared to the conventional coaxial wire method. The modified method developed during the present work may also be used to measure kicker constants of kickers using relation between pickup and kickers properties.

Thesis work reported here comprises six chapters. **Chapter 1** presents introduction to pickups and kickers commonly used as diagnostics devices in the particle accelerators. The next four chapters provide detailed description of simulation, measurements, results and discussion of the specific topic under investigation in chronological order. Finally, summary of the research work pursued for the thesis is presented in **Chapter 6**. Brief description of each chapter is given below.

Chapter 1 contains the general introduction to the particle accelerator and role of pickups and kickers as diagnostics tool for these machines. The fundamentals of capacitive pickups, shoe box BPM, button electrode BPM and striplines are presented. Important properties of pickup and kicker viz., transfer impedance, position sensitivity, kicker constants and shunt impedance are discussed. In principle, a device which is used as pickup can also be used as kicker and vice versa, therefore a general relation between pickup and kicker properties are discussed. Panofsky Wenzel theorem allows one to calculate the transverse effect (kick) of a kicker purely in terms of longitudinal field for a given mode of excitation. Thus, the relationship between transverse and longitudinal effects on a beam due to kicker device is also discussed.

Stripline is basically a transmission line which has definite characteristic impedance that is governed by its geometry. The fringe field between stripline electrodes (strips) and vacuum chamber body has significant effect on effective width of the strip. Due to fringe field, the effective width of a strip gets enhanced compared to its physical width, thereby the characteristic impedance of stripline depends on the intensity of fringe field. The net current flowing through stripline electrode is proportional to the effective width of the strip, thus fringe fields also have significant effect on its properties like transfer impedance, kicker constant, shunt impedance etc.

In Chapter 2, study of effect of fringe field on effective width of the strip is presented. A correction factor for the fraction of beam current intercepted by strip is obtained by considering the fringe field between electrode and the vacuum pipe. Validation of proposed expression of current induced in the stripline electrode through simulations performed using CST MW Studio Suite is presented. Finally, effect of change in effective width (hence induced current) of a stripline electrode on various properties of stripline is discussed.

Cross talk between pickup electrodes is an important phenomenon in capacitive beam position monitors (like shoe box BPM). The origin of inter-electrode cross talk is inter-electrode capacitance which allows induced current to flow from one electrode to other and vice-versa. In the absence of inter-electrode cross talk, the position sensitivity of the capacitive BPM depends only on the geometry of the BPM and does not depend on working frequency. In practical situation, due to inter-electrode capacitance, the position sensitivity is a function of frequency. This effect becomes significant when inter-electrode capacitance is comparable to the capacitance between pickup electrode and beam pipe.

Chapter 3 presents study of effect of inter-electrode cross talk on position sensitivity of a beam position monitor with two pickup electrodes. A generalized mathematical expression for normalized difference signals (difference over sum signal) for a two electrodes BPM having inter-electrode cross talk is presented. Inter-electrode cross talk can be very significant in shoe box BPM, therefore effect of cross talk on position sensitivity of shoe box BPM is discussed. An analytical expression for position sensitivity of shoe box BPM along with its validation through simulation and summary of the investigation are presented in **Chapter 3**.

Chapter 4 focuses on button electrodes beam position monitors designed for Indus-2 for various applications. The old BPMs of Indus-2 were designed more than 13 years ago for commissioning of Indus-2. Since commissioning of Indus-2, it has undergone many upgrades in beam diagnostics. In order to meet present requirements of beam position monitors, new button electrode BPMs, called upgraded beam position indicator (UPBPI), have been designed to replace old BPMs in Indus-2.

In addition to UPBPI, another type of button electrodes BPMs have also been designed and deployed in Indus-2 for monitoring of beam position at entry and exit of insertion devices in Indus-2. To differentiate these BPMs from UPBPI, these BPMs are called insertion device beam position indicator (IDBPI). This chapter presents design, simulations, measurement and results of UPBPI and IDBPI. The performance of new BPM (UPBPI) has also been compared with the old BPM.

Chapter 5 presents design and development of a modified setup of coaxial wire method to measure transfer impedance of button electrode BPMs of Indus-2. In conventional coaxial wire method, impedance matching between external circuit and device under test (DUT) is a necessary requirement. Generally, the implementation of impedance matching is carried out using impedance matching electrical networks or long tapered physical structures. The implementation of impedance matching is practically tedious task. Therefore, to simplify the setup of coaxial wire method, a modified coaxial wire method is conceived in which impedance matching elements are eliminated. The effect of impedance mismatch has been analyzed mathematically and the new expressions for transfer impedance are derived for different configurations of modified coaxial wire setup. The modified setup is validated through simulation of a test BPM using different methods in CST Studio Suite and applied to measure transfer impedance of the beam position monitors developed for Indus-2.

Chapter 5 presents the theory of modified coaxial wire method along with its validation through simulation. This is followed by description of measurement of transfer impedance of button electrode BPMs of Indus-2 using modified coaxial wire method and comparison of measured results with simulation of the BPMs.

Chapter 6 presents summary of the thesis. Important results obtained during this course of investigation are discussed in this chapter. The new results presented in the thesis are:

i. A correction factor for the effective width of strip (electrode) of a coaxial stripline is obtained by considering the fringe fields between strip and the vacuum pipe. Expressions of beam current intercepted by strip, characteristic impedance and kicker constant are also reformulated subsequently.

ii. Considering inter-electrode cross talk, a generalized mathematical expression for normalized difference signal (difference over sum signal) for a two electrodes BPM and analytical expression for position sensitivity of shoe box BPM are obtained.

iii. A modified coaxial wire method (set up) for measurement of transfer impedance of capacitive BPMs is developed and transfer impedance of a button electrode BPM is measured using this set up.

iv. New button electrode beam position monitors having improved performance are designed for Indus-2.

Future scope of work in pickups & kickers for applications in particle accelerators is discussed at the end of this chapter.

LIST OF FIGURES

LIST OF TABLES

CHAPTER-1

ROLE OF PICKUPS & KICKERS FOR THE PARTICLE ACCELERATORS

Beam diagnostics play vital role for any accelerator facility. It provides measurement of different parameters associated with beam during commissioning, smooth operation, troubleshooting, re-starting after a shut-down and upgrade of an accelerator. Pickups [1,2] or beam position monitors (BPMs) are the devices which interact with electromagnetic field associated with the beam of charge particles and generate electrical signals. Kickers [1,2] are the devices which work just opposite to the pickups. Kicker generates electromagnetic field inside the vacuum chamber when it is driven by an external source. The field generated by the kicker interacts with the beam and provides kick (momentum change) to the beam. In principle, a device that is used as pickup can also be used as kicker. Pickups and kickers are integral part of particle accelerator (circular, linear, electron, proton/hadron etc.) and beam transport lines. These devices (pickups and kickers) have numerous applications like monitoring of beam position or trajectory, measurement of betatron tunes, detection of instabilities, measurement of beam phase, measurement of energy through time of flight, tune feedback system, instability control feedback system, orbit correction and feedback system etc. [3-10].

This chapter presents important accelerator activities at Raja Ramanna Centre for Advanced Technology (RRCAT), motivation and objectives of this thesis work, fundamental properties of pickups and kickers, brief theory of specific pickup/kicker and applications of pickups and kickers in particle accelerators.

1.1 Indus accelerators and accelerator for proposed Indian Spallation Neutron Source (ISNS)

Indus-1 [11,12] and Indus-2 [11-16] are two frontline national Synchrotron Radiation facilities (established in year 1997 and 2006) serving for research and development in the country for condensed matter physics, material science, protein crystallography etc.. The schematic of Indus accelerator complex is [17] shown in Fig. 1.1. Indus accelerator complex consists of 20 MeV microtron, 550 MeV booster synchrotron, two electron storage rings [Indus-1 and Indus-2] and beam transport lines (TL-1, TL-2 and TL-3). Microtron and booster synchrotron are common injectors of Indus-1 and Indus-2. A 20 MeV electron beam from microtron is injected into booster synchrotron which boosts its energy up to 450 MeV for injection into Indus-1 and up to 550 MeV for injection into Indus-2. Indus-2 is a booster cum storage ring with stored beam energy of 2.5 GeV. The parameters of Indus-1 and Indus-2 are given in table 1.1.

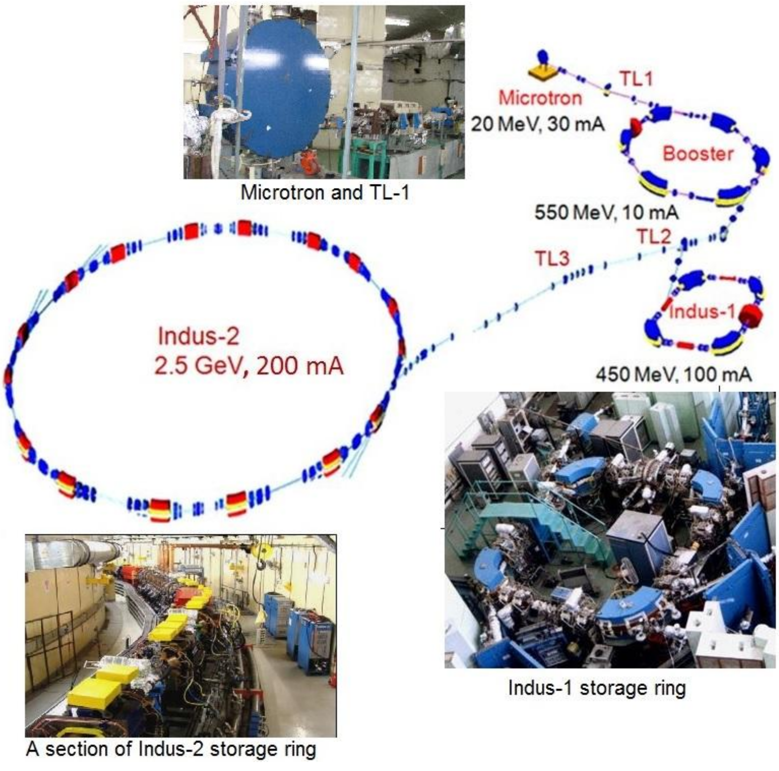

Fig. 1.1 Schematic of Indus accelerator complex; (ref. 17).

Table 1.1 Parameters of Indus-1 and Indus-2			
Sr. No.	Parameter	Indus-1	Indus-2
1	Stored beam energy	450 MeV	2.5 GeV
2	Injection beam energy	450 MeV	550 MeV
3	Beam Current	100 mA	200 mA
4	Critical wavelength	61 A^0	1.98 A^0
5	Beam emittance	$7x10^{-8}$ m-rad (H) $7x10^{-9}$ m-rad (V)	$5.8x10^{-8}$ m-rad (H) $5.8x10^{-9}$ m-rad (V)
6	Dipole magnet	4	16
7	Periodicity	4	8
8	Harmonic number	2	291
9	Rf system frequency	31.613 MHz	505.812 MHz
10	Circumference	18.97 m	172.47 m

Design of high intensity proton accelerator [18,19] of 1 GeV beam energy, 1 MW average power with 2 ms pulse duration and 50 Hz pulse repetition rate for the proposed Indian Spallation Neutron Source (ISNS) is another important activity being pursued at RRCAT. It consists of 50 keV H^- ion source, low energy beam transport line (LEBT), 3.0 MeV radio frequency quadrupole (RFQ), medium energy beam transport line (MEBT), 1 GeV linac, high energy beam transport line (HEBT) and 1 GeV proton accumulator ring. Schematic of 1 GeV linac for ISNS is shown in Fig. 1.2. Important parameters of ISNS accelerator are shown in table 1.2.

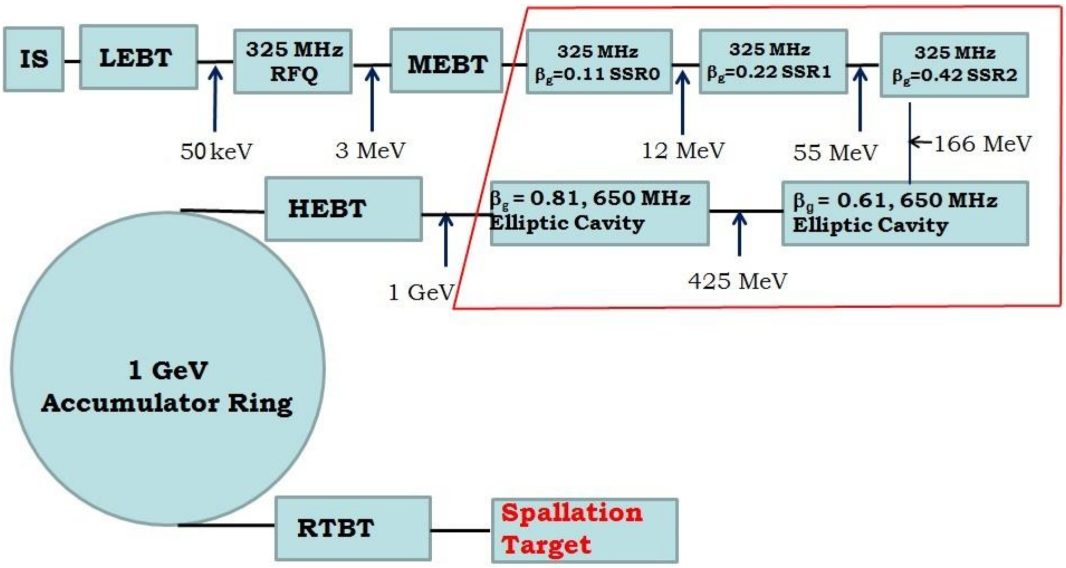

Fig. 1.2 Schematic of accelerator for proposed ISNS.

Table 1.2 Important parameters of ISNS accelerator

Sr. No.	Parameter	Value
1	Ion type (Front end, Linac, HEBT)	H^-
2	Ion type (Ring)	proton
3	Pulse repetition rate	50 Hz
4	Pulse length (linac)	2 ms
5	Average pulse current (Linac)	10 mA
6	Beam kinetic energy (Linac exit)	1.0 GeV
7	Beam kinetic energy (Accumulator ring)	1.0 GeV
8	Pulse length (on target)	680 ns
9	Proton beam power on target	1.0 MW
10	Front end length (ion source, LEBT, RFQ, MEBT)	9.1 m
11	Ring circumference	262 m
12	Ring filling time	2.0 ms

13	Average beam current on target	1 mA
14	Proton per pulse on target	1.25×10^{14}
15	Injection into the ring	2000 turns
16	Pulsed neutron peak flux	10^{16} n cm^{-2} sec^{-1}

1.2 Motivation and objectives of the thesis work

There are different accelerating structures and beam transport lines in ISNS accelerator (see Fig. 1.2). Striplines and capacitive electrodes (shoe box, split electrode) are most suitable and commonly used BPMs for proton (or H^-) linacs and synchrotrons [20-28]. Thus, different types of striplines/capacitive BPMs would be required for beam diagnostics purpose for ISNS accelerator. In addition to this, new striplines and button electrode BPMs [29-35] are also required for the up-gradation of beam diagnostics in Indus-1 and Indus-2. Thus, prime motivation of the thesis work is study of pickups/kickers for beam diagnostic applications for ISNS accelerator and up-gradation of beam diagnostics of Indus accelerators. The main objectives of the present thesis work are

i. Study of the effect of fringe field and inter-electrode cross talk on characteristics of stripline and capacitive BPMs.

The geometry of pickup electrodes and physical phenomena like fringe field and inter-electrode coupling play important role in performance of the devices like stripline and capacitive BPMs. The characteristic impedance of the stripline is very important design parameter. Like other transmission lines, the characteristic impedance of the stripline depends on dimension and geometry of strip (electrode) and vacuum chamber (outer conductor). Fringe field has significant effect on effective width of the strip [36] and plays important role in design and analysis of the striplines. The study of the effect of the fringe field on characteristics of the circular stripline (stripline with circular cross section of strip and vacuum chamber) is carried out and modified expressions of effective width of strip and other associated parameters like characteristic impedance have been derived by considering fringe field [37]. The modified expressions produce results which are in better agreement with simulation results as compared to the earlier expressions.

The inter-electrode coupling (cross talk) has significant effect on position sensitivity of capacitive BPMs. Due to inter-electrode capacitive coupling the current induced on one electrode can flow towards another electrode and vice-versa. The capacitive coupling increases with increasing frequency and output load for a given BPM. Thus, due to inter-electrode capacitive coupling, the position sensitivity becomes a function of the signal frequency and load impedance [38-42]. A generalized expression for normalized difference signal is derived for a two electrodes BPM and the effect of inter-electrode cross talk on position sensitivity of shoe box BPM is analyzed in detail [43].

The study of fringe field effect in striplines and inter-electrode cross talk in capacitive BPMs is presented in Chapter 2 and Chapter 3.

ii. Design and measurement of new button electrode BPMs (having improved performance) for beam diagnostics upgrades in Indus-2.

Since commissioning, Indus-2 has undergone many upgrades [44-48] and advancements like installation of coupled bunch instability feedback system, close orbit measurement and feedback system, installation of insertion devices etc. These upgrades generated the requirement of new BPMs having higher transfer impedance, similar response in both of the transverse planes (equal position sensitivity), resonance free structure over wide frequency range and fast decaying wake-fields as compared to the old BPMs. Commissioning of insertion devices (undulators) has also put requirement of additional

BPMs to monitor beam position at entry and exit of these devices. To meet these requirements, new button electrodes BPMs have been designed [49,50] for Indus-2.

Bench measurement of transfer impedance is an important part of characterization of any BPM. Electromagnetic field distribution of a charge particle moving with relativistic velocity inside a conducting vacuum chamber approximates to the field distribution of TEM mode inside coaxial transmission line. Therefore, coaxial wire method [51-61] is widely used technique for the bench measurement of beam coupling and transfer impedance of various components in particle accelerators. Generally, the characteristic impedance of coaxial structure formed by wire and device under test (DUT) does not match with the characteristic impedance of external circuit. To simulate realistic situation of DUT and particle beam, impedance matching between DUT and external electronics is employed. In conventional wire method, impedance matching (between DUT and external circuit) is carried out using impedance matching elements like tapered structures or impedance matching networks which is generally a tedious task.

To simplify the setup of conventional wire method, a modified setup of coaxial wire method has been conceptualized and used to measure transfer impedance of button electrodes beam position monitors of Indus-2 [62]. In modified setup of coaxial wire method, the impedance matching elements have been eliminated. The effect of impedance mismatch arising due to impedance mismatch is analyzed mathematically and modified expression of transfer impedance is derived accordingly. The modified coaxial wire method is easy to implement (no impedance matching is required) and immune to any change in impedance of coaxial structure arising due to change in wire diameter or any other factor.

The design and characterization of new button electrode BPMs for Indus-2 are presented in Chapter 4 and Chapter 5.

1.3 Pickups

Pickups interact with electromagnetic field associated with the beam of charge particles and generate electrical signals. Depending on interaction of the pickup with electromagnetic field, pickups can be classified as capacitive pickup (button electrode, shoe box, split electrodes), magnetic pickup (magnetic loop) and electromagnetic pickup (stripline) and RF cavities. The inductive pickup and RF cavity are also used as BPM but beyond the scope of this thesis.

The work presented in this thesis mainly deals with capacitive pickups (button electrode BPM, shoe box BPM) and stripline that are commonly used as beam position monitors and transverse kickers in particle accelerators and transport lines. Thus, a brief introduction of specific devices like capacitive pickups (shoe box and button BPM) and stripline is given in following sections.

1.3.1 General capacitive pickup

Consider a pickup electrode of length L, placed inside a chamber as shown in Fig. 1.3. For relativistic beam velocity, the distribution of electromagnetic field associated with the beam can be approximated to transverse electromagnetic field (TEM) distribution [29]. Let the beam current be represented by $I_b\ (t)$ and its velocity by v_b. If the bunch length (wavelength in frequency domain) is much larger than the length of pickup electrode, the charge induced on the electrode is given by

$$q(t) = -\eta L \frac{I_b(t)}{v_b} \tag{1.1}$$

Here η is a geometric factor which depends on beam position and geometry of pickup electrode and vacuum chamber. $\eta = \frac{\phi}{2\pi}$ for curved electrode having azimuthal width ϕ.

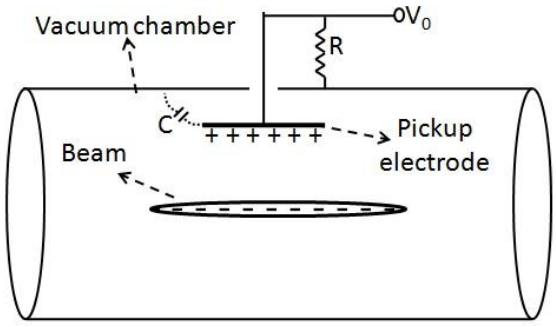

Fig. 1.3 Schematic of single electrode capacitive pickup.

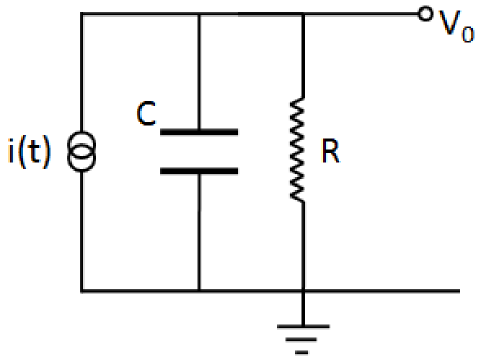

Fig 1.4 Equivalent circuit of capacitive pickup with single electrode.

Generally, the pickup electrode is terminated with a load impedance (resistance R) to measure voltage induced between pickup electrode and vacuum chamber. The equivalent circuit of pickup electrode, connected to a load resistance (R), is shown in Fig. 1.4 [29]. The rate of change of the charge induced on the electrode drives a current flowing into the electrode. The current flowing through the capacitance is given by

$$i(t) = -\eta \frac{L}{v_b} \frac{dI_b(t)}{dt} \tag{1.2}$$

From Fig. 1.4, the pickup voltage in frequency domain is given by

$$V_0(\omega) = -\eta \frac{L}{v_b} \frac{dI_b(\omega)}{dt} \left(\frac{R}{1 + j\omega CR} \right) \tag{1.3}$$

Expressing beam current as $I_b(\omega)= |I_b(\omega)|e^{j\omega t}$, equation (1.3) becomes

$$V_0(\omega) = -\eta \frac{L}{v_b}\left(\frac{j\omega R}{1 + j\omega CR}\right) I_b(\omega) \qquad (1.4)$$

Equation (1.4) shows that the response of the capacitive pickup is equivalent to a high pass filter. Therefore a capacitive pickup does not respond to a dc beam. The cut off frequency of capacitive pickup is $\omega_{cut} = 1/(RC)$. Depending on capacitance and output resistance (hence cut off frequency) the different working regions of capacitive pick up are explained below.

Case 1 High frequency region: ω >>1/(RC)

When the frequency is quite high, the impedance offered by the capacitance becomes much smaller as compared to the load 'R'. In this situation most of the induced current passes through the capacitance and gets integrated. Since the induced current is differentiation of beam current, therefore the temporal profile of the output voltage is similar to the beam current or bunch structure (Fig. 1.5). The output voltage is given by

$$V_0(\omega) = -\eta \frac{L}{v_b C} I_b(\omega) \qquad (1.5)$$

Mathematically, equation (1.5) can be obtained by putting $(1+j\omega CR) \approx j\omega CR$ in equation (1.4). The output resistor is kept very high to get low cut off frequency. This type of configuration is used for long bunches.

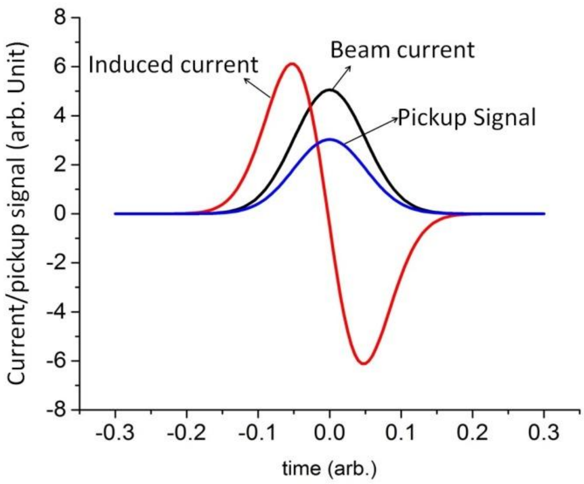

Fig. 1.5 Capacitive pickup signal for ω>>1/RC.

Case 2 Low frequency region: ω <<1/(RC)

When working frequency is much lower than the cut off frequency (1/(RC)), the impedance offered by capacitance is much higher as compared to the load 'R'. In this situation most of the induced current passes through load and the output of the pickup is 90^0 (π/2) out of phase with the beam current and the output signal is differentiated form of the beam current as shown in Fig. 1.6. The output voltage, in this case, is given by

$$V_0(\omega) = -\eta \frac{L}{v_b}\left(\frac{j\omega R}{1}\right) I_b(\omega) \tag{1.6}$$

This configuration is used for small bunch length. The output resistance is kept low (generally 50 Ω) to keep working frequency below cut off frequency.

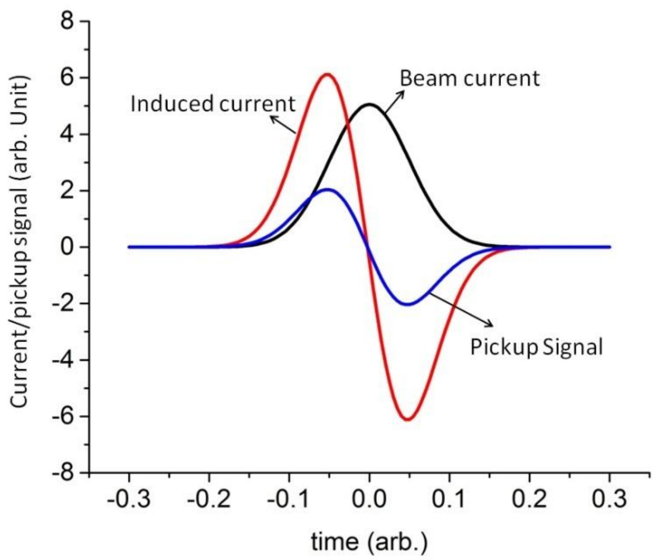

Fig. 1.6 Capacitive pickup's output signal for ω<<1/RC.

1.3.2 Linear response pickup (Shoe box BPM)

Linear response pickup is a variant of capacitive BPM. The electrodes of the BPM are designed in such a manner that the charge (hence pickup voltage) induced on the pickup electrodes varies linearly with the beam position or beam offset from the BPM axis. Generally, a linear response beam position monitor has a hollow tube of circular or rectangular aperture which is bisected diagonally to make two electrodes [4, 5, 29].

Typical example of capacitive linear response beam position monitor is shoe box BPM. Fig. 1.7 shows schematic of a general shoe box beam position monitor. In shoe box BPM, if the beam is displaced by an amount 'x' towards one electrode, the geometrical factor for that electrode is given by [29]

$$\eta = \frac{1}{2}\left(1 + \frac{x}{b}\right) \tag{1.7}$$

Using equation (1.7) in equation (1.4) we get

$$\frac{\Delta V}{\Sigma V} = \frac{|V_R| - |V_L|}{|V_R| + |V_L|} = \frac{x}{b} \tag{1.8}$$

In equation (1.8), $\frac{\Delta V}{\Sigma V}$ is normalized difference signal, V_R is voltage signal of right hand side pickup electrode, V_L is voltage signal of left hand side pickup electrode and b is half of the BPM aperture.

Equation (1.8) shows that the normalized difference signal varies linearly with beam offset 'x'. This is true only when the two electrodes are completely isolated from each other. In reality, due to inter-electrode coupling, the normalized difference signal is not only a function of beam offset but it also depends on signal frequency and load impedance [38-42]. The effect of inter-electrode coupling on normalized difference signal and position sensitivity of shoe box BPM is described in Chapter-3.

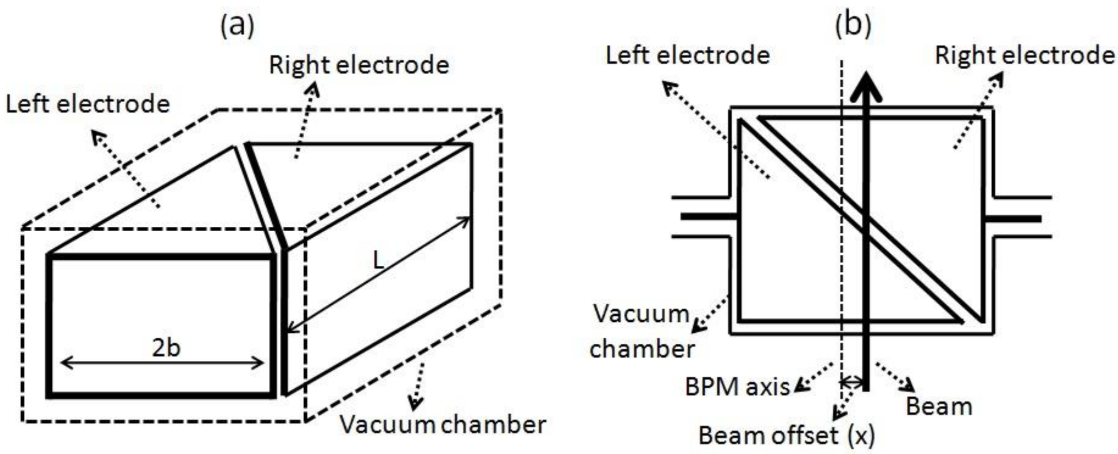

Fig. 1.7 Schematic of shoe-box BPM (a) perspective view (b) top view with x-z cut plane.

1.3.3 Button electrode monitor

Button electrode BPM [29-35] is a capacitive type beam position monitor. Unlike shoe box BPM, button electrodes BPMs have very small pickup electrodes. Due to small size, the impedance due to capacitance between button and ground is negligible as compared to the output load. Neglecting capacitance in equivalent circuit of capacitive pickup (Fig. 1.4), the output voltage for button electrode is given by

$$V_0(t) = Ri(t) = -\eta \frac{RL}{v_b} \frac{dI_b(t)}{dt} \quad (1.9)$$

For rectangular curved electrodes of length 'L' and azimuthal width 'ϕ', the geometrical factor 'η' for centered beam is

$$\eta = \frac{\phi}{2\pi} \quad (1.10)$$

For circular electrodes (button) of radius r, the factor ϕL should be replaced with electrode area divided by radius of beam pipe 'b'. Thus equation (1.9) can be written as

For rectangular electrode

$$V_0(t) = -\frac{\phi}{2\pi} \frac{RL}{v_b} \frac{dI_b(t)}{dt} \quad (1.11)$$

For circular electrode

$$V_0(t) = -\frac{r^2}{2b} \frac{R}{v_b} \frac{dI_b(t)}{dt} \quad (1.12)$$

In frequency domain, representing beam current as $I_b(\omega) = |I_b(\omega)|e^{j\omega t}$, equations (1.11) and (1.12) give

For rectangular electrode

$$V_0(t) = -j\omega \frac{\phi}{2\pi} \frac{RL}{v_b} I_b(\omega) \quad (1.13)$$

For circular electrode

$$V_0(t) = -j\omega \frac{r^2}{2b}\frac{R}{v_b} I_b(\omega) \qquad (1.14)$$

Equations (1.11) to (1.14) show that the output signal is 90^0 ($\pi/2$) out of phase with beam current.

1.3.4 Stripline

If the length of the capacitive pickup electrode is increased then it forms a transmission line type structure. This transmission line, if not terminated properly, produces resonance at discrete frequencies. Special type of electrode structure called stripline [4-6, 29] is designed to avoid this problem. The striplines are used as pickups (BPMs) as well as kickers in accelerator.

Striplines are basically the transmission lines having fixed characteristics impedance. The analysis of stripline is done by considering propagation of signal (along the stripline) in the form of electromagnetic wave between electrode (also called strip) and vacuum chamber. This consideration makes stripline useful for the bunch (wavelength in frequency domain) shorter than the electrode length. Whereas for capacitive pickup, the analysis fails for wavelengths which are shorter or of the order of electrode’s length. Striplines are widely used as pickups as well as kickers for different applications in particle accelerators.

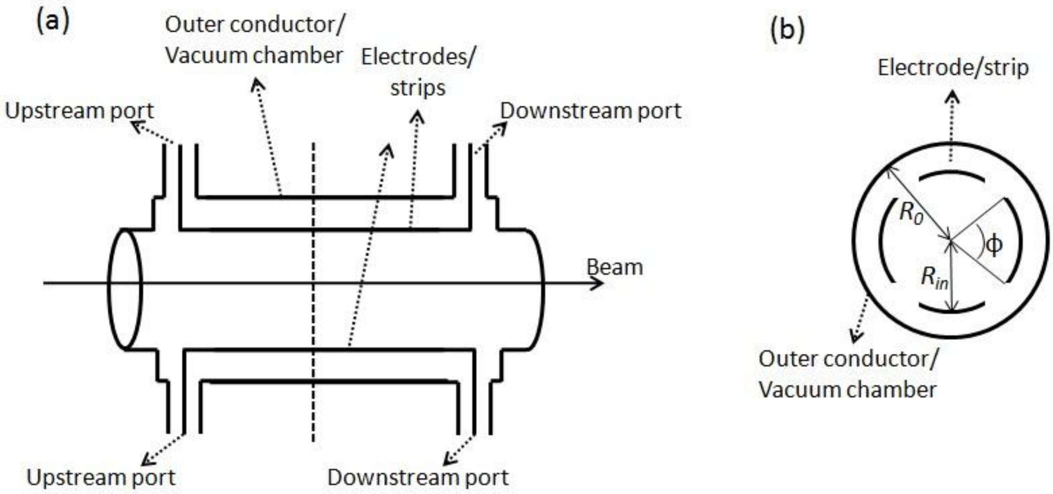

Fig. 1.8 schematic of stripline; (a) side view (b) cross sectional view.

Consider an electrode (strip) of angular width ϕ, length L, radius R_{in} placed inside vacuum chamber having radius R_0 (Fig. 1.8). Let the characteristic impedance of the transmission line formed by strip and the outer conductor (vacuum chamber) is Z_0. The upstream and downstream ends of the strip are terminated with R_u and R_d respectively. When bunch approaches upstream end of the strip, the wall current (image charge) crosses the gap between beam pipe and the strip. It induces voltage signal across the gap. This voltage launches TEM waves in two directions. One signal appears across the load R_u and second signal travels towards downstream end. If $R_u = Z_0$, the wall current crossing the gap will see two equal impedance in parallel. Thus, the voltage induced at upstream port is

$$V_1 = \eta \frac{Z_0}{2} I_b(t) \tag{1.15}$$

Here η is geometrical factor and it represents fraction of beam current intercepted by a given electrode. For stripline matched at downstream port (R_d=Z_0), the signal traveling towards downstream port will be completely absorbed by R_d (no reflection at the downstream port).

If the velocity of the bunch is v_b, the bunch arrives downstream end of the stripline at time L/v_b. This time the wall current crosses the gap from the strip to the vacuum chamber and again induces a voltage across the gap between vacuum chamber and strip. The signal generated at downstream port by bunch crossing downstream gap has equal magnitude but opposite polarity as given by equation (1.15). This signal travels in two directions. One signal appears across the output resistance R_d. The second signal travels towards the upstream port and is completely absorbed by R_u at time $t + \left({L}/{v_b} + {L}/{v_s}\right)$. Here v_s is velocity of signal travelling along the stripline. The voltage signals at upstream and downstream ends are super-imposition of the signals generated at both ends. Mathematically, the voltage at upstream and downstream port (ends) at time t is given by

At upstream port

$$V_u = \eta \frac{Z_0}{2} \left[I_b(t) - I_b\left(t - {L}/{v_b} - {L}/{v_s}\right) \right] \tag{1.16}$$

At downstream port

$$V_d = \eta \frac{Z_0}{2} \left[I_b\left(t - {L}/{v_b}\right) - I_b\left(t - {L}/{v_s}\right) \right] \tag{1.17}$$

If $v_s = v_b$=c then no signal will appear at downstream port and signal at upstream port is given by

$$V_u = \eta \frac{Z_0}{2} \left[I_b(t) - I_b\left(t - {2L}/{c}\right) \right] \tag{1.18}$$

Graphically, the signal of stripline is illustrated in Fig. 1.9.

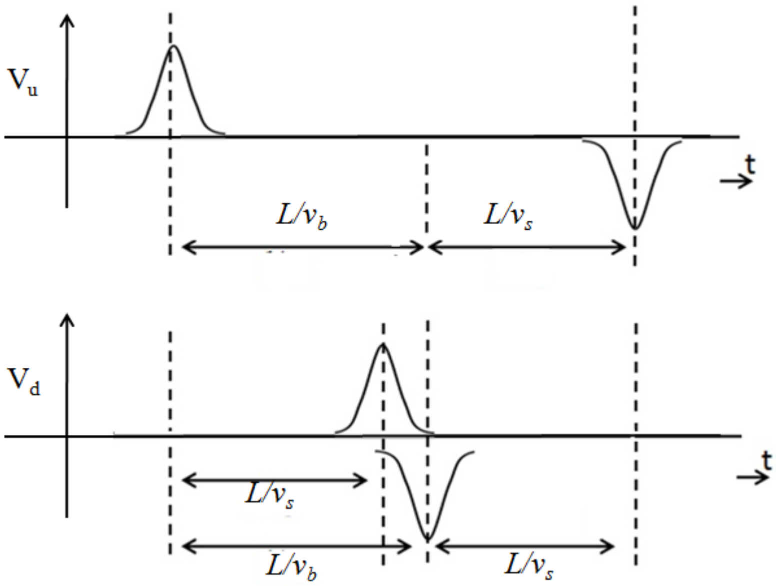

Fig. 1.9 Graphical representation of stripline signals at upstream and downstream ports.

In frequency domain, representing beam current as $I_b(\omega,t)= |I_b(\omega)|cos(\omega t)$, equation (1.18) gives

$$V_u(\omega,t) = -\eta Z_0|I_b(\omega)|cos\left(\omega t + \frac{\pi}{2} - \frac{\omega L}{c}\right) sin\left(\frac{\omega L}{c}\right) \qquad (1.19)$$

In equation (1.19), $\left(\frac{\pi}{2} - \frac{\omega L}{c}\right)$ is phase difference between stripline signal and beam current. The amplitude of the signal is given by

$$|V_u(\omega,t)| = \eta Z_0|I_b(\omega)|\left|sin\left(\frac{\omega L}{c}\right)\right| \qquad (1.20)$$

1.3.5 Transfer impedance of pickup

The strength of the pickup signal ($V_0(\omega)$) is proportional to the beam current ($I_b(\omega)$). The quantity which relates pickup voltage with beam current is called transfer impedance. Mathematically the transfer impedance ' Z_T ' is defined as

$$Z_T(\omega) = \frac{V_0(\omega)}{I_b(\omega)} \qquad (1.21)$$

The transfer impedance of the pickup is independent of beam current and it is inherent property of the pickup. It depends upon size and geometry of the pickup.

1.3.6 Position sensitivity of pickup

In order to get information about the position of the beam, more than one (two or four) electrodes are generally used. The signal induced on a particular electrode is uniquely related with the beam offset through η. The relative amplitude of the signals on different electrodes is used to calculate beam position.

For example, consider a four electrode BPM as shown in Fig. 1.10. The normalized difference signal of the BPM along a particular axis is proportional to the beam offset along that direction. Therefore,

$$\left(\frac{\Delta V}{\Sigma \mathrm{V}}\right)_x = \frac{V_R - V_L}{V_R + V_L} = S_x x \quad \text{(horizontal plane)} \tag{1.22}$$

$$\left(\frac{\Delta V}{\Sigma \mathrm{V}}\right)_y = \frac{V_U - V_D}{V_U + V_D} = S_y y \quad \text{(vertical plane)} \tag{1.23}$$

Here S_x and S_y are proportionality constants called position sensitivity in horizontal and vertical planes respectively. The position sensitivity depends on geometry of pickup electrodes and vacuum chamber. In reality, the position sensitivity itself can be a function of beam position corresponding to non linear response of pickup signal with respect to beam position. Mathematically position sensitivity can be written as

For x- axis (horizontal plane)

$$S_x = {}^{\partial}\!/_{\partial x} \left(\frac{\Delta V}{\Sigma \mathrm{V}}\right)_x \tag{1.24}$$

For y- axis (vertical plane)

$$S_y = {}^{\partial}\!/_{\partial y} \left(\frac{\Delta V}{\Sigma \mathrm{V}}\right)_y \tag{1.25}$$

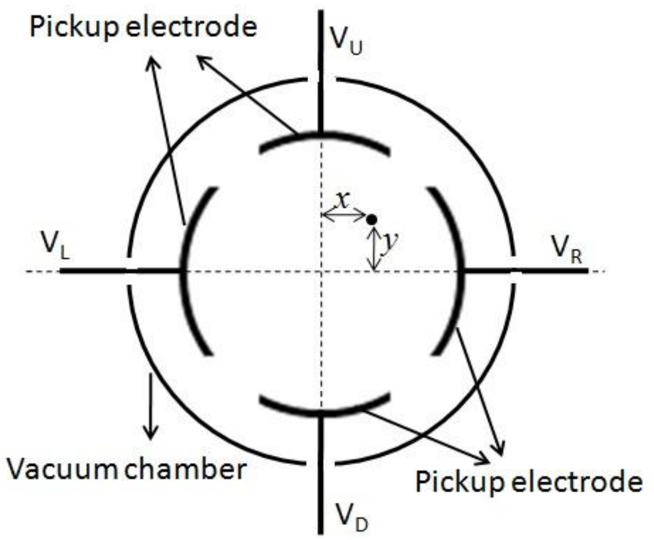

Fig. 1.10 Four electrodes BPM and pickup signal used for defining position sensitivity.

1.4 Kickers

Kickers when driven by an external source, generates electromagnetic field inside the vacuum chamber and provides kick to the beam. In principle, a device that serves as pickup can also be used as kicker. For practical application, the designs of pickup and kicker are generally different, but the relation between pickup and kicker properties of the device is very useful for its design and analysis. For example, the kicker constant or shunt impedance of a stripline can be obtained from its transfer impedance and position sensitivity. The following section presents important properties of the kicker.

1.4.1 Kicker constant

The kick experienced by the beam is proportional to the electromagnetic field excited by the kicker in the path of the beam or voltage applied to the kicker. The relation between applied voltage and kick experienced by the beam is represented as kicker constant [1,2].

1.4.1.1 Longitudinal kicker constant

Longitudinal kicker constant is defined as the ratio of the change of the particle's energy (in electron volt) per unit charge of particle to the applied voltage V_k. Mathematically it is represented as

$$K_{//} = \frac{\Delta\varepsilon/_e}{V_k} = \frac{1}{V_k} \int_{-L/2}^{L/2} e^{j\frac{\omega}{v_b}z} E_z dz \qquad (1.26)$$

Here Δε is energy change of the particle, L is length of the kicker, e is charge on particle, E_z is z-component of the electric field at position z and time t along the beam path and v_b is particle velocity.

The quantity represented by numerator of equation (1.26) is effective voltage experienced by the charge particle passing through the kicker. The instantaneous voltage drop across the kicker is defined as

$$V_{//} = \int_{-L/2}^{L/2} E_z dz \qquad (1.27)$$

The ratio of effective voltage to the instantaneous voltage is known as transient time factor given by

$$T = \frac{\int_{-L/2}^{L/2} e^{j\frac{\omega}{v_b}z} E_z dz}{\int_{-L/2}^{L/2} E_z dz} \qquad (1.28)$$

Factor $e^{j\frac{\omega}{v_b}z}$ in numerator of equation (1.26) accounts for transient time factor.

1.4.1.2 Transverse kicker constant

Transverse kicker constant is defined as the complex ratio of the product of the transverse momentum change (Δp_x) and particle velocity (v_b) per unit charge of particle to the applied voltage (V_k). It is given by

For horizontal plane (x-direction)

$$\boldsymbol{K_x} = \frac{\Delta \boldsymbol{p_x} v_b / e}{V_k} = \frac{1}{V_k} \int_{-L/2}^{L/2} e^{j\frac{\omega}{v_b}z} \left[\boldsymbol{E_x} + \boldsymbol{v_b} \times \boldsymbol{B_y}\right] dz \tag{1.29}$$

For vertical plane (y-direction)

$$\boldsymbol{K_y} = \frac{\Delta \boldsymbol{p_y} v_b / e}{V_k} = \frac{1}{V_k} \int_{-L/2}^{L/2} e^{j\frac{\omega}{v_b}z} \left[\boldsymbol{E_y} + \boldsymbol{v_b} \times \boldsymbol{B_x}\right] dz \tag{1.30}$$

Similar to the longitudinal case, the effective transverse voltage experience by charge particle passing through kicker is less than instantaneous transverse voltage drop across the kicker.

1.4.2 Shunt impedance of a kicker

The kicker constant relates the kick received by a charge particle with the applied voltage. For a given input power, the input voltage changes with input impedance. Hence, kicker constant does not relate kick with input power uniquely. To evaluate efficiency of a device as a kicker, one should relate kick and input power. The quantity that uniquely relates the input power to the kick received by the beam is called shunt impedance [1,2].

1.4.2.1 Longitudinal shunt impedance

Analogous to the RF cavities, the shunt impedance of kicker may be defined as the ratio of the square of the instantaneous voltage drop across the kicker to the input power 'P'. Therefore for longitudinal direction the shunt impedance is

$$(R_{sh})_{//} = \frac{\left[\int_{-L/2}^{L/2} E_z dz\right]^2}{2P} \tag{1.31}$$

The quantity of importance in kicker is effective voltage experienced by the beam. Therefore, effective shunt impedance of kicker may also be defined as ratio of square of effective voltage experienced by beam to the input power. The effective shunt impedance is given by

$$(R_{sh})_{//}^{eff} = T^2 (R_{sh})_{//} \tag{1.32}$$

1.4.2.2 Transverse shunt impedance

Transverse shunt impedance of kicker is defined as the ratio of the square of the instantaneous transverse voltage drop across the kicker and input power 'P'. Mathematically transverse shunt impedance is represented as

For x- direction (horizontal plane)

$$(R_{sh})_x = \frac{\left|\int_{-L/2}^{L/2} (\boldsymbol{E_x} + \boldsymbol{v_v} \times \boldsymbol{B_y}) dz\right|^2}{2P} \tag{1.33}$$

For y- direction (vertical plane)

$$(R_{sh})_y = \frac{\left|\int_{-L/2}^{L/2} (\boldsymbol{E_y} + \boldsymbol{v_b} \times \boldsymbol{B_x}) dz\right|^2}{2P} \tag{1.34}$$

Effective shunt impedance for transverse plane can be written as

$$(R_{sh})_x^{eff} = T^2 (R_{sh})_x \quad \text{(horizontal),} \tag{1.35}$$

$$(R_{sh})_y^{eff} = T^2 (R_{sh})_y \quad \text{(vertical),} \tag{1.36}$$

1.4.3 Relation between kicker constant and shunt impedance

Kicker constant relates voltage experienced by charge particle passing through it with applied (input) voltage, whereas shunt impedance relates it with input power. For a given input impedance (source input), the input voltage and input power are related with each other. Therefore, shunt impedance can be represented in terms of kicker constant and input impedance [1,2]. For input voltage V_k and input impedance Z_0, the average input power is

$$P = \frac{(V_k)^2}{2Z_0} \tag{1.37}$$

From equations (1.26), (1.28), (1.31) and (1.37) we have

$$(R_{sh})_{//} T^2 = Z_0 {K_{//}}^2 \tag{1.38}$$

Similarly, for transverse case, we have

$$(R_{sh})_x T^2 = Z_0 |\boldsymbol{K_x}|^2 = Z_0 {K_x}^2 \quad \text{(horizontal),} \tag{1.39}$$

$$(R_{sh})_y T^2 = Z_0 \left|\boldsymbol{K_y}\right|^2 = Z_0 {K_y}^2 \quad \text{(vertical),} \tag{1.40}$$

1.4.4 Relation between transverse and longitudinal effect

According to the Panofsky Wenzel theorem [63-65], for a charge particle moving in time varying electromagnetic field, the transverse deflection can be expressed purely in terms of the longitudinal component of electric field (longitudinal kick). Applying Panofsky Wenzel theorem to pickup/kicker we get [1,2] (see Appendix-A)

$$\frac{\partial K_{//}}{\partial \mathrm{x}} = -j\frac{\omega}{v_b}K_x \qquad \text{(horizontal),} \qquad (1.41)$$

$$\frac{\partial K_{//}}{\partial \mathrm{y}} = -j\frac{\omega}{v_b}K_y \qquad \text{(vertical),} \qquad (1.42)$$

Equations (1.41) and (1.42) are very important as they represent transverse properties of a kicker purely in terms of its longitudinal properties. From equations (1.41) and (1.42) one can also infer that a structure with no longitudinal electric field (no longitudinal kick) cannot produce transverse kick.

Important point to be noted here is that, a given kicker can be used as transverse kicker in one mode of excitation and as longitudinal kicker in another mode of excitation. For such case, the Panofsky Wenzel theorem does not predict transverse behavior of kicker in terms of its longitudinal field. On the other, the Panofsky Wenzel theorem predicts transverse behavior of the kicker in terms of its longitudinal field for same mode of excitation.

1.4.5 Relation between pick-up and kicker characteristics

Any device which serves as pickup can also be used as kicker. The pickup characteristics of the device, if used as pickup, have definite relation with kicker characteristics of the same device when used as kicker. Following Lorentz reciprocity theorem [66-68], the relations between pickup (transfer impedance and position sensitivity) and kicker properties (kicker constant or shunt impedance) of a device are given in table 1.3 [1,2] (see Appendix-B).

Table 1.3. Relation between kicker and pickup characteristics of a general pickup/kicker.				
Sr. No.	Parameter	Longitudinal	Transverse	
			Horizontal	Vertical
1	Kicker constant	$K_{//} = \frac{2Z_T}{Z_0}$	$K_x = j\frac{2v_{bZ_TS_x}}{\omega Z_0}$	$K_y = j\frac{2v_{bZ_TS_y}}{\omega Z_0}$
2	Shunt impedance	$(R_{sh})_{//}T^2 = 4\frac{{Z_T}^2}{Z_0}$	$(R_{sh})_x T^2 = 4\left(\frac{v_b}{\omega}\right)^2\frac{{Z_T}^2{S_x}^2}{Z_0}$	$(R_{sh})_y T^2 = 4\left(\frac{v_b}{\omega}\right)^2\frac{{Z_T}^2{S_y}^2}{Z_0}$

1. 5 Beam diagnostics applications of pickups and kickers

Pickups and kickers have numbers of applications in particle accelerators [3-8]. Few important applications of pickups/kickers are explained briefly in following sections.

1.5.1 Beam position monitoring

Beam position is defined as the transverse position (co-ordinate) of the beam with respect to the reference beam path or trajectory. Measurement of beam position is important for efficient transmission of the beam through different sections of the linear accelerators and transport lines. In circular machine, like synchrotrons, beam position monitoring system plays important role in measurement and minimization of closed orbit distortion which improves quality and life time of the beam.

The most commonly used beam position monitors in electron accelerators (like electron synchrotrons and storage rings) are button electrode BPMs. In proton synchrotron, linear accelerators and beam transfer lines, where bunch length is relatively larger as compared to the electron beam accelerators due to particle energy or space charge, shoe box BPM and striplines are commonly used for beam position measurement.

1.5.2 Tune measurement and feedback system

In synchrotron, there are periodic focusing and defocusing fields, thus the particles oscillate about some reference point or orbit. The oscillations in transverse direction are called betatron oscillations [63,69,70] and oscillations in longitudinal direction are called synchrotron oscillations [63,69,70]. The number of oscillations per turn is called tune. For transverse and longitudinal oscillations, the tunes are classified as betatron tune and synchrotron tune respectively.

There are different techniques (RF excitation, RF knock out etc.) to measure betatron or synchrotron tunes. Principally, the measurement of tune involves excitation of beam using kickers and then measurement of beam oscillation frequency using pickups (BPM). For transverse direction (betatron tune), striplines are commonly used for transverse excitation (kicker mode) and measurement of the betatron oscillations (pickup mode).

Stability of tune is very important in synchrotron as slight change of tune from designed value can kill the beam. Therefore, tune feedback systems are also employed in such machines to ensure non interrupted operation of the machine.

1.5.3 Instability detection and control feedback system

When a bunch of charge particles (beam) moves in an accelerator, the electromagnetic field associated with it interacts with surrounding elements like diagnostic devices, RF cavity, vacuum chamber etc. Such interactions can produce counter field that can interact back with the beam itself. The counter field generated due to interaction between beam and surroundings is known as wakefield [66, 71, 72]. The wakefield interacting back with the beam can produce unwanted oscillations in the beam. These unwanted oscillations of beam are called beam instability. Pickup and kicker play vital role in detection and control of the beam instabilities. The signature of beam instability appears as oscillations in the pickup signal. Beam position monitors (pickups) are used to detect such unwanted oscillations or beam instabilities.

The beam instability has serious impact on beam quality as well as beam lifetime of the machine. Therefore, beam instability control feedback systems are deployed to suppress these beam instabilities. Essential devices deployed for controlling any beam instability through control feedback system are pickups (BPM) and kickers. Pickup is used to sense beam instability (beam oscillations) and kicker is used to apply correction kick of certain amplitude and phase on the beam to suppress the beam oscillations.

1.5.4 Beam Energy (Time of flight)

Measurement of beam energy using time of flight technique is very useful in accelerators like low energy proton linac or transport lines where particles have non relativistic velocities. The schematic of time of flight system for energy measurement is shown in Fig. 1.11.

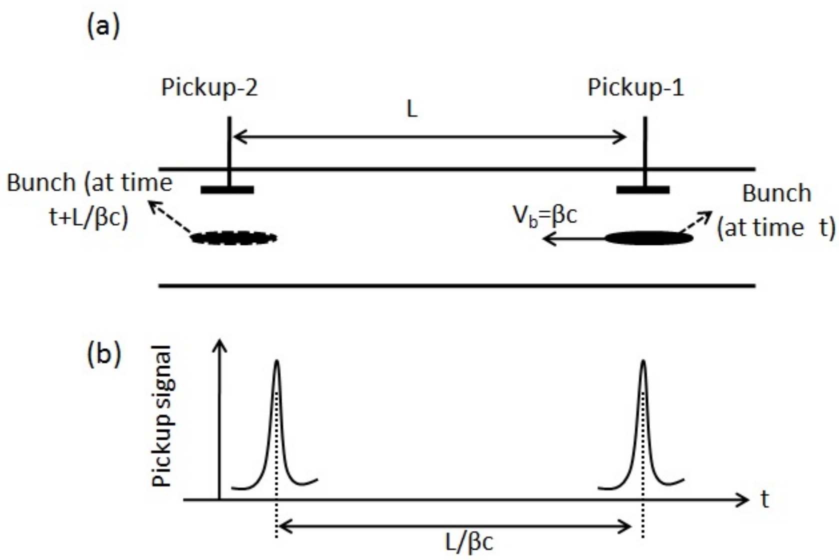

Fig. 1.11 Schematic of Time of flight (TOF) technique for energy measurement; (a) Schematic of setup (b) Pickup signals for TOF measurement.

Beam energy is calculated from the time taken by the beam to travel distance 'L' from pickup-1 to pickup-2 (Fig. 1.11). Time of flight (T_{TOF}) between pickups is given by

$$T_{TOF} = \frac{L}{\beta c} \tag{1.43}$$

Here β=v/c with v is beam velocity and c is velocity of the light. In actual measurement, phase difference between the signals of pickup-1 and pickup-2 is measured. Let time of flight can be represented as

$$T_{TOF} = \frac{2\pi}{\omega} N + \Delta t \tag{1.44}$$

Here N is an integer number of RF cycle, ω is frequency and Δt is fractional part of T_{TOF}. Converting T_{TOF} into phase difference, we get

$$\omega T_{TOF} = 2\pi N + \Delta\varphi \tag{1.45}$$

Here Δφ=ωΔt is actual/measured phase difference between two pickup signals. From equations (1.43) and (1.45) we can write

$$\beta = \frac{L}{\lambda\left(N + \frac{\Delta\varphi}{2\pi}\right)} \tag{1.46}$$

Kinetic energy of the beam is given by

$$W = W_0\left(\frac{1}{\sqrt{1-\beta^2}} - 1\right) \tag{1.47}$$

Here W_0 is rest mass energy of the beam. From equations (1.46) and (1.47) we get

$$W = W_0\left(\frac{1}{\sqrt{1-\left(\frac{L}{\lambda\left(N+\frac{\Delta\varphi}{2\pi}\right)}\right)^2}} - 1\right) \tag{1.48}$$

Equation (1.48) gives kinetic energy of the beam in terms of phase difference between signals of pickup-1 and pickup-2.

1.5.4.1 Error estimation

The error in β due to uncertainties in distance (δL) between pickup-1 and pickup-2, and measurement of phase difference (δ(Δφ)) is given by

$$\frac{\delta\beta}{\beta} = \sqrt{\left(\frac{\delta L}{L}\right)^2 + \left(\frac{\delta\left(\frac{\Delta\varphi}{2\pi}\right)}{N+\frac{\Delta\varphi}{2\pi}}\right)^2} \tag{1.49}$$

Differentiating equation (1.47) with β we get

$$\frac{dW}{W} = \gamma(\gamma+1)\frac{d\beta}{\beta} \tag{1.50}$$

Here $\gamma = \frac{1}{\sqrt{1-\frac{\beta}{c}}}$. From equations (1.49) and (1.50) we get

$$\frac{dW}{W} = \gamma(\gamma+1)\sqrt{\left(\frac{\delta L}{L}\right)^2 + \left(\frac{\delta\left(\frac{\Delta\varphi}{2\pi}\right)}{N+\frac{\Delta\varphi}{2\pi}}\right)^2} \tag{1.51}$$

Equation (1.51) shows that the error in measured energy increases with increasing γ. therefore time of flight (TOF) method is used for particle/beam having non relativistic velocity.

CHAPTER-2

EFFECT OF FRINGE FIELD ON STRIPLINE PROPERTIES

Fringe field between stripline electrode (strip) and vacuum chamber has significant effect on effective width of the electrode (strip). The parameters like characteristic impedance, transfer impedance and kicker constant (shunt impedance) depend on effective width of strip. Considering fringe field, the modified expressions for effective width of strip and characteristic impedance of stripline are derived.

This chapter is broadly divided into two parts. First part presents derivation of modified expressions for different parameters of circular stripline (stripline having circular cross section) considering fringe field. Second part presents validation of modified expressions and analysis of fringe field effect on effective width of the strip and characteristic impedance of stripline through simulations performed using CST EM Studio and CST MW Studio.

2.1 Coaxial transmission line and its characteristic impedance

Coaxial transmission line is simply a transmission cable that has a tubular outer conductor with a coaxial narrow inner conductor. An insulator or a dielectric is used to isolate these conductors electrically. The coaxial transmission line transmits signal through propagation of electromagnetic wave (TEM mode) between the inner and the outer tubular conductors.

Consider a circular coaxial transmission line having outer conductor of radius R_0 and inner conductor of radius R_{in} as shown in Fig. 2.1. The characteristic impedance of loss-less transmission line can be written as [66,73]

$$Z_0 = \sqrt{\frac{L}{C}} \tag{2.1}$$

Here L and C are inductance and capacitance per unit length, of a transmission line, given by equations (2.2) and (2.3).

$$L = \frac{\mu}{2\pi} ln\left(\frac{R_0}{R_{in}}\right) \tag{2.2}$$

$$C = \frac{2\pi\epsilon}{ln\left(\frac{R_0}{R_{in}}\right)} \tag{2.3}$$

In equations (2.2) and (2.3), μ and ε are magnetic permeability and electric permittivity of the medium between inner and outer conductors. From equations (2.1) to (2.3) we get

$$Z_0 = \frac{1}{2\pi}\sqrt{\frac{\mu}{\epsilon}}\ ln\left(\frac{R_0}{R_{in}}\right) \tag{2.4}$$

For vacuum we have

$$Z_0 \approx 60\ ln\left(\frac{R_0}{R_{in}}\right) \tag{2.5}$$

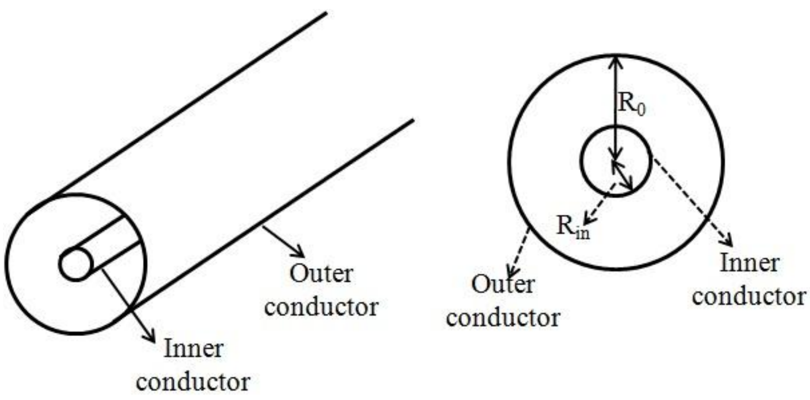

Fig. 2.1 Schematic of circular coaxial transmission line showing inner and outer conductors.

2.2 Circular Stripline

Striplines are important diagnostics devices which are commonly used as beam position monitors (pickups) and kickers in electron, proton and heavy ion particle accelerators. Striplines have long electrodes of finite width which are placed inside vacuum chamber. Fig. 2.2 shows the schematic of circular cross section stripline (circular stripline) having four electrodes (strips). It consists of a cylindrical pipe called outer conductor or vacuum chamber and four curved electrodes called strips. The strips and the vacuum chamber form a transmission lines like structure having well defined characteristic impedance. The strip acts as inner conductor and the vacuum chamber acts as outer conductor similar to the coaxial transmission line. The beam passing through the stripline induces image current on strips [29]. The flow of image current generates electromagnetic wave between strip and vacuum chamber similar to the transmission line.

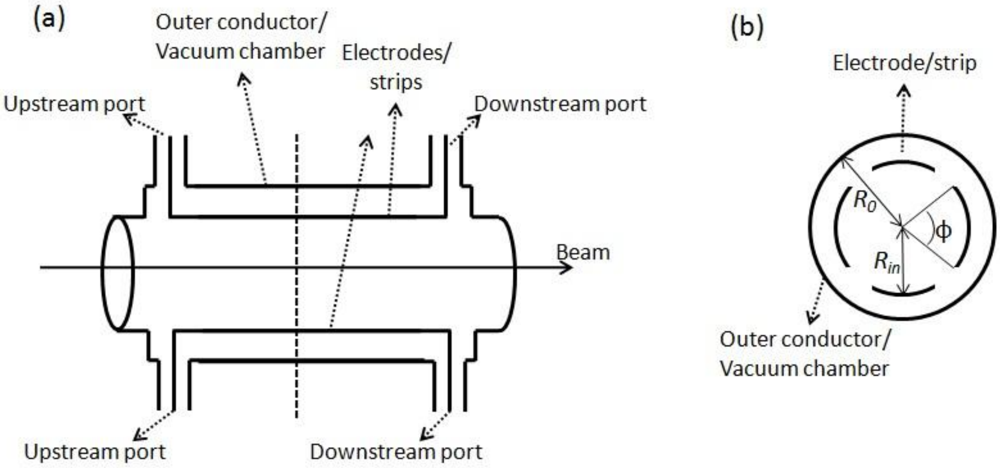

Fig. 2.2 Schematic of four electrodes circular stripline.

2.2.1 Characteristic impedance of stripline without fringe field

Consider a stripline shown in Fig. 2.2. Let the azimuthal width of the strip be ϕ, radius of the strip be R_{in} and radius of vacuum chamber (outer conductor) be R_0. For single strip, the surface area of inner conductor (strip) is reduced by a factor of $\frac{\phi}{2\pi}$ as compared to the inner conductor of the conventional circular transmission line having same dimension (Fig. 2.1). Therefore, neglecting fringe field at the edges of the strip, the capacitance per unit length of transmission line formed by the single strip and vacuum chamber can be written as

$$C = \frac{\phi}{2\pi} \frac{2\pi\epsilon}{ln\left(\frac{R_0}{R_{in}}\right)} \tag{2.6}$$

Characteristic impedance of transmission line is inversely proportional to the capacitance per unit length as shown in equations (2.3) and (2.4). Therefore, the characteristic impedance of single strip is given by

$$Z_0 = \frac{1}{\phi}\sqrt{\frac{\mu}{\epsilon}}\ ln\left(\frac{R_0}{R_{in}}\right) \tag{2.7}$$

Generally, the stripline have vacuum between the electrode and the outer conductor, thus the characteristic impedance of stripline (single electrode) is given by

$$Z_0 = \frac{1}{\phi/_{2\pi}} 60\ ln\left(\frac{R_0}{R_{in}}\right) \tag{2.8}$$

In equation (2.8), $\frac{\phi}{2\pi}$ is called geometrical factor and it is represented by η. Physically, geometrical factor represents fraction of wall current (image current) intercepted by strip.

2.3 Fringe field in circular stripline

The geometry and size of the strip and vacuum chamber play an important role in stripline design. For example, the current flowing through a stripline electrode (strip) depends on its width, thereby the quantities like characteristic impedance, transfer impedance, kicker constant, shunt impedance are functions of strip width [1,2,29].

The expression of the characteristic impedance given by equation (2.8) is based on the fact that the field only exists between the strip and the outer conductor. In reality, the field between strip and the outer conductor is uniform whereas it gradually decays to zero going outwards from the edge of the strip due to finite gap between consecutive strips. This is known as fringe field and it causes enhancement in the effective width of the strip as compared to its (strip's) physical width. The illustration of fringe field in a circular stripline is shown in Fig. 2.3.

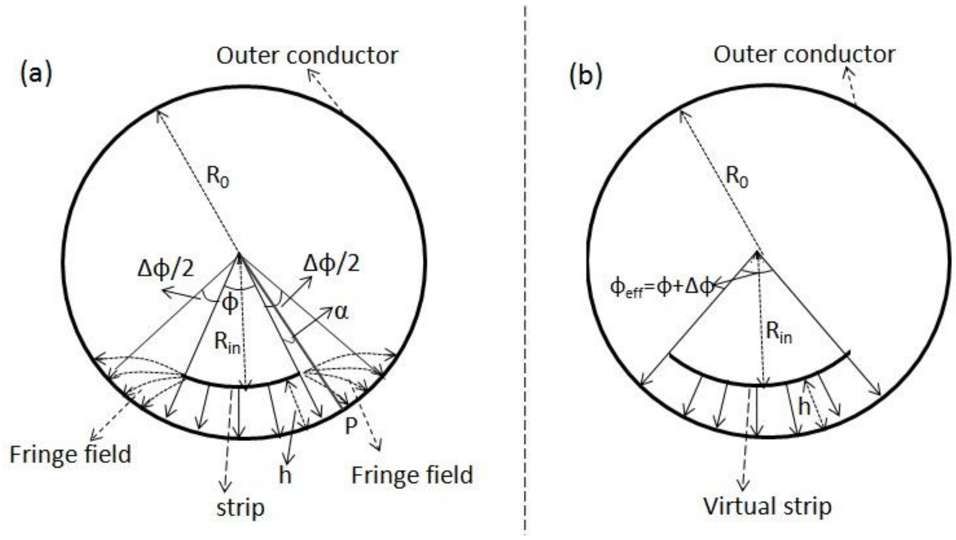

Fig. 2.**3** (a**)** Actual **s**tripline with fringe field; and (b) its equivalent imaginary stripline without fringe field.

2.3.1 Effective width of strip

Let us imagine another stripline (Fig. 2.3(b)) in which there is no fringe field. If the total field between strip and outer conductor in both of the striplines (actual and imaginary striplines) are equal, then (for same radii of the strip and outer conductor) the azimuthal width of the strip in imaginary stripline is equal to the effective width of the strip in actual stripline.

The fringe field at a point 'P' on outer conductor decays as $1/r^2$, where r is the distance of the point on outer conductor from the edge of the strip. The normal field between strip and outer conductor is proportional to $1/h^2$, where h is the distance between radii of the strip and the outer conductor. Thus, neglecting thickness of the strip, the integrated field in actual stripline is proportional to

$\frac{1}{h^2}\phi + 2\int_0^{\psi} \frac{1}{{R_{in}}^2+(R_{in}+h)^2-2R_{in}(R_{in}+h)cos\alpha}\, d\alpha$

Here α is azimuthal angle between radii passing through the edge of the strip and the point on the outer conductor. The integrated field in imaginary stripline is proportional to

$\frac{1}{h^2}(\phi + \Delta\phi)$

Here ϕ+Δϕ is azimuthal width of the imaginary stripline which is equal to the effective width (ϕ_{eff}) of the actual stripline, ψ is integration limit which is decided by the extent of the fringe field, R_{in} is radius of the strip, h is distance between the strip and the outer conductor.

Equating both fields we get

$$\frac{1}{h^2}\phi_{eff} = \frac{1}{h^2}(\phi + \Delta\phi)$$

$$= \frac{1}{h^2}\phi + 2\int_0^{\psi} \frac{1}{{R_{in}}^2 + (R_{in}+h)^2 - 2R_{in}(R_{in}+h)cos\alpha}\, d\alpha \qquad (2.9)$$

Factor 2 with second term of equation (2.9) arises mainly due to contribution of fringe field by both edges of the strip. Simplifying equation (2.9), the virtual enhancement in width of strip ($\Delta\phi$) is given by

$$\Delta\phi = 2h^2\int_0^{\psi} \frac{1}{{R_{in}}^2 + (R_{in}+h)^2 - 2R_{in}(R_{in}+h)cos\alpha}\, d\alpha \qquad (2.10)$$

Equation (2.10) is similar to the equation presented by J-P. Papis and L. Vos, in CERN report [36]. In reference [36], the limit of integration has been taken from 0 to π giving following equations.

$$\Delta\phi = 2\pi\frac{h}{2R_{in} + h} \qquad (2.11)$$

$$\phi_{eff} = \phi + \Delta\phi = \phi + 2\pi \frac{h}{2R_{in} + h} \quad (2.12)$$

$$\eta = \frac{\phi + \Delta\phi}{2\pi} = \frac{1}{2\pi}\left\{\phi + 2\pi \frac{h}{2R_{in} + h}\right\} \quad (2.13)$$

Generally, striplines used as pickups have two or four strips and due to presence of other strips the fringe field of a given strip can only extend to a maximum value of ψ but not π. While designing a stripline for pickup mode, the strips are assumed to be at same potentials, thus a perfect magnetic plane exists between two consecutive strips (Fig. 2.4). The perfect magnetic plane forces normal component of electric field to be 0 at this plane and the lines of fringe field emerging from the side end of one strip can only extend up to the middle of the gap between two consecutive strips. Thus, the upper limit of integration (ψ) of the fringe field should be equal to half the angular separation between the side ends of consecutive electrodes as illustrated in Fig. 2.4.

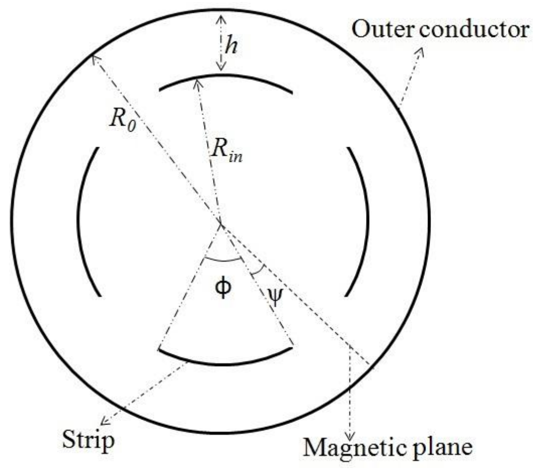

Fig. 2.**4**. Illustration of magnetic plane and limit of integration (ψ).

In general, for a stripline having N electrodes each of azimuthal width ϕ, the limit of integration of fringe field is from 0 to $\psi = \frac{1}{2}\left(\frac{2\pi}{N} - \phi\right)$. Using $\psi = \frac{1}{2}\left(\frac{2\pi}{N} - \phi\right)$ in equation (2.10), the expression for the virtual increase in the width of the strip becomes

$$\Delta\phi = \frac{4h}{2R_{in} + h} atan\left[\frac{2R_{in} + h}{h} tan\left(\frac{1}{4}\left(\frac{2\pi}{N} - \phi\right)\right)\right] \qquad (2.14)$$

The new expression for effective width ($\Delta\phi$) and geometrical factor (η) of strip can be written as

$$\phi_{eff} = \phi + \Delta\phi = \phi + \frac{4h}{2R_{in} + h} atan\left[\frac{2R_{in} + h}{h} tan\left(\frac{1}{4}\left(\frac{2\pi}{N} - \phi\right)\right)\right] \qquad (2.15)$$

$$\eta = \frac{\phi + \Delta\phi}{2\pi} = \frac{1}{2\pi}\left\{\phi + \frac{4h}{2R_{in} + h} atan\left[\frac{2R_{in} + h}{h} tan\left(\frac{1}{4}\left(\frac{2\pi}{N} - \phi\right)\right)\right]\right\} \qquad (2.16)$$

2.3.2 Characteristic impedance under fringe field

Equation (2.8) shows that the characteristic impedance of the strip depends on width of the strip. Due to fringe field, the effective width of the strip gets enhanced, therefore the characteristic impedance of the strip reduces. In reality, the characteristic impedance of stripline calculated using equation (2.8) differs from its actual value [74]. In the presence of fringe field the correct expression for the characteristic impedance of the strip can be obtained by using effective width of the strip in equation (2.8). From equations (2.8) and (2.15), the expression for the characteristic impedance of the circular stripline becomes

$$Z_0 = \frac{2\pi}{\phi + \frac{4h}{2R_{in} + h} atan\left[\frac{2R_{in} + h}{h} tan\left(\frac{1}{4}\left(\frac{2\pi}{N} - \phi\right)\right)\right]} 60\, ln\left(\frac{R_0}{R_{in}}\right) \qquad (2.17)$$

Here $R_0=R_{in}+h$. Equation (2.17) is an important relation as the characteristic impedance is an important design parameters for any stripline.

For sake of comparison the expression of characteristic impedance derived by J-P Papis and L. Vos [36] is given by (using equation (2.12) in equation (2.8))

$$Z_0 = \frac{2\pi}{\phi + 2\pi\frac{h}{2R_{in}+h}} 60\, ln\left(\frac{R_0}{R_{in}}\right) \tag{2.18}$$

2.3.3 Effect of fringe field on transfer impedance and kicker constant

For stripline, matched at downstream end, the output voltage is given by [29]

$$V(\omega) = -\eta Z_0 I_b(\omega) sin\left(\frac{\omega l}{c}\right) sin\left(\omega t - \frac{\omega l}{c}\right) \tag{2.19}$$

Here $I_b(\omega)$ is beam current at frequency ω and l is length of the strip (electrode). The transfer impedance is the ratio of pickup voltage to the beam current. Thus we have

$$Z_T = \frac{V(\omega)}{I_b(\omega)} = -\eta Z_0 sin\left(\frac{\omega l}{c}\right) sin\left(\omega t - \frac{\omega l}{c}\right) \tag{2.20}$$

$$\Longrightarrow |Z_T| = \eta Z_0 sin\left(\frac{\omega l}{c}\right) \tag{2.21}$$

From equations (2.16), (2.17) and (2.21) we get

$$|Z_T| = 60\, ln\left(\frac{R_0}{R_{in}}\right) sin\left(\frac{\omega l}{c}\right) \tag{2.22}$$

The relation between kicker constant ($k_{//}$) and transfer impedance of the stripline is [1,2]

$$Z_T = \frac{Z_0 k_{//}}{2} \tag{2.23}$$

From equations (2.21) and (2.23) we get

$$|k_{//}| = 2\eta sin\left(\frac{\omega l}{c}\right) \tag{2.24}$$

Equation (2.22) shows that the transfer impedance of stripline (matched at downstream end) depends on $\frac{R_0}{R_{in}}$ and length of strip/electrode (l), and it is independent (apparently) of azimuthal width. As explained in section 2.3.2, the characteristic impedance of a stripline depends on the ratio $\frac{R_0}{R_{in}}$ and effective width of the strip (equation 2.17). Therefore, for particular characteristic impedance, the ratio $\frac{R_0}{R_{in}}$ depends on effective width of strip which is governed by fringe field.

Regarding kicker constant, equation (2.24) explicitly shows that for a given structure of stripline, the longitudinal kicker constant depends on η which in turn depends on fringe field through equation (2.16).

2.4. Simulations

2.4.1 Simulation of η and ϕ_{eff}

Equation (2.16) gives relationship between effective width of the strip (ϕ_{eff}) and geometrical factor (η) or fraction of wall current intercepted by strip. According to the quasi-electrostatic model, the fraction of the wall current intercepted by the strip can be obtained by calculating charge induced (image charge) at the inner surface of the strip due to a uniform line charge distribution along the axis of the stripline. Most of the striplines have either two or four electrodes. Therefore, simulations presented here concentrate on two and four electrodes configurations of the striplines. Similar analysis can be done for the stripline having any number of electrodes.

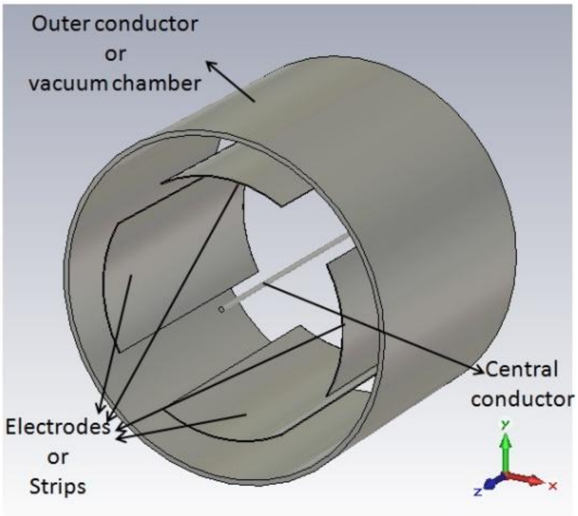

Fig. 2.5 CST model of a stripline showing four strips, an outer conductor and a central conductor (simulating line charge distribution).

Computer model of a stripline having four strips, an outer conductor and a central conductor (simulating line charge distribution) is shown in Fig. 2.5. To calculate η we need not to model whole stripline structure (like feed-through assembly etc.). Only the outer conductor with four strips is designed in CST EM Studio [75]. At upstream and downstream ends of the strip, the fringe field emerging from the sides of the strip results in enhancement of effective width of the strip, whereas the fringe field emerging from the curved edges (ends of the strip) of the stripline results in enhancement of effective length of the strip. Thus, to avoid this effect (change in length of the strip), the length of the outer conductor and strips are considered to be equal. To define longitudinal uniform charge distribution along the axis, a cylindrical conductor (central conductor) along the stripline axis is designed and an arbitrary charge Q is assigned to it.

In principle (for quasi-electrostatic model), the actual length of the beam pipe and the central conductor should be infinite. Same condition is obtained for simulation by defining a tangential boundary condition (forces normal electric and magnetic field to be zero at the boundary) at the upstream and the downstream ends of the stripline model. The outer conductor and the strips are grounded by assigning a fixed potential of 0 V. The charge induced on strip is obtained for an arbitrary charge Q of central conductor using E-static solver. The fraction (η) of the wall current intercepted by strip is the ratio of the charge induced at the strip to the total charge (Q) assigned to the central conductor.

A comparison of the fraction of the wall current intercepted by the strip obtained using expression ($\eta = \frac{\phi}{2\pi}$), equation (2.13), equation (2.16) and simulation is presented in Figs. 2.6 to 2.11. The effective width of the strip may be calculated from η using equation (2.16). Simulations (Figs. 2.6 to 2.11) show that, the modified equation (2.16) derived in this chapter produces results which are more close to the simulation results as compared to the conventional equation $\eta = \frac{\phi}{2\pi}$ and equation (2.13). The conventional equation under estimates whereas equation (2.13) over estimates η.

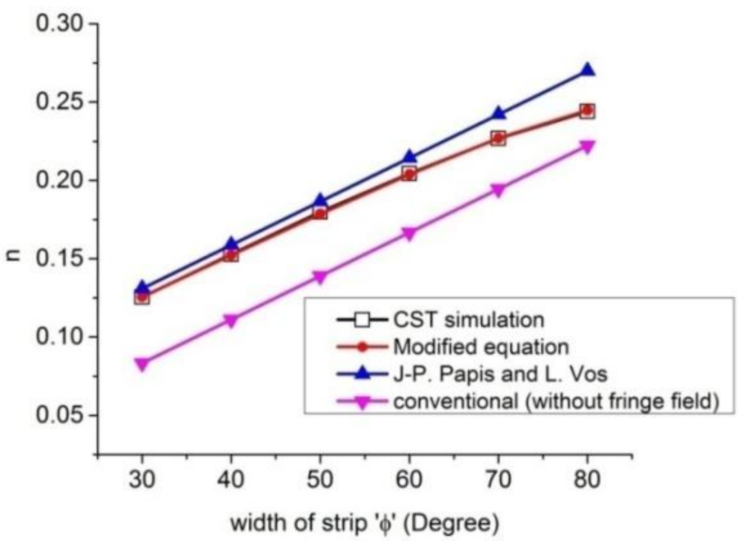

Fig. 2.6 Variation of η with ϕ for four electrodes stripline structure (R_0/R_{in}=1.1).

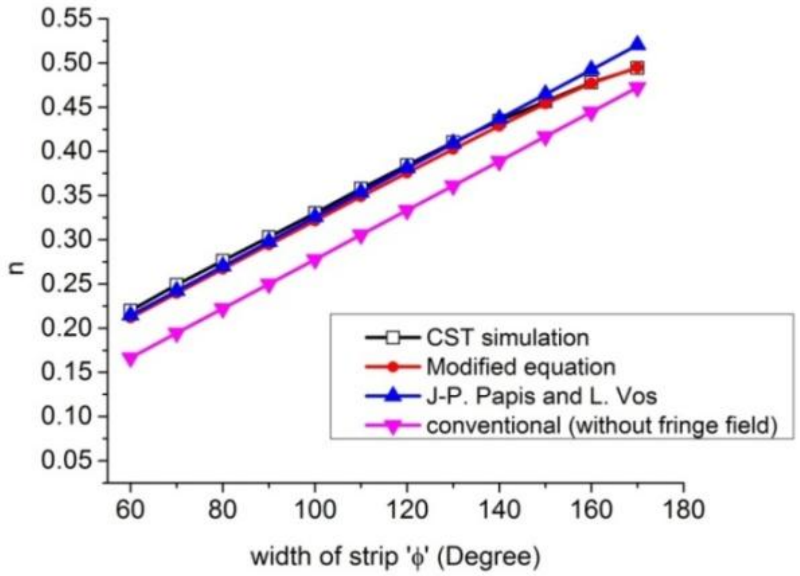

Fig. 2.7 Variation of η with ϕ for two electrodes stripline structure (R_0/R_{in}=1.1).

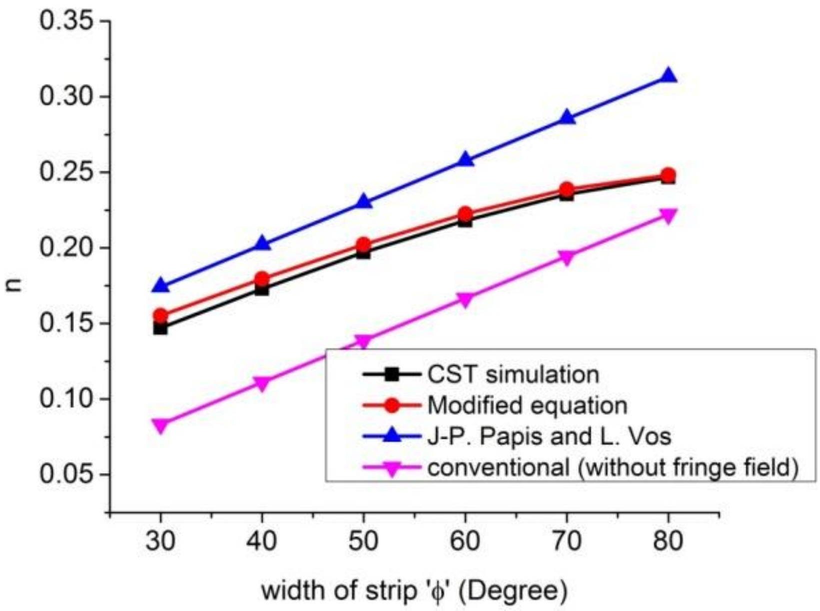

Fig. 2.8 Variation of η with ϕ for four electrodes stripline structure (R_0/R_{in}=1.2).

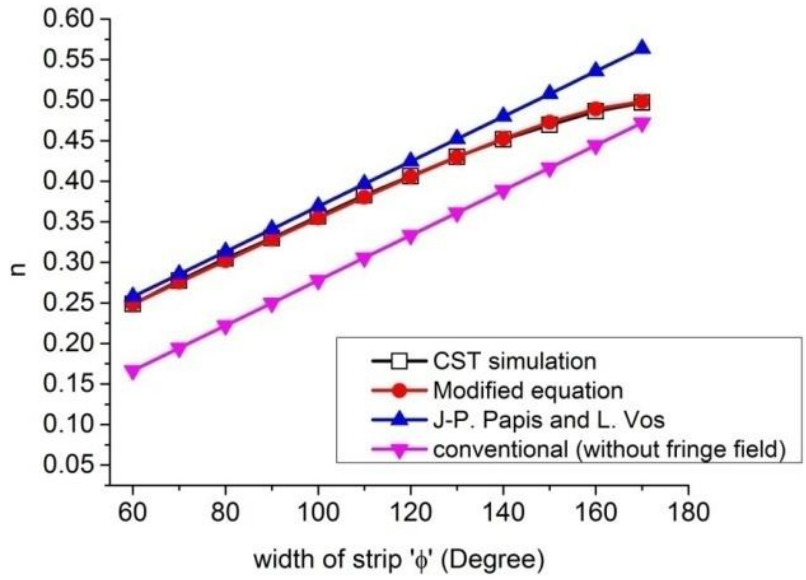

Fig. 2.9 Variation of η with ϕ for two electrodes stripline structure (R_0/R_{in}=1.2).

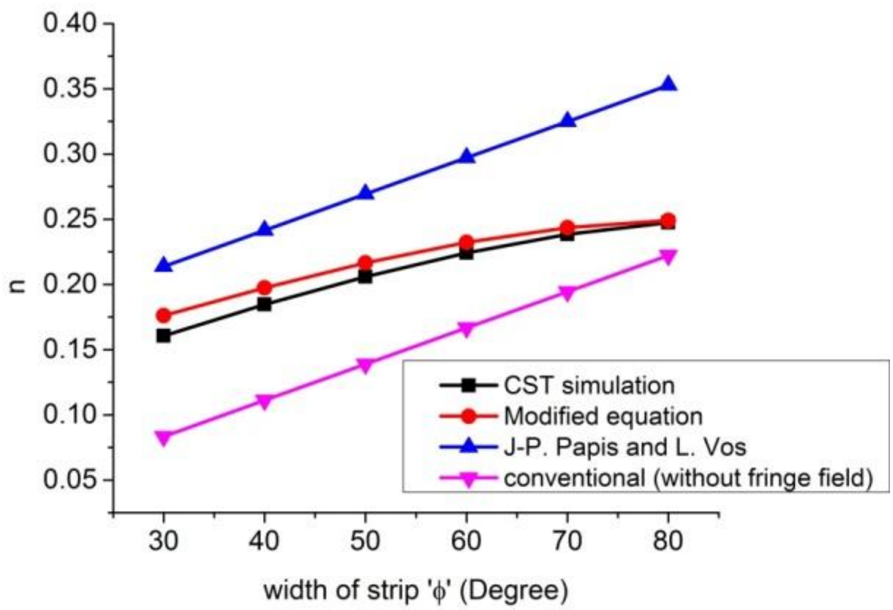

Fig. 2.10 Variation of η with ϕ for four electrodes stripline structure (R_0/R_{in}=1.3).

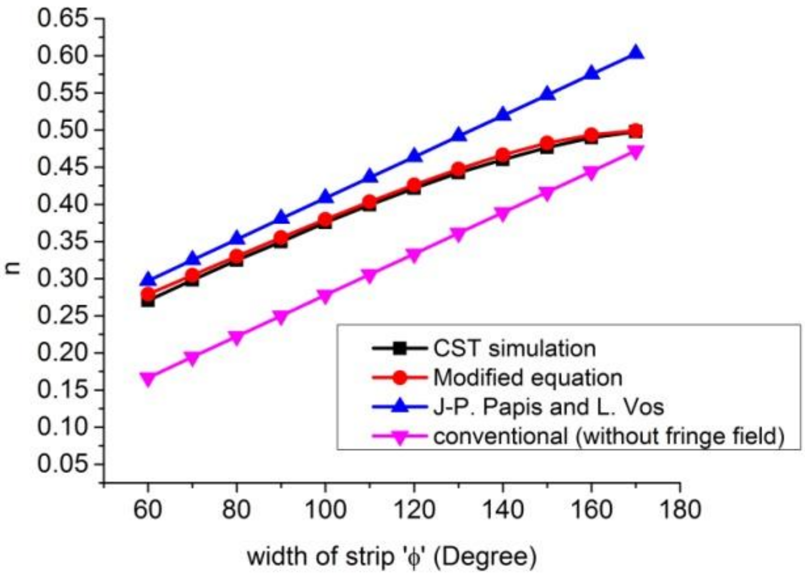

Fig. 2.11 Variation of η with ϕ for two electrodes stripline structure (R_0/R_{in}=1.3).

2.4.2 Simulation of Characteristic impedance

Equation (2.17) is also validated through simulation performed using CST Microwave Studio for two and four electrodes stripline structures. Stripline (outer conductor and strips) is modeled in CST Microwave Studio and characteristic impedance is obtained from line impedance using Transient Solver of CST Microwave Studio. For multipin type waveguide port in even mode, the line impedance given by CST MW Studio is calculated for net current flowing through all electrodes (strips). Therefore, to calculate characteristic impedance of single electrode (strip), the line impedance is multiplied by number of center conductors (here strips). Fig. 2.12 shows line impedance and electric field distribution for a typical four electrodes stripline obtained through simulation performed using CST Microwave Studio.

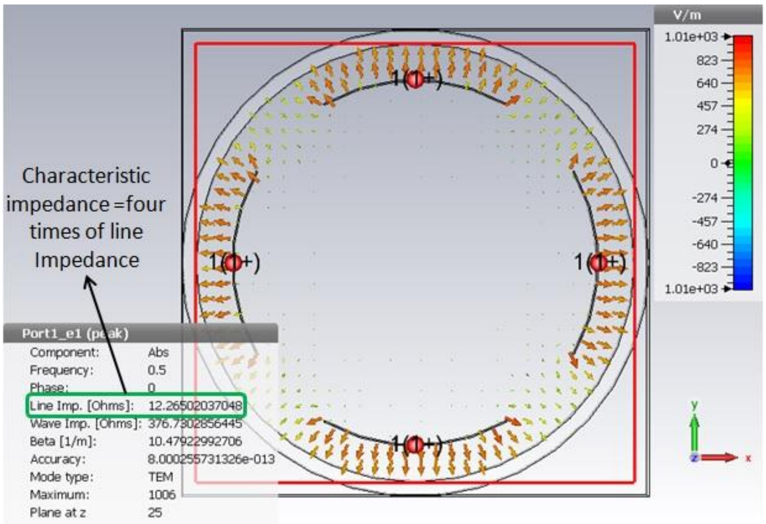

Fig. 2.12 Port impedance of a general four electrodes stripline simulated using CST Microwave Studio.

Generally, the striplines used for the diagnostic purpose are designed to have 50 Ω characteristic impedance. Therefore, to represent the practical scenario, simulations of two and four electrodes striplines are carried out for different combinations of ϕ and $\frac{R_0}{R_{in}}$such that the characteristic impedance of the stripline under simulation is close to 50 Ω. Comparison of characteristic impedance obtained through simulation with equations (2.17) and (2.18) is shown in Figs. 2.13 and 2.14. Simulation results show that, the equation (2.17) produces much better results as compared to the conventional equation (2.8). Comparing equation (2.17) and with equation (2.18), the Figs. 2.13 and 2.14 show that the equation (2.17) produces much better results as compared to the equation (2.18). The difference between results obtained using equations (2.17) and (2.18) is significantly large for stripline with large strip width. For example, in a four electrodes stripline having strip width 60^0 and $\frac{R_0}{R_{in}}$=1.2, the characteristic impedance obtained using equation (2.17) and equation (2.18) is 49.13 Ω and 42.4 Ω respectively.

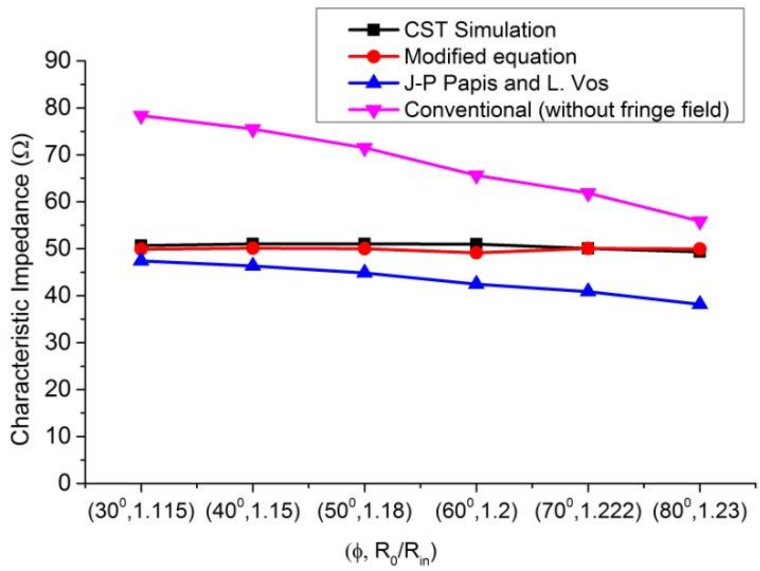

Fig. 2.13 Comparison of characteristic impedance for four electrodes stripline.

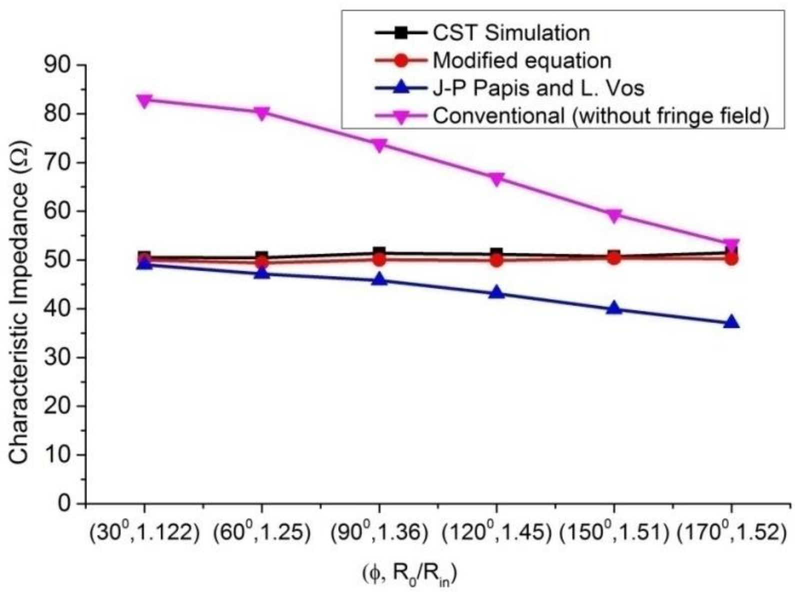

Fig. 2.14 Comparison of characteristic impedance for two electrodes stripline.

2.5 Summary

The fringe field primarily affects the effective width of the strip. The properties like characteristic impedance, wall current intercepted by strip and kicker constant are function of effective width of the strip. The modified expressions produce results which are in close agreement with the simulation results as compared to old expressions conventionally used in the literature. The study and analysis of effect of fringe field on effective width of the strip and characteristic impedance of two and four electrodes striplines presented in this chapter is very useful for design and understanding of simulation results of striplines for future projects like up-gradation of beam diagnostics of Indus-2 accelerators and High Intensity Linear Accelerator for Indian Spallation Neutron Source.

CHAPTER-3

EFFECT OF INTER-ELECTRODE CROSS TALK ON POSITION SENSITIVITY OF CAPACITIVE BEAM POSITION MONITOR

Inter-electrode coupling (cross talk) has significant effect on position sensitivity of the beam position monitors (BPM). Due to inter-electrode capacitive coupling the current induced on one electrode can flow towards another electrode and vice-versa. The capacitive coupling increases with increasing frequency and output load for a given BPM. Thus, the position sensitivity becomes dependent on the signal frequency and load impedance due to cross talk [38-42].

The effect of inter-electrode cross talk on the position sensitivity of the capacitive BPM is studied. A generalized expression for normalized difference signal is derived for a two electrodes BPM and the effect of inter-electrode cross talk on position sensitivity of shoe box BPM is analyzed in detail. This chapter is divided into two parts. First part presents mathematical derivation of expression for normalized difference signal for two electrodes BPM and position sensitivity of the shoe box BPM. Second part describes simulation studies of shoe box BPM and comparison of position sensitivity obtained through simulation with analytical expression presented in this chapter.

3.1 Normalized difference signal in two electrodes BPM

Schematic of a general two electrodes BPM is shown in Fig. 3.1. It consists of two electrodes (called pickup electrodes) placed opposite to each other inside a vacuum chamber. The pickup electrodes are terminated with output loads R_L and R_R towards left and right side of the electrode as shown in Fig. 3.1. A beam of charge particles, passing through the BPM, generates voltage signals across the output loads. The difference in voltage signals induced on the pickup electrodes is proportional to the offset of the beam from the BPM axis. The difference voltage signal is used to calculate position of the beam. Generally, to make difference voltage signal independent of the beam current, it is normalized with respect to the sum of the voltage signals.

If the voltage signals generated at left and right hand side electrodes are V_L and V_R respectively then, normalized difference signal is defined as

$$\frac{\Delta V}{\Sigma V} = \frac{|V_R| - |V_L|}{|V_R| + |V_L|} \tag{3.1}$$

Here $\Delta V=|V_R|-V_L|$ is difference or delta signal and $\Sigma V=|V_R|+|V_L|$ is sum signal.

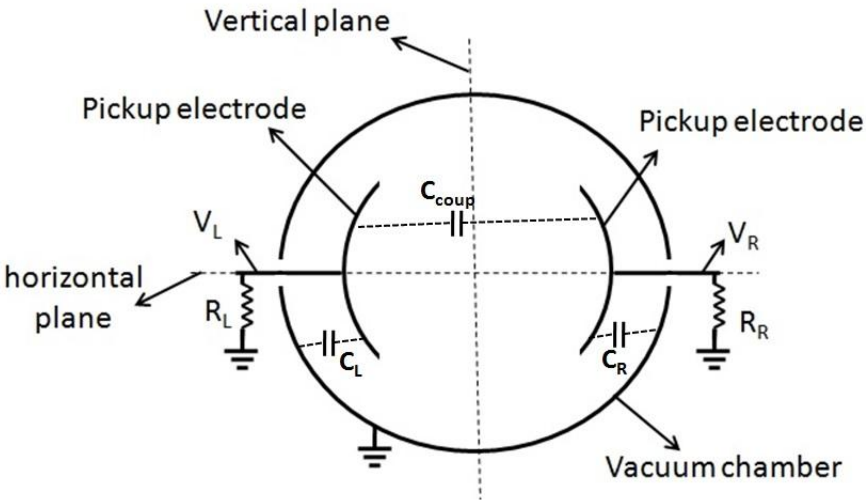

Fig. 3.1 Schematic of two electrodes BPM.

3.2 Inter-electrode cross talk

The equivalent circuit of two electrodes capacitive BPM is shown in Fig. 3.2. In this, C_R and C_L are capacitances between pickup electrodes and vacuum chamber for the right and left electrodes, C_{coup} is inter-electrode capacitance (capacitance between right and left hand side electrodes), R_L and R_R are output loads, and i_L and i_R are current induced on left and right hand side electrodes respectively [29].

Due to inter-electrode coupling between left and right hand side electrodes, the current induced on left electrode can flow towards right electrode and vice versa. As a result, the signal induced on pickup electrode is not purely governed by the current induced on that electrode alone; rather, it is also governed by the inter-electrode coupling current through C_{coup}.

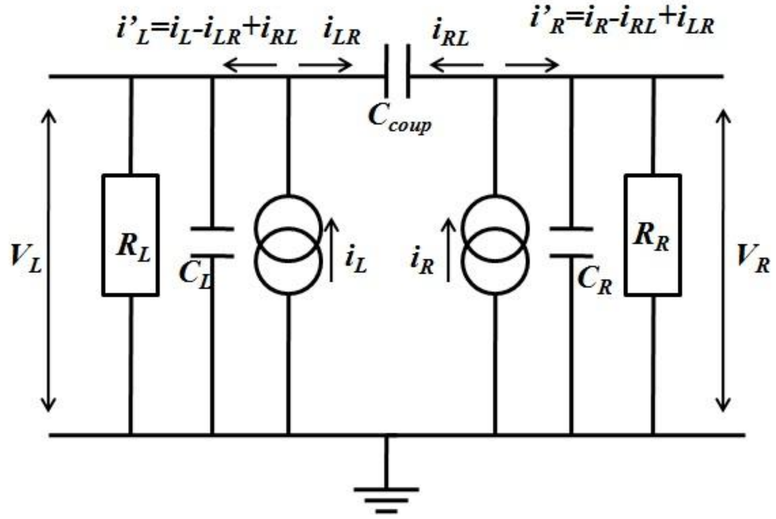

Fig. 3.2 Equivalent circuit of two electrodes BPM.

3.2.1 Normalized difference signal

In the presence of inter-electrode coupling, the current (i_L) induced on left electrode will divide into two paths; i) fraction of current will pass through parallel combination of R_L and C_L and ii) remaining fraction of current will flow towards right electrode through inter-electrode coupling. Similarly, The current (i_R) induced on right electrode will also divide into two paths; i) fraction of current will pass through parallel combination of R_R and C_R and ii) remaining fraction of current will flow towards left electrode.

Let i_{RL} represents fraction of current induced on right electrode that flows towards left electrode and i_{LR} is fraction of current induced on left electrode that flows towards right electrode through inter-electrode coupling. Using superposition principle, i'_L and i'_R can be written as

$$i'_L = i_L - i_{LR} + i_{RL} \tag{3.2}$$

$$i'_R = i_R - i_{RL} + i_{LR} \tag{3.3}$$

For identical electrodes the normalized difference signal is derived and the derivation is presented in Appendix-C. The normalized difference signal is given by

$$\frac{\Delta V}{\Sigma V} = \frac{(i_R + i_L)(i_R - i_L)[1 - 2\alpha]}{[|i'_R| + |i'_L|]^2} \tag{3.4}$$

Here α is given by (see Appendix-C for further detail**)**

$$\alpha = \frac{\omega^2 R^2 C_{coup}\left(2C_{coup} + C\right)}{1 + \omega^2 R^2 \left(2C_{coup} + C\right)^2} \tag{3.5}$$

In equation (3.5), $C=C_R=C_L$ and $R=R_R=R_L$ (for identical electrodes and loads). Equation (3.4) is a generalized equation of difference over sum signal of two electrodes capacitive BPM having inter-electrode cross talk. Mathematically, derivative of equation (3.4) with respect to beam position 'x' gives position sensitivity of the BPM.

3.3 Position sensitivity of shoe box BPM

3.3.1 Position sensitivity at BPM axis

In shoe box BPM, the current induced on pickup electrodes is given by R. E. Shafer [29].

$$i_R = \frac{1}{2}\left(1 + \frac{x}{b}\right)\frac{L}{v_b}\frac{dI_b(t)}{dt} \tag{3.6}$$

$$i_L = \frac{1}{2}\left(1 - \frac{x}{b}\right)\frac{L}{v_b}\frac{dI_b(t)}{dt} \tag{3.7}$$

Here (see Fig. 1.7) $2b$ is aperture of the shoe box BPM, x is beam offset towards right hand side electrode, L is length of the electrode, I_b is beam current and v_b is velocity of the beam.

For small offset of the beam from the BPM axis (x<<<b), we have $[|i'_R| + |i'_L|]^2 = [i_R + i_L]^2$. Using $[|i'_R| + |i'_L|]^2 = [i_R + i_L]^2$ in equation (3.4) we get

$$\frac{\Delta \mathrm{V}}{\Sigma \mathrm{V}} = \frac{(i_R - i_L)}{(i_R + i_L)}[1 - 2\alpha] \tag{3.8}$$

Equations (3.5)-(3.8) give

$$\frac{\Delta \mathrm{V}}{\Sigma \mathrm{V}} = \frac{x}{b}\left[1 - 2\frac{\omega^2 R^2 C_{coup}\left(2C_{coup} + C\right)}{1 + \omega^2 R^2 \left(2C_{coup} + C\right)^2}\right] \tag{3.9}$$

Position sensitivity '*S*' is defined as the rate of change of normalized difference signal with respect to change in beam offset (*x*). Differentiating equation (3.9) with respect to 'x' we get

$$S = \frac{1}{b}\left[1 - 2\frac{\omega^2 R^2 C_{coup}\left(2C_{coup} + C\right)}{1 + \omega^2 R^2 \left(2C_{coup} + C\right)^2}\right] \tag{3.10}$$

Equation (3.10) shows that the position sensitivity of shoe box BPM is not constant but it depends on ωR (signal frequency and output load). As an illustration, variation of the position sensitivity with ωR is shown in Fig. 3.3.

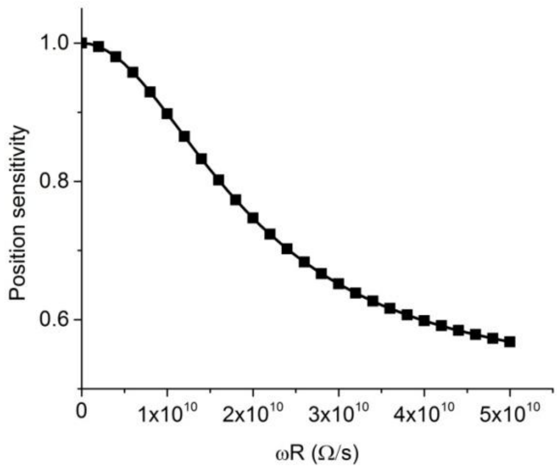

Fig. 3.3 Variation of position sensitivity with ωR (product of signal frequency and output load); for C_{coup}/C=0.5. The sensitivity is normalized with respect to b (half of the BPM aperture).

3.3.2 Position sensitivity at off axis

For deriving equation (3.10) we assumed that $[|i'_R| + |i'_L|]^2 = [i_R + i_L]^2$. Theoretically, this is true only at BPM axis and the value of $\frac{[i_R+i_L]^2}{[|i'_R|+|i'_L|]^2}$ depends on beam offset. For offset from the BPM axis, the accuracy of the equation (3.10) depends on offset and inter-electrode coupling. Let δ represents the fractional difference between $[|i'_R| + |i'_L|]^2$ and $[i_R + i_L]^2$ defined as

$$\delta = \frac{[|i'_R| + |i'_L|]^2 - [i_R + i_L]^2}{[i_R + i_L]^2} \tag{3.11}$$

For identical electrodes, using equations (3.2), (3.3), (3.6), (3.7), and equations (C.5), (C.6) of Appendix-C in equation (3.11) we get

$$\delta = \left(\left|\frac{1}{2}\left(1 + \frac{x}{b}\right) - f\,\frac{x}{b}\right| + \left|\frac{1}{2}\left(1 - \frac{x}{b}\right) + f\,\frac{x}{b}\right|\right)^2 - 1 \tag{3.12}$$

Here *f* is inter-electrode coupling factor (see equation (C.14) for details given in Appendix-C).

The variation of δ with ωR for different beam offset (x/b) at constant C_{coup}/C is shown in Fig 3.4. Whereas, the variation of δ with ωR for different C_{coup}/C at constant beam offset (x/b) is shown in Fig. 3.5. The maximum value of δ (peak of the curves in Fig. 3.4 and Fig. 3.5) increases with increasing x/b and C_{coup}/C. The variation of maximum value of δ with C_{coup}/C (shown in Fig. 3.6) indicates that, for C_{coup}/C=0.5 and $x/b=0.5$ the maximum value of δ is less than 2% and for C_{coup}/C=1 and $x/b=0.5$ it is ~ 3%. Therefore, for most of the practical cases, we have $[|i'_R| + |i'_L|]^2 \approx [i_R + i_L]^2$ giving equation (3.10) for position sensitivity.

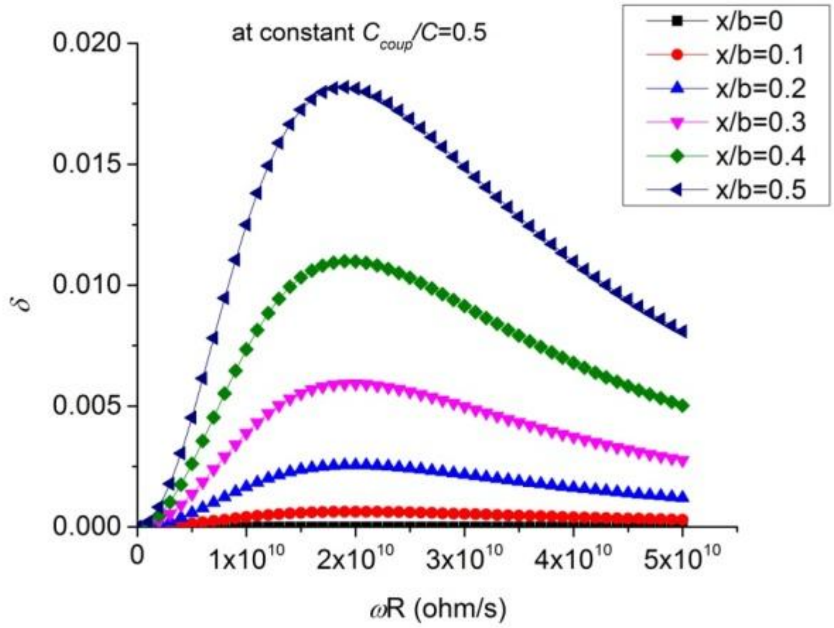

Fig. 3.4 Variation of δ with ωR for different beam offset '*x/b*' at constant C_{coup}/C=0.5.

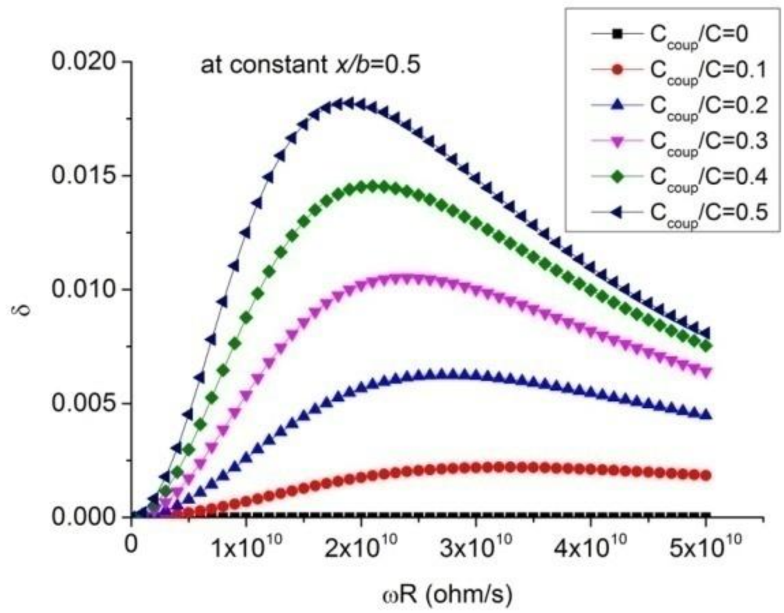

Fig. 3.5 Variation of δ with ωR for different values of C_{coup}/C at constant beam offset

x/b=0.5.

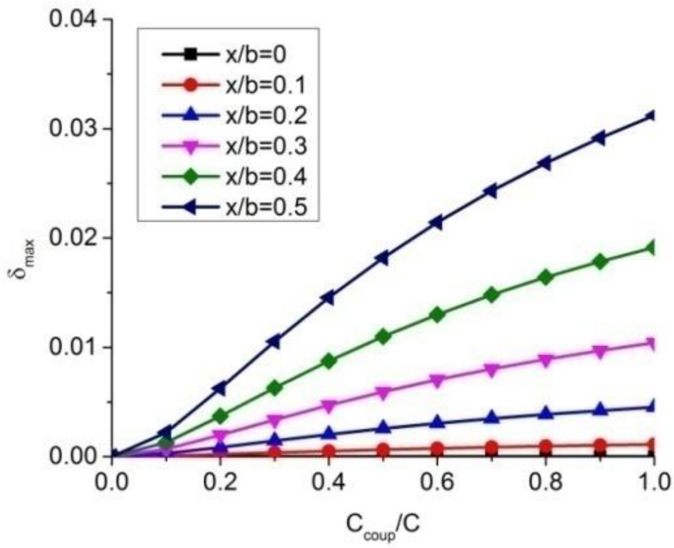

Fig. 3.6 Variation of maximum value of δ (δ_{max}) with C_{coup}/C at different beam offset *(x/b)*.

3.4 Simulation of shoe-box BPM

The effect of cross talk on position sensitivity of a general shoe box BPM is also studied through simulations performed using CST Studio Suite [75]. A general shoe box BPM shown in Fig. 3.7 is simulated. The position sensitivity obtained through simulation is compared with equation (3.10). The parameters of shoe-box BPM (considered as test BPM) are given in table 3.1.

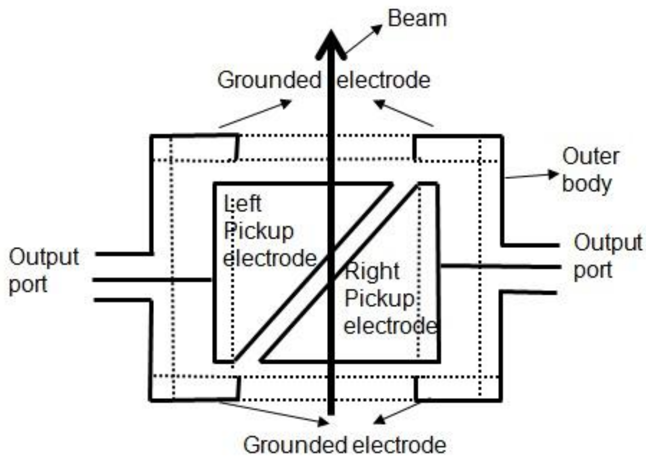

Fig. 3.7 Layout of shoe-box BPM considered for simulation of position sensitivity.

Table 3.1. Geometrical parameters of shoe-box BPM.		
Sr. No.	Geometrical parameter	Value
1	Length of pick up electrodes	100 mm
2	Thickness of pickup electrode	3 mm
3	Horizontal separation between pick up electrodes	6 mm
4	Horizontal aperture of pickup electrodes	106 mm
5	Vertical aperture of pickup electrodes	50 mm
6	Horizontal aperture of outer body	132 mm
7	Vertical aperture of outer body	76 mm
8	Distance between pickup electrodes and ground electrode	3 mm
9	Thickness of ground electrodes	2 mm

3.4.1 Simulation of normalized difference signal

Test BPM with geometrical parameters given in table 3.1 is modeled in CST Particle Studio as shown in Fig. 3.8. All the components of BPM like pick-up electrodes, outer body, grounded electrodes etc. are defined as perfect conductors. A particle beam having Gaussian temporal distribution of r.m.s. bunch length of 225 mm (gives frequency range over 300 MHz) is defined to travel along the BPM axis. The wakefield solver simulates interaction of beam with pickup electrodes and gives electrode voltage. Generally, the electronics used in beam position monitors have input impedance of 50 Ω or in the range of 100 kΩ or higher (using buffers). Thus simulations are performed for both 50 Ω and 100 kΩ output loads.

The normalized difference signal $\left(\frac{\Delta V(\omega,x)}{\Sigma \mathrm{V}(\omega,x)}\right)$ obtained through simulations is defined as

$$\frac{\Delta V(\omega,x)}{\Sigma \mathrm{V}(\omega,x)}=\frac{|V_R(\omega,x)|-|V_L(\omega,x)|}{|V_R(\omega,x)|+|V_L(\omega,x)|} \tag{3.13}$$

Here $|V_R(\omega,x)|$ and $|V_L(\omega,x)|$ are voltage amplitudes generated at right and left hand side pickup electrodes respectively at frequency 'ω' for beam offset 'x'. The simulations are performed for different beam offsets. The normalized difference signals calculated using equation (3.13), for beam offset $x = \pm 2$ mm, are shown in Figs. 3.9 and 3.10.

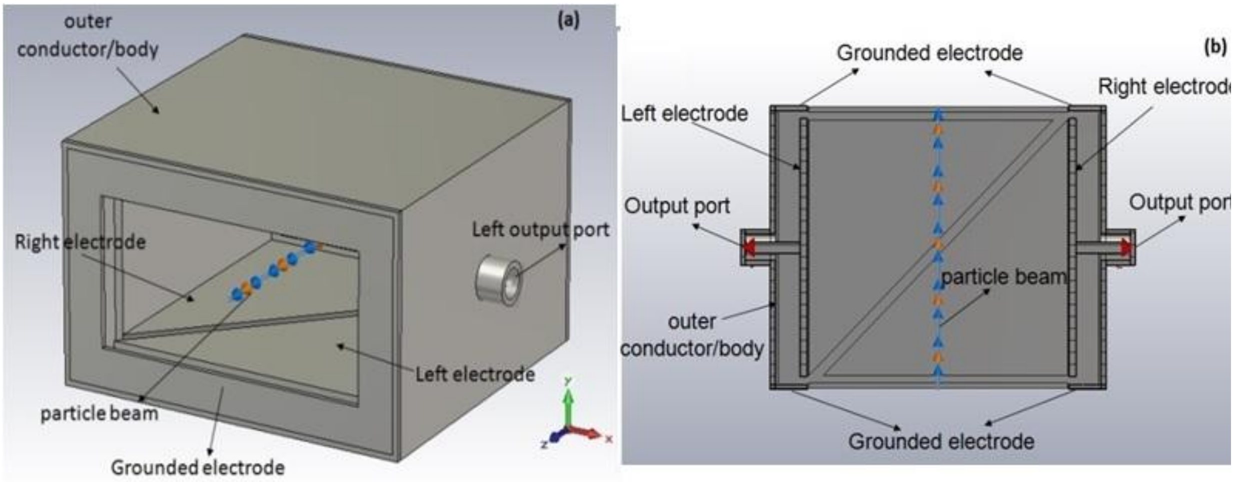

Fig. 3.8 CST model of test BPM for validation of analytical expression of position sensitivity with simulation results. (a) perspective view (b) top view with x-z cut plane.

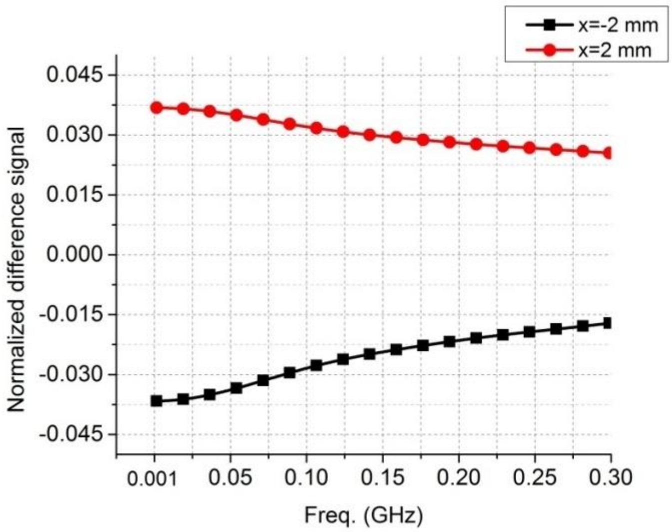

Fig. 3.9 Normalized difference signal obtained through simulation of test BPM with 50 Ω output load.

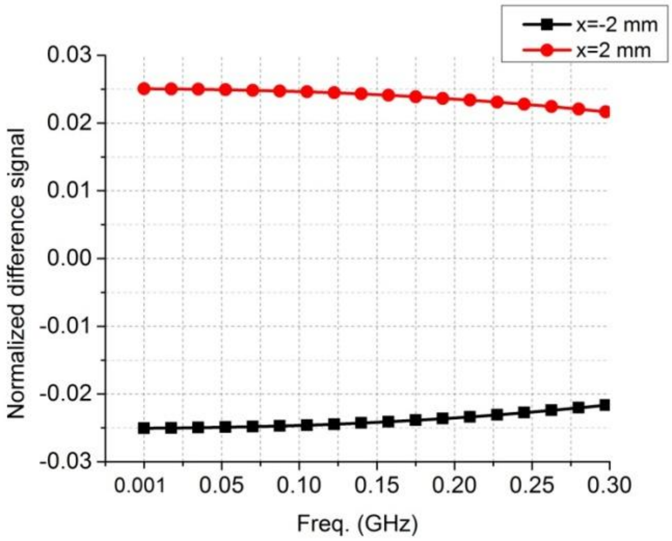

Fig. 3.10 Normalized difference signal obtained through simulation of test BPM with 100 kΩ output load.

3.4.2 C_{coup} and C through simulation

To calculate position sensitivity using equation (3.10), C_{coup} and C are calculated using E-static solver of CST EM Studio. CST model similar to that shown in Fig. 3.8 (except particle beam and port impedances) is simulated to obtain values of required capacitance. The values of C_{coup} and C obtained through simulations are 5.1 pF and 24.9 pF respectively.

3.5 Simulation versus analytical results

From the simulation of difference over sum signal (Figs. 3.9 and 3.10), the position sensitivity '*S*' of the BPM is calculated using following equation.

$$S(\omega) = \frac{1}{(x_1 - x_2)}\left[\frac{\Delta(\omega, x_1)}{\Sigma(\omega, x_1)} - \frac{\Delta(\omega, x_2)}{\Sigma(\omega, x_2)}\right] \qquad (3.14)$$

Here x_1 and x_2 are transverse offsets (±2 mm) of the beam. The position sensitivity obtained through simulation is shown in Figs. 3.11 and 3.12 along with the position sensitivity calculated using C_{coup} and C in equation (3.10).

Figs. 3.11 and 3.12 show that the results obtained using equation (3.10) matches closely with the results obtained through simulations at lower frequencies. Nevertheless, as the frequency increases (above 150 MHz), the simulation results deviate from the theoretical predictions. The possible reason for the difference in the simulation and the theoretical results could be because of the fact that the assumption of lumped elements (capacitances) considered for equivalent circuit of shoe-box BPM fails altogether at higher frequencies. Another reason of the deviation could be the resonance occurring in the BPM. Figs. 3.13 and 3.14 show that there is resonance in the test BPM at ~ 1 GHz having its tail towards lower frequencies. Due to resonance, the BPM deviates from the quasi-electrostatic models given by R. E. Shafer [29] which is the fundamental base of equivalent circuit (Fig. 3.2) and all associated equations.

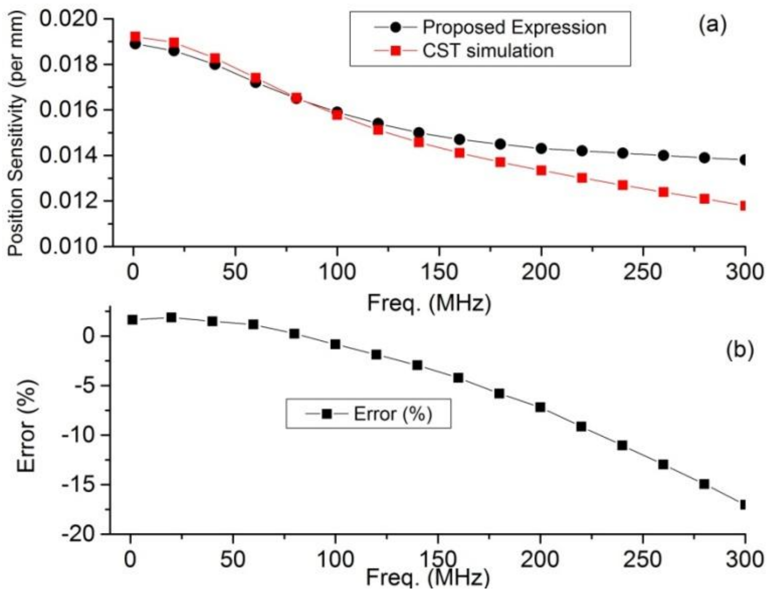

Fig. 3.11 Variation of position sensitivity with frequency of shoe-box BPM for 50 Ω output load with proposed new expression (filled circles) and CST simulations with filled rectangles) (a). Difference between them is shown as (%) error with filled rectangles (b).

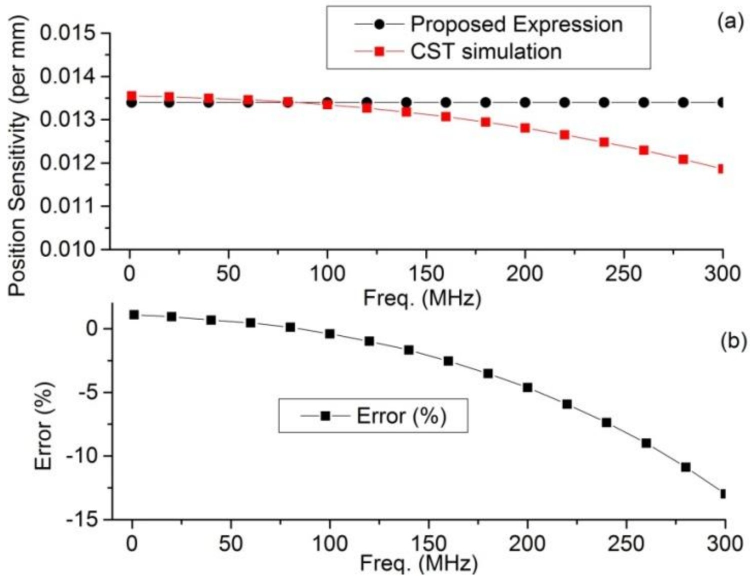

Fig. 3.12 Variation of position sensitivity with frequency of shoe-box BPM for 100 kΩ output load with proposed new expression with filled circles and CST simulations with filled rectangles (a). Difference between them is shown as (%) error with filled rectangles (b).

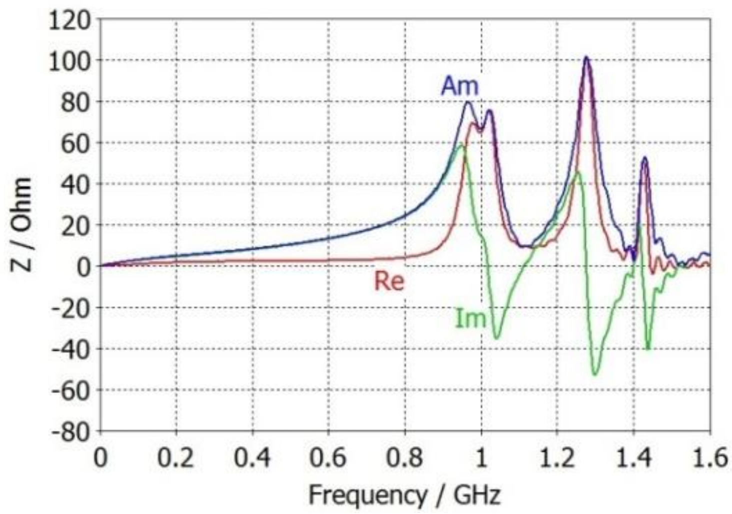

Fig. 3.13 Beam coupling impedance of BPM showing resonance in the structure for 50 Ω output load.

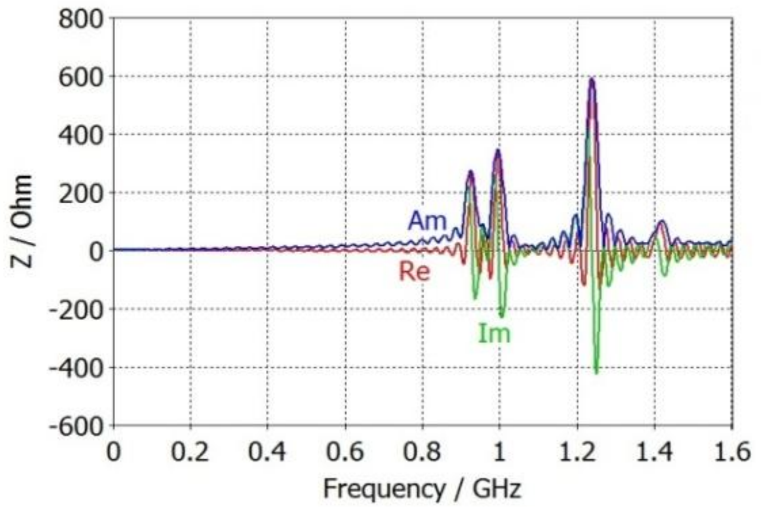

Fig. 3.14 Beam coupling impedance of BPM showing resonance in the structure for 100 k Ω output load.

3.6 Summary and discussion

The analytical expression presented in this chapter quantitatively explains the effect of inter-electrode capacitive coupling (cross talk) on position sensitivity of two electrodes BPM. It shows that the position sensitivity of the BPM depends on the inter-electrode capacitance and capacitance between pick-up electrode and vacuum chamber. The values of the capacitances depend on the geometry and dimensions of pick-up electrodes and vacuum chamber. Therefore, the analytical expression presented in this chapter provides an analytical tool to calculate position sensitivity as a function of inter-electrode capacitance and capacitance between electrode and vacuum chamber for a given frequency and output load. For upcoming projects like up-gradation of beam diagnostics in Indus accelerators and High Intensity Linear Accelerator for Indian Spallation Source, different types of beam position monitors are required. Therefore, the study presented in this chapter would be helpful in designing of new BPMs like (shoe-box, split electrodes, striplines etc.) by optimizing the geometry and size of different parts (electrodes etc.) of BPM to achieve required position sensitivity at desired frequency or frequency range.

The analysis (mathematical and simulation) presented in chapter mainly focuses on shoe-box BPM, but the theory and mathematical expressions derived in this chapter can be applied to any two electrodes BPM having capacitive inter-electrode coupling (cross talk). Equation (3.10) shows that the position sensitivity of shoe-box BPM is product of position sensitivity of the BPM without inter-electrode cross talk ($\frac{1}{b}$) and factor arising due to inter-electrode coupling $\left(1-2\frac{\omega^2 R^2 C_{coup}\,(2C_{coup}+C)}{1+\omega^2R^2\left(2C_{coup}+C\right)^2}\right)$. This fact is applicable on any two electrodes capacitive BPM having capacitive coupling (provided $|i'_R| + |i'_L| \approx [i_R + i_L]$). For example, for curved electrodes BPM (similar to the case shown in Fig. 3.1), $\frac{I_R - I_L}{I_R + I_L}$ is given by [29]

$$\frac{I_R - I_L}{I_R + I_L} = \frac{4sin\left(\phi/_2\right)}{\phi}\frac{x}{b} + \ higher\ order\ terms\ of\ x \tag{3.15}$$

Here b is radius of the pickup electrode and ϕ is its azimuthal width. Using equation (3.15) in equation (3.8) and neglecting higher order terms we get

$$\frac{\Delta V}{\Sigma V} = \frac{4sin\left(\phi/_2\right)}{\phi}\frac{x}{b}[1-2\alpha] \tag{3.16}$$

$$\Rightarrow \frac{\Delta V}{\Sigma V} = \frac{4sin\left(\phi/_2\right)}{\phi}\frac{x}{b}\left[1-2\frac{\omega^2 R^2 C_{coup}\left(2C_{coup}+C\right)}{1+\omega^2R^2\left(2C_{coup}+C\right)^2}\right] \tag{3.17}$$

$$\Longrightarrow S = \frac{1}{b}\frac{4sin\left({}^{\phi}\!/_{2}\right)}{\phi}\left[1 - 2\frac{\omega^2 R^2 C_{coup}\left(2C_{coup} + C\right)}{1 + \omega^2 R^2\left(2C_{coup} + C\right)^2}\right] \qquad (3.18)$$

Also, to incorporate fringe field between pickup electrodes and vacuum chamber, the azimuthal width of electrode should be replaced by effective width of the electrodes as explained in Chapter 2.

CHAPTER-4

NEW BUTTON ELECTRODE BEAM POSITION MONITORS FOR INDUS-2

Upgraded beam position indicator (UPBPI) and Insertion device beam position indicator (IDBPI) are two different types of button electrode beam position monitors (BPMs) which are designed for up-gradation of beam position monitors in Indus-2. UPBPI and IDBPI have improved performance like higher transfer impedance, similar response in both of the transverse planes, resonance free structure over wider frequency range and fast decaying wakefield as compared to the old BPMs of Indus-2. The transfer impedance and time domain signals of UPBPI and IDBPI are measured with real beam during Indus-2 operation to compare their performance with designed values and performance of old BPMs. This chapter presents design, simulations and measurements carried out for abovementioned new BPMs (UPBPI and IDBPI).

4.1 Various beam position monitors in Indus-2

Indus-2 is a 2.5 GeV electron storage ring being used as national synchrotron light source facility [11-16]. The button electrode beam position monitors are main diagnostic devices in the Indus-2 storage ring. There are different types of button electrode BPMs deployed in Indus-2. In Indus-2 context, button electrode BPM is also known as beam position indicator (BPI). Broadly, the button electrode BPMs in Indus-2 are classified as individual BPMs, integrated BPMs and insertion device (ID) BPMs [76]. The integrated BPMs are integrated with dipole chambers of Indus-2, whereas individual BPMs are separate BPMs distributed in straight sections of Indus-2. The individual and integrated BPMs have cross-section similar to the cross-section of vacuum chamber of Indus-2. Layout of integrated and individual BPMs per unit cell of Indus-2 is shown in Fig. 4.1.

Commissioning of insertion devices (undulators) required additional BPMs having cross sections similar to the vacuum chamber of insertion devices. These BPMs are called Insertion Device Beam Position Indicator (IDBPI) to differentiate them from integrated and individual BPMs in Indus-2. The IDBPIs are installed at entry and exit of the insertion devices (undulators).

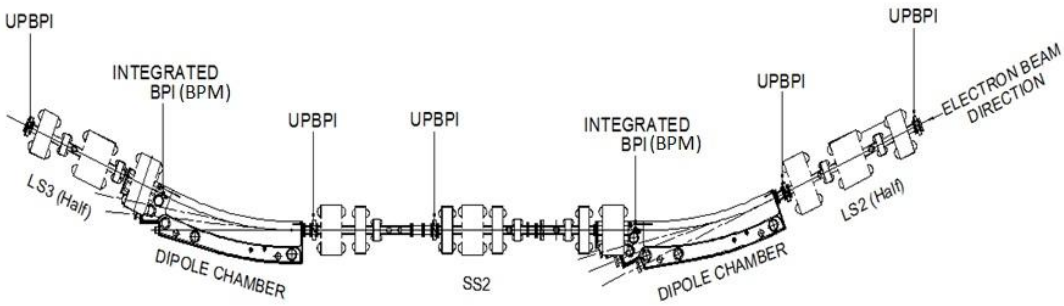

Fig. 4.1 Layout of individual type BPMs (UPBPI or old BPM) in unit cell of Indus-2.

4.2 Up-graded beam position indicator (UPBPI)

Earlier BPMs (old individual type BPMs) of Indus-2 were designed and installed more than 13 years ago at the time of commissioning of Indus-2 [77]. Since then, Indus-2 has undergone many upgrades and advancements [44-48].These upgrades generated the requirement of BPMs having higher transfer impedance, similar response (equal position sensitivity) in both transverse planes, resonance free structure over wide frequency range and fast decaying wake-field as compared to the old BPMs. Therefore, an improved version of individual type button electrode BPM is designed to replace the erstwhile (old) BPMs. The improved version of individual type button electrode BPM is called upgraded beam position indicator (UPBPI) in the context of Indus-2.

4.2.1 UPBPI design

Pickup electrode assemblies of UPBPI and old BPMs are shown in Fig. 4.2. In old BPMs, the transition from button electrodes to electrical feedthrough has large variation in geometry of inner and outer conductors. Therefore, the structure has multiple reflections and resonances resulting into loss of signal (low transfer impedance) and poor signal quality (resonances). The pickup electrode assembly of UPBPI is designed to overcome this limitation of old BPMs. It consists of a button electrode, tapered central conductor, dielectric insulator and commercially available SMA electrical feedthrough. The radius of button is 5.9 mm and the annular gap between button electrode and housing is 1 mm. The characteristic impedance of the coaxial structure formed by button and housing is ~ 9.2 Ω. The transition from button (~9.2 Ω) electrode to electrical feedthrough (50 Ω) is achieved through a tapered central conductor and a dielectric (macor) ring. The dielectric ring provides rigidity to the central conductor. It also eliminates the requirement of sudden reduction in size of the outer diameter of electrode assembly to match with outer conductor of electrical feedthrough. This type of electrode assembly reduces the beam coupling impedance and resonances.

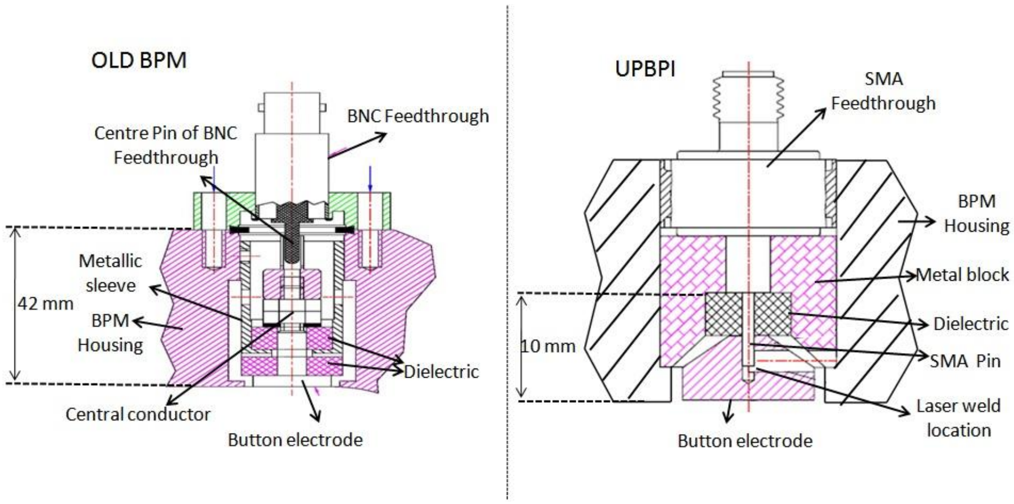

Fig. 4.2. Pickup electrode assemblies of old BPM and UPBPI.

Complete UPBPI consists of four identical pickup electrode assemblies and BPM body called housing. The schematic of electrodes configuration is shown in Fig. 4.3.The housing of UPBPI has racetrack geometry with 36 mm by 86 mm vertical and horizontal aperture respectively. Two pickup electrodes are located at the top and other two electrodes are located at the bottom of the horizontal plane. The strength of signal induced on a particular electrode increases with decrease in the distance of the beam from the that electrode. Let $V_{1,2,3,4}$ are voltage signals at different electrodes as shown in Fig. 4.3. Close to the BPM axis (linear region), the normalized difference signals (defined by equations (4.3) and (4.4)) are proportional to the beam shift from the BPM axis. The proportionality constant is called position sensitivity (equations (4.5) and (4.6)). The beam position is obtained from the normalized difference signals using position sensitivity factors.

Position sensitivity of the BPM depends on horizontal and vertical separation between the button electrodes. The vertical separation between the button electrodes is fixed by the vertical aperture of the vacuum chamber (BPM housing). In old BPMs, the horizontal separation between button electrodes is 32 mm which gives higher position sensitivity in horizontal plane as compared to the vertical plane. To enhance position sensitivity in vertical plane and achieve similar response in both of the transverse planes, the horizontal separation between button electrodes is optimized for UPBPI. The position sensitivity (S_x/S_y) is defined as

$$S_x = \frac{\partial\left(\frac{\Delta V}{\Sigma \mathrm{V}}\right)_x}{\partial(x_b)} \tag{4.1}$$

For horizontal plane.

And for vertical plane

$$S_y = \frac{\partial\left(\frac{\Delta V}{\Sigma \mathrm{V}}\right)_y}{\partial(y_b)} \tag{4.2}$$

Here $\left(\frac{\Delta V}{\Sigma V}\right)_x$ and $\left(\frac{\Delta V}{\Sigma V}\right)_y$ are difference signals normalized with respect to sum signals and x_b , y_b are beam co-ordinates (position) in horizontal and vertical planes respectively. In four electrodes BPM, shown in Fig. 4.3, the normalized difference signals are defined as

$$\left(\frac{\Delta V}{\Sigma V}\right)_x = \frac{[(V_1 + V_2) - (V_3 + V_4)]}{[V_1 + V_2 + V_3 + V_4]} \tag{4.3}$$

and

$$\left(\frac{\Delta V}{\Sigma V}\right)_y = \frac{[(V_1 + V_4) - (V_2 + V_3)]}{[V_1 + V_2 + V_3 + V_4]} \tag{4.4}$$

For identical electrodes and small displacement of beam from BPM axis, the position sensitivity at BPM axis can be represented as

$$S_x = \frac{1}{x_b}\frac{[(V_1 + V_2) - (V_3 + V_4)]}{[V_1 + V_2 + V_3 + V_4]} \tag{4.5}$$

and

$$S_y = \frac{1}{y_b}\frac{[(V_1 + V_4) - (V_2 + V_3)]}{[V_1 + V_2 + V_3 + V_4]} \tag{4.6}$$

For a given beam current, the voltage at a particular pickup electrode is proportional to the charge induced at that electrode. The charge induced at the button electrodes is calculated using boundary element method **[**78**]** for different locations (horizontal separations) of button electrodes. The variation of horizontal and vertical sensitivities as a function of horizontal separation between the electrodes is shown in Fig. 4.4. The sensitivity of the UPBPI is same in horizontal and vertical planes for horizontal separation of ~22 mm. Thus horizontal separation (centre to centre) of 22 mm is chosen between the button electrodes placed in same horizontal plane.

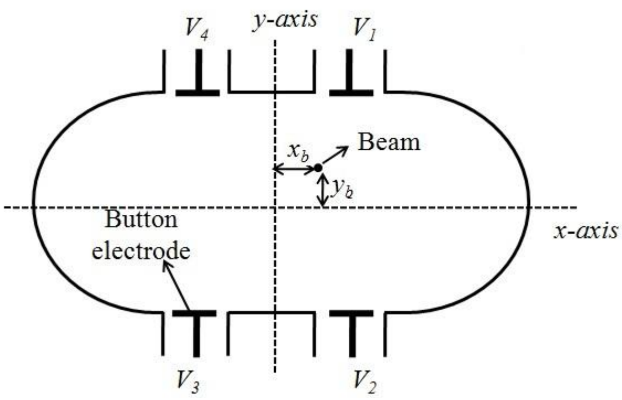

Fig. 4.3 Schematic electrodes configuration of UPBPI.

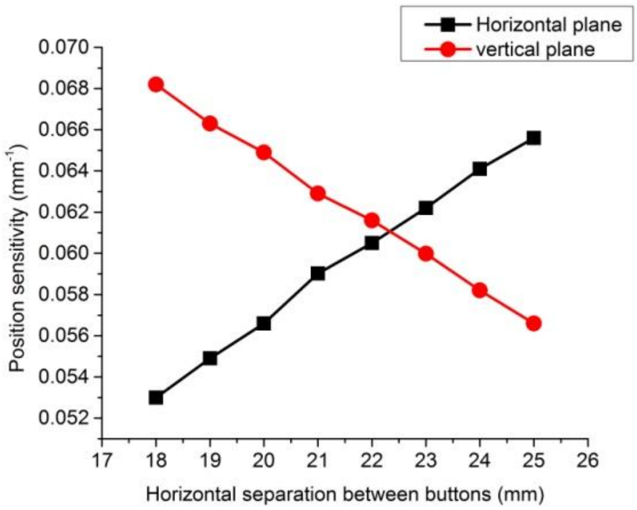

Fig. 4.4 Horizontal and vertical sensitivity of UPBPI

as a function of button separation.

4.2.2 UPBPI simulation

Most widely used model for the analysis of button electrode BPM is quasi-electrostatic model [29]. According to the quasi-electrostatic model, the frequency domain pickup signal ($V_0(\omega)$) of button electrode BPM is given by equation (4.7)

$$V_0(\omega) = \frac{k}{v_b}\left(\frac{j\omega R}{1 + j\omega CR}\right) I_b(\omega) \tag{4.7}$$

In equation (4.7), k is constant which depends on geometry of pickup electrode, I_b is beam current, v_b is beam velocity, C is capacitance between button electrode and BPM housing (vacuum chamber) and R terminating load. Factor 'k' and capacitance 'C' depend on shape, size and geometry of the button electrode and vacuum chamber.

Analytically, the pickup signal can be calculated using equation (4.7), but due to fringe field, the estimation of exact values of η and C is not possible in most of the practical situations. Moreover, the quasi-electrostatic model assumes C as lumped element and it does not incorporate inductance (in case of resonance) of electrode assembly. Therefore, for wide frequency range and resonance in the electrode assembly, the electromagnetic simulation is very important in BPM designing.

A 3-D model of UPBPI (Fig. 4.5) is created in CST Particle Studio. The electromagnetic simulation of the UPBPI is performed using wakefield solver of the CST Studio Suite [75]. The characteristics parameters like pickup signal, transfer impedance, beam coupling impedance, wakefield, loss factor and response obtained through simulation of the UPBPI are presented below.

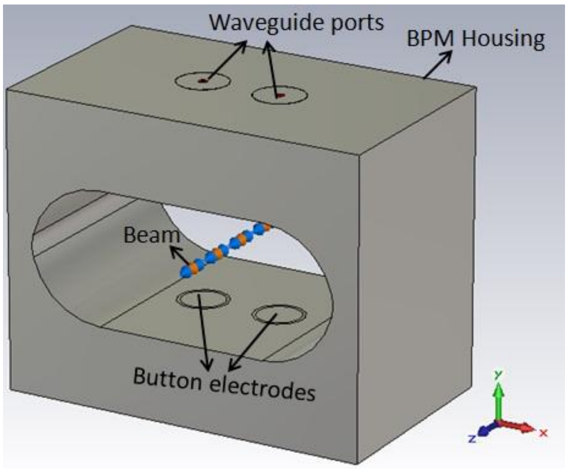

Fig. 4.5 3-D model of UPBPI created in CST Particle Studio for electromagnetic simulation.

4.2.2.1 Output signal and transfer impedance

Wakefield solver of CST Studio Suite simulates interaction of the particle beam with pickup electrodes and gives resultant pickup signals. Fig. 4.6 shows temporal signal of UPBPI obtained through wakefield solver. The output signal of the BPM is approximately differentiation of Gaussian beam (beam used for simulation) and there is no ringing in the output signal. This indicates that there is no reflection in the pickup electrode assembly. The difference in positive (upper) and negative (lower) amplitudes of the signal is due to finite capacitance between button electrode and the vacuum chamber.

Transfer impedance of BPM is the quantity which relates its output signal to the beam current. The Fourier transform of time domain voltage signal and beam current is calculated to eventually calculate the transfer impedance of the BPM. The frequency domain BPM voltage and corresponding beam current are shown in Figs. 4.7 and 4.8 respectively. The transfer impedance is calculated from the ratio of BPM voltage and beam current which is shown in Fig. 4.9. At lower frequencies, the transfer impedance of improved BPM increases linearly with frequency and becomes constant at higher frequencies as expected. At 505.8 MHz *(rf* frequency of Indus-2), the transfer impedance of the BPM is ~0.56Ω.

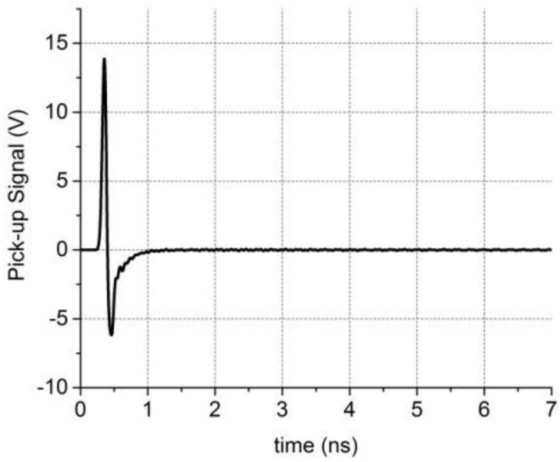

Fig. 4.6 UPBPI signal (V) as a function of time (ns).

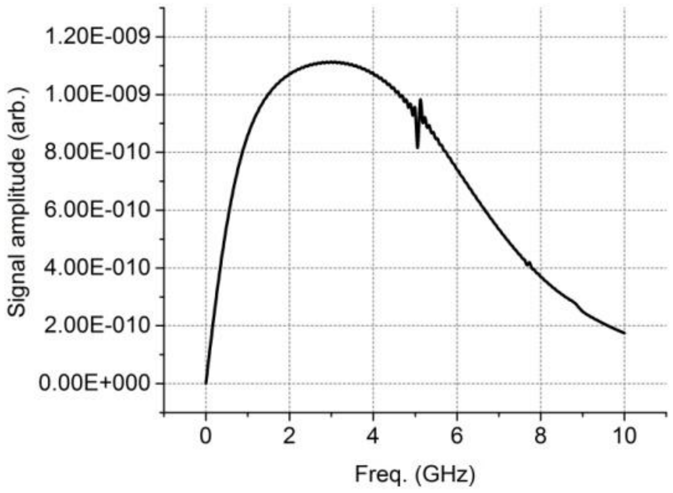

Fig. 4.7 UPBPI output: Amplitude (arbitrary) as a function of frequency (GHz).

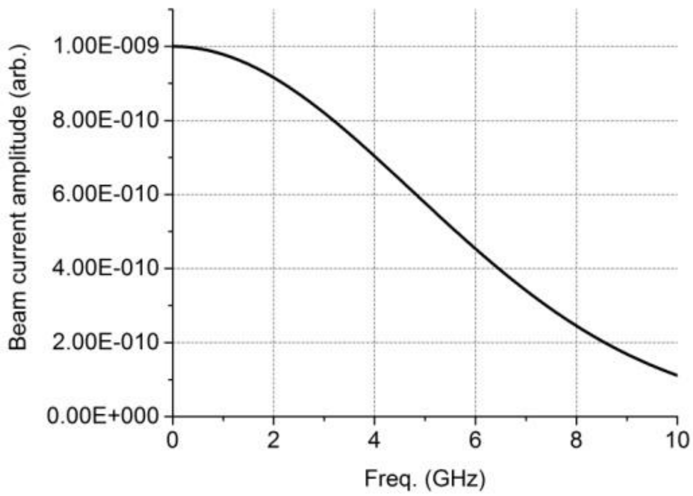

Fig. 4.8 Spectrum of the bunch used for simulation of the UPBPI.

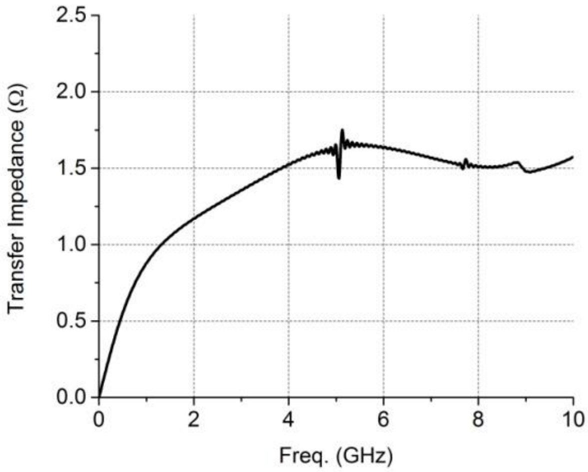

Fig. 4.9 Transfer impedance (Ω) of UPBPI as a function of freq. (GHz).

4.2.2.2 Wakefield and beam coupling impedance

When a charge particle or a beam passes through a discontinuity of vacuum chamber it generates electromagnetic field in the chamber. The field generated by the particle can stay in the structure even after the particle (beam) has passed through it. These fields are known as wakefield. Generally wakefield is represented as an integrated force (wake potential) due to field on a test particle of unit charge passing through the structure at a fix distance (s) behind the source particle (beam). Longitudinal wake potential (wakefield) of UPBPI is shown in Fig. 4.10.

Frequency domain counterpart of wake potential is called beam coupling or wake impedance [**65**]. The longitudinal wake impedance of UPBPI is very smooth except one peak at ~8.7 GHz (Fig. 4.11). The resonant peak shown in Fig. 4.11 is generated due to the trapped electromagnetic field (TE_{11} mode) in the coaxial structure formed by button electrode and UPBPI housing. The frequency of this resonant mode can be estimated by equation **(**4.8**)** [30,31,**79**].

$$f_{11} = \frac{c}{2\pi}\frac{1}{\left[r_b + \frac{g}{2}\right]} \tag{4.8}$$

In equation (4.8), c is velocity of the light, r_b is radius of button electrode and g is annular gap between button and BPM housing. For button radius 5.9 mm and annular gap 1 mm, the frequency of trapped mode comes out to be ~ 7.5 GHz. This frequency is smaller than 8.7 GHz obtained through simulation. This difference can be attributed to the presence of tapered structure immediately after button electrode which reduces the effective radius of the button electrode.

A bunch of charge particle loses some of its energy when it interacts with wakefield generated by itself. The energy lost by the bunch is proportional to the square of its charge. The proportionality constant is known as loss factor [**65**]. For a given BPM, the loss factor depends on longitudinal distribution and length of bunch. For a Gaussian bunch of r.m.s. length 10 mm, the loss factor of UPBPI, calculated through wakefield solver, is 2.1e-3 V/pC. Taking bunch repetition rate 505.81 MHz and average beam current 300mA, the power loss is ~0.36W. This indicates that the power dissipation by beam in UPBPI is not a serious issue.

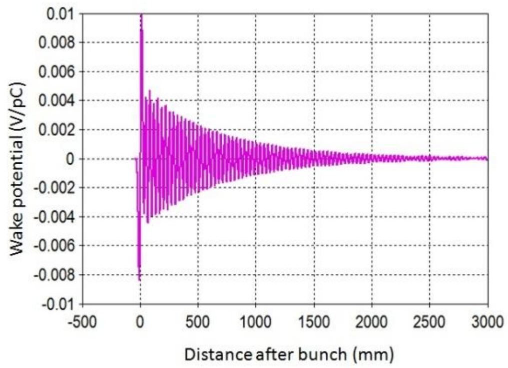

Fig. 4.10 Wake potential of UPBPI (for bunch length 10 mm) as function of distance after the bunch.

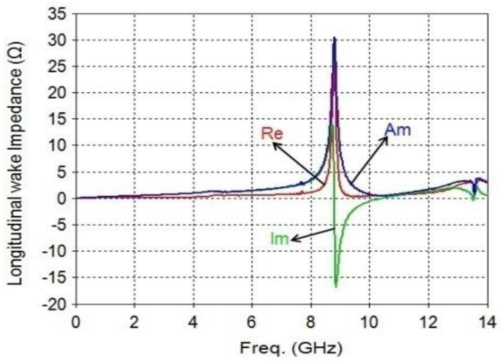

Fig. 4.11 Longitudinal coupling impedance of UPBPI (calculated using bunch length 10 mm).

4.2.2.3 Response and position sensitivity

The response of the BPM is defined as the variation of the normalized difference signal (equations (4.3) and (4.4)) with beam position. For UPBPI, normalized difference signal is calculated using wakefield solver of CST Particle Studio.

The plots between normalized difference signal and frequency for different beam offsets are shown in Figs. 4.12 and 4.13. It is clear from Figs. 4.12 and 4.13 that the normalized difference signal is almost independent of frequency indicating that there is no inter-electrode coupling between different pickup electrodes of UPBPI. The response of UPBPI at 505.8 MHz is shown in Fig. 4.14.The slope of the response curve gives position sensitivity of the BPM. From Fig. 4.14 the position sensitivity (near BPM axis)of UPBPI comes out to be ~0.060 mm^{-1}in both of the transverse planes. This value is quite close to the value obtained through numerical method (boundary element technique).

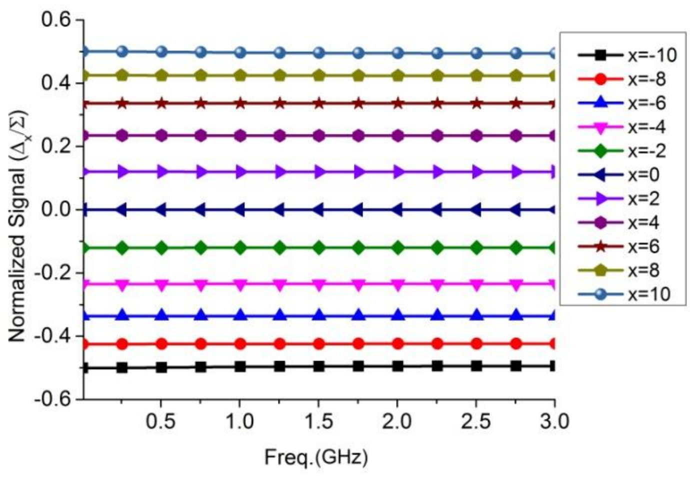

Fig. 4.12 Variation of normalized difference signal with frequency for different beam positions along x-axis frequency (UPBPI).

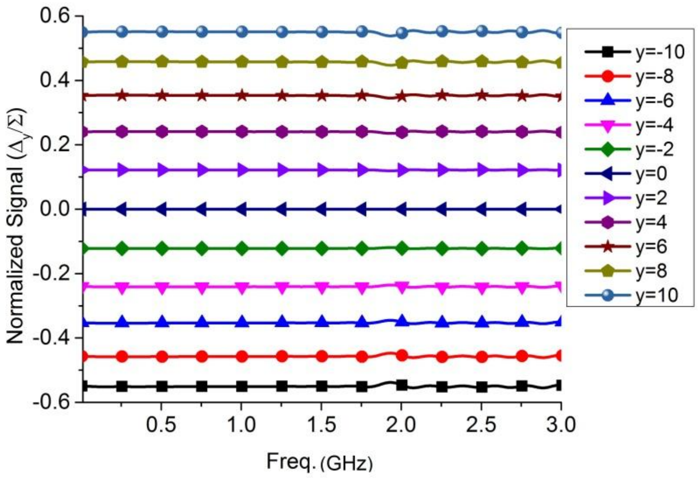

Fig. 4.13 Variation of normalized difference signal with frequency for different beam positions along y-axis frequency (UPBPI).

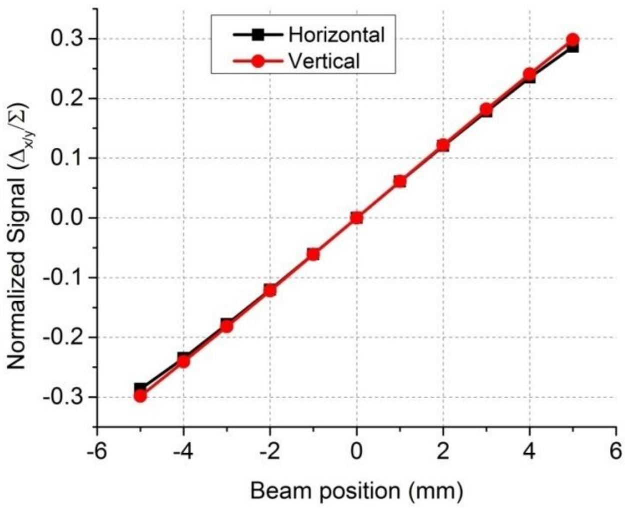

Fig. 4.14 Response of UPBPI at 505.8 MHz.

4.3 IDBPI

IDBPIs are button electrodes BPMs designed to monitor beam position at entry and exit of insertion devices (undulators) in Indus-2. Conceptual design of pickup electrode assembly of IDBPI is similar to UPBPI electrode assembly. Vertical aperture of insertion device is quite low as compared to the vacuum chamber in straight section of Indus-2. Therefore IDBPI (Fig. 4.15) and UPBPI have following differences.

1. The diameter of IDBPI is reduced to 9 mm from 11.8 mm.

2. The horizontal separation between pickup electrodes (center to centre) is reduced to 12 mm from 22 mm.

3. Unlike UPBPI, pickup electrodes of same horizontal plane have longitudinal separation (centre to centre) of 16 mm to provide minimum separation of 20 mm between buttons for mechanical feasibility.

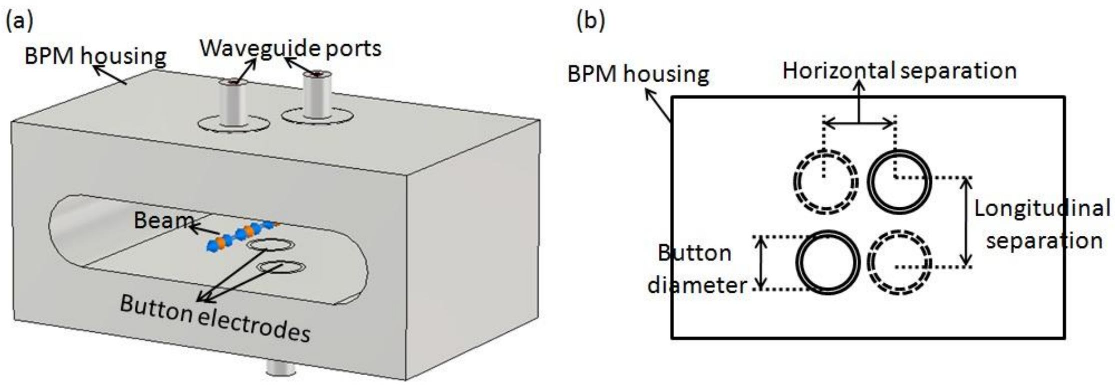

Fig. 4.15 (a) CST model of IDBPI (b) sketch of IDBPI showing different dimensions.

Reducing horizontal separation between pickup electrodes ensures equal position sensitivity in both of the transverse planes. Reduction in horizontal separation between pickup electrodes and vertical aperture also increases transfer impedance. Therefore, diameter of pickup electrode is reduced to push resonance mode given by equation (4.8) to higher frequency without sacrificing transfer impedance. Electrode assembly of IDBPI is shown in Fig. 4.16.

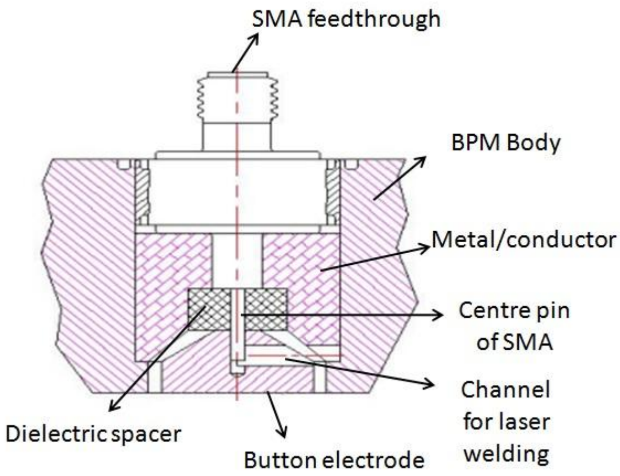

Fig. 4.16 Pickup electrode assembly of IDBPI.

4.3.1 IDBPI simulation

Similar to UPBPI, simulation of IDBPI is also performed using CST Studio Suite. The important characteristic parameters like pickup signal, transfer impedance, position sensitivity, wakefield and beam coupling impedance are presented below.

4.3.1.1 Output signal and transfer impedance

The temporal response of the IDBPI is shown in Fig. 4.17. The difference in upper (positive) and lower (negative) amplitude of the signal is due to finite capacitance between button and vacuum chamber. There is no ringing in the output signal which indicates that there is no reflection/resonance in the button electrode. The transfer impedance of IDBPI is shown in Fig. 4.18. At 505.8 MHz, the transfer impedance of IDBPI is ~0.7Ω.

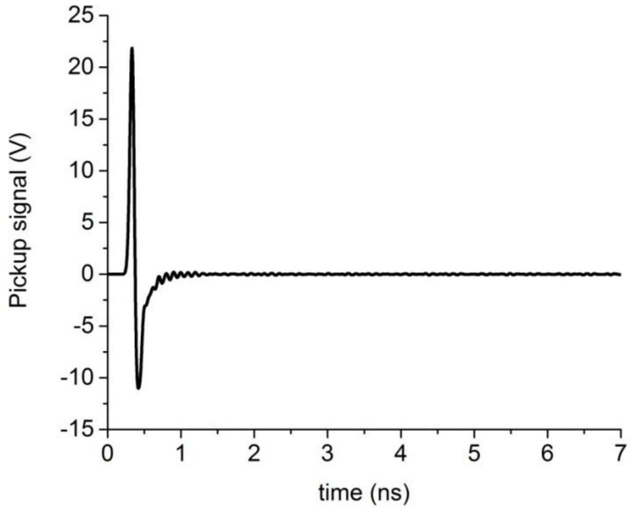

Fig. 4.17 Output signal of IDBPI as a function of time.

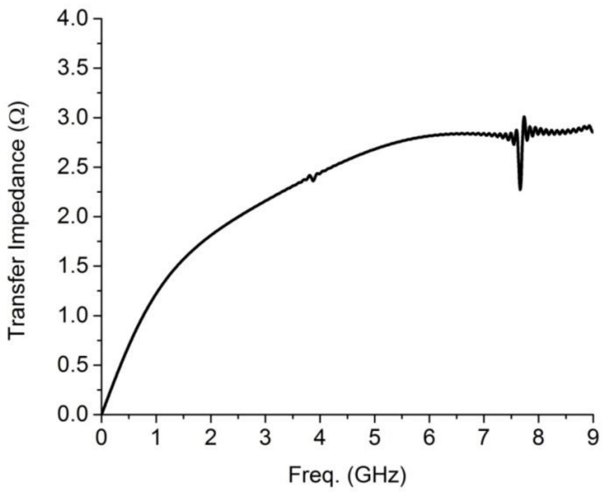

Fig. 4.18 Transfer impedance of IDBPI as a function of frequency.

4.3.1.2 Wakefield and beam coupling impedance

The longitudinal wake potential and beam coupling impedance (wake impedance) of IDBPI are shown in Figs. 4.19 and 4.20 respectively. There is no resonance in the structure up to 10 GHz. The only sharp peak is seen at frequency ~10 GHz. The frequency of this peak can be compared with TE_{11} mode given by equation (4.8).

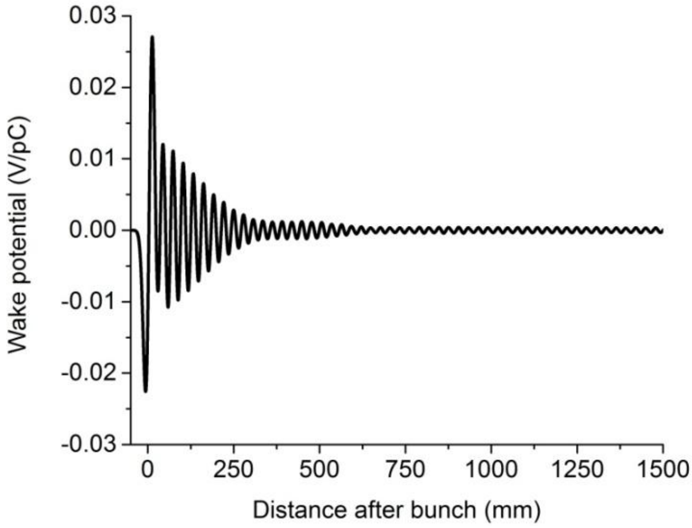

Fig. 4.19 Longitudinal wake potential of IDBPI as a function of distance after the bunch (mm).

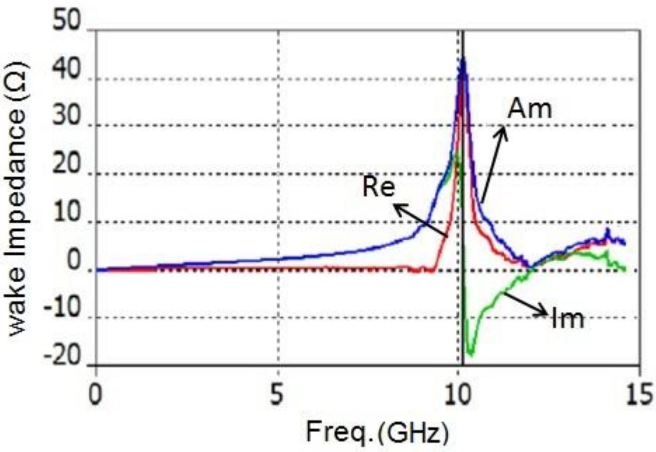

Fig. 4.20 Longitudinal coupling (wake) impedance of IDBPI as a function of frequency.

4.3.1.3 Response and position sensitivity

Similar to the UPBPI, the response and position sensitivity of the IDBPI are also simulated using wakefield solver of CST Particle Studio. The plots between normalized difference signals of IDBPI and frequency are shown in Figs. 4.21 and 4.22. The response (at 505. 8 MHz) of the IDBPI is shown in Fig. 4.23. The position sensitivity, calculated from the slope of the response curves given in Fig. 4.23 is ~0.12 mm^{-1} for both of the transverse planes. For racetrack geometry, the expected value of position sensitivity of the button electrodes BPM is of the order of the inverse of the distance between BPM axis and the button electrodes. For IDBPI, the distance between centre of the button electrode and BPM axis is ~10 mm giving position sensitivity of the order of 0.1 mm^{-1}. Thus the simulated value of ~0.12 mm^{-1} is close to the expected value.

For ~ 0.7 Ω transfer impedance and 0.12 mm^{-1} position sensitivity, the intrinsic resolution (resolution defined by thermal noise) of IDBPI comes out to be ~1 μm at 1 mA (~0.1 μm at 10 mA) beam current for 1.738 MHz bandwidth (turn by turn beam position measurement). Vertical size of beam at undulator location is ~ 35 μm (r.m.s.), therefore the position sensitivity (0.12 mm^{-1}) of IDBPI is sufficient for our requirement.

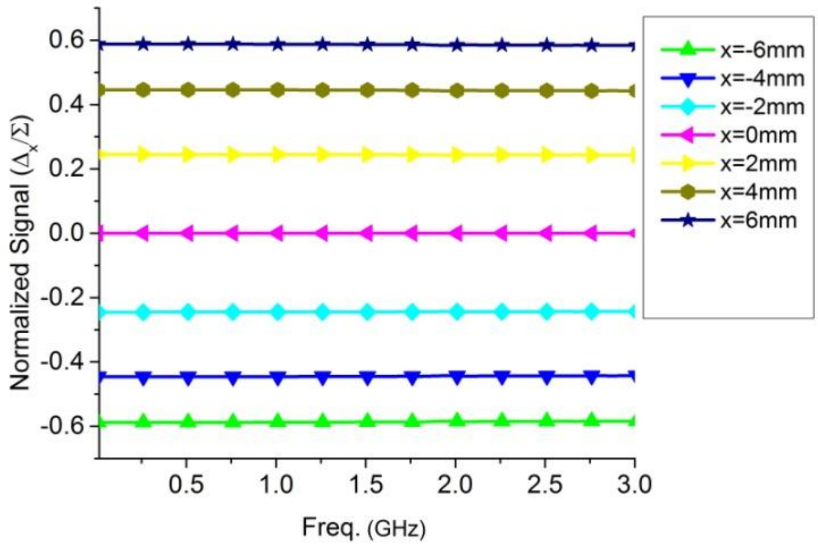

Fig. 4.21 Variation of normalized difference signal with frequency for different beam positions along x-axis frequency (IDBPI).

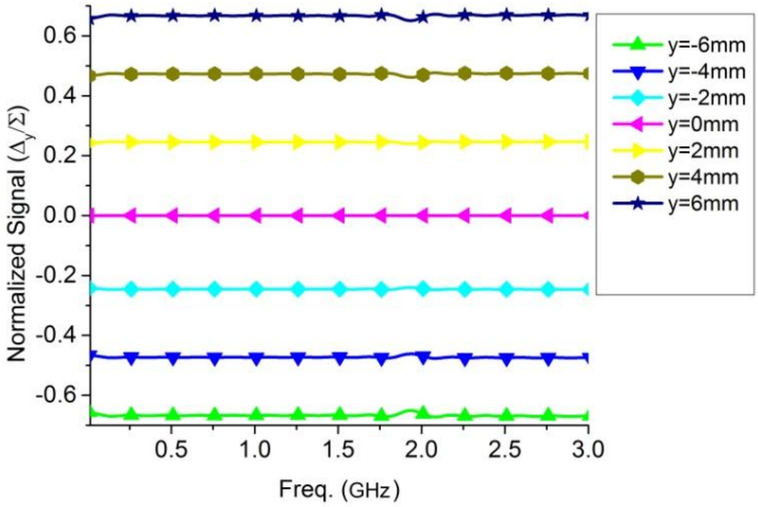

Fig. 4.22 Variation of normalized difference signal with frequency for different beam positions along y-axis frequency (IDBPI).

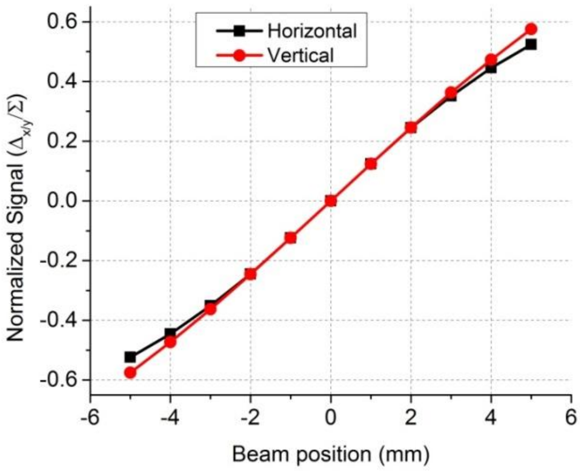

Fig. 4.23. Response of IDBPI at 505.8 MHz.

4.4 Measurements

4.4.1 Beam based measurement

Measurement on UPBPI, IDBPI and old button electrode BPM in Indus-2 is carried out with real electron beam during Indus-2 operation. Time domain signal and transfer impedance are measured to compare their performance relative to each other and with simulation results.

4.4.1.1 Time domain signal

Figs. 4.24 and 4.25 show that the time domain signal of UPBPI and IDBPI are well separated at bunch repetition time of ~2 ns as expected based on BPM simulation. On the other hand, in old BPM there is significant ringing with no clear differentiating signal as shown in Fig. 4.26.

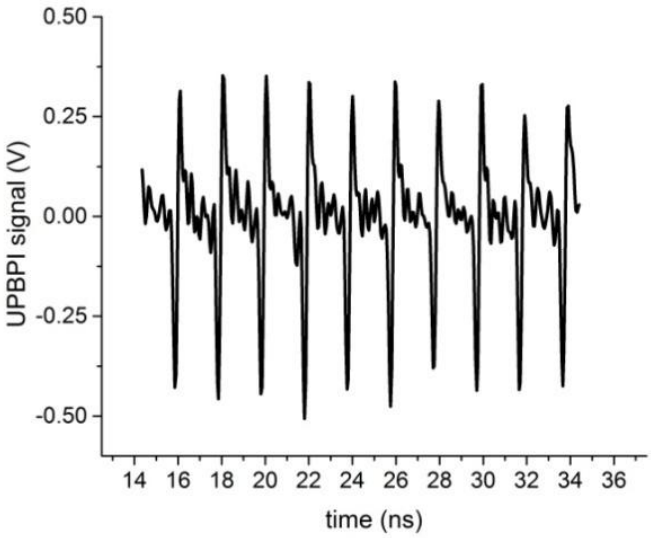

Fig. 4.24 Time domain signal of UPBPI measured during operation of Indus-2.

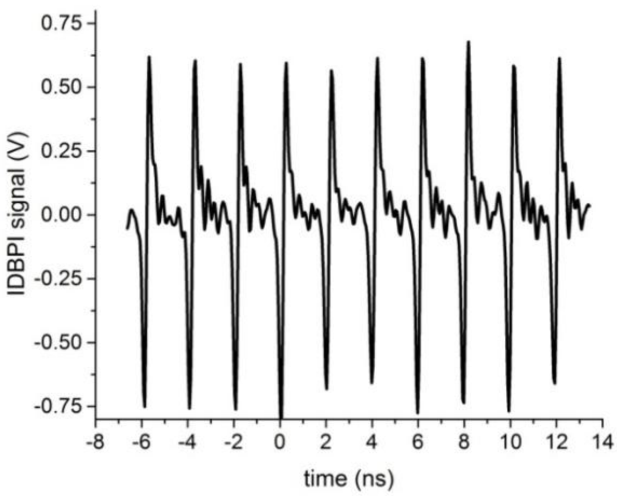

Fig. 4.25 Time domain signal of IDBPI measured during operation of Indus-2.

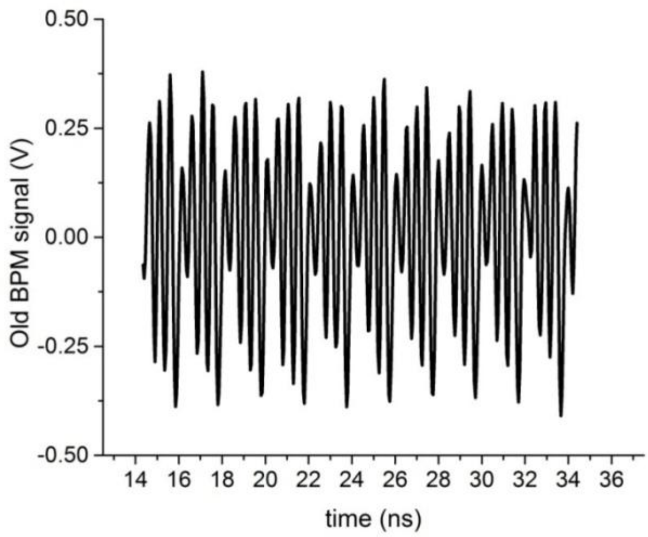

Fig. 4.26 Time domain signal of earlier (old) BPM measured during operation of Indus-2.

4.4.1.2 Transfer impedance

Transfer impedance of different BPMs (UPBPI, IDBPI and old BPM) is calculated from the pickup signal measured in the instrument gallery. For a given pickup voltage and beam current the transfer impedance is given by equation (4.9).

$$Z_T(\omega) = \frac{V_0(\omega)}{2A(\omega)I_{dc}} \tag{4.9}$$

In equation (4.9), $A(\omega)$ is amplitude factor of beam current at frequency ω and I_{dc} is dc beam current. Indus-2 has Gaussian bunch with r.m.s. length ~50 ps. Therefore, at 505.81 MHz A(ω) is ~ 1.

Voltage signal at the pickup electrode is calculated from the signal power. Table 4.1 shows signal power measured in instrument gallery. The attenuation factor of different cables running from pickup electrodes to instrument gallery is given in table 4.2. The power at the button electrode is difference of the signal power (dBm) in the instrument gallery and the attenuation factor (dB) of the respective cable. The power at pickup electrodes (after subtracting effect of cable loss) is given in table 4.3. The pickup voltage is calculated from power at button electrode for 50 Ω load impedance. The pickup voltage at different electrodes is shown in table 4.4. The signal corresponding to the beam passing through the axis of the BPM is calculated by taking average of the signals of four pickup electrodes of a given BPM. The BPM voltage (average of four electrodes voltage signals) and transfer impedances of old and improved BPMs are shown in table 4.5.

Table 4.1. Pickup powers (dBm) of UPBPI, IDBPI and old BPMs measured in instrument gallery of Indus-2.

Sr. No.	BPM type	Signal power (dBm)				DC beam current 'I_{dc}' (mA)
		electrode-1	electrode-2	electrode-3	electrode-4	
1	UPBPI (close to ID-2 entrance)	-16.2	-15.4	-15.2	-16.3	68
2	UPBPI (close to ID-2 exit)	-16.7	-16.8	-16.1	-16.1	68
3	UPBPI (straight section)	-16.3	-15.3	-16.4	-17.3	63.4
4	Old BPM (straight section)	-20.3	-19.9	-18.9	-19.6	68
5	IDBPI (at ID-2 entrance)	-16.1	-15.9	-14.1	-14.2	68
6	IDBPI (at ID-2 exit)	-14.7	-14	-14.7	-15.4	68

Table 4.2. Cable attenuation factor (dB) of UPBPI, IDBPI and old BPMs measured in instrument gallery of Indus-2.

Sr. No.	BPM type	Cable attenuation (dB)			
		electrode-1	electrode-2	electrode-3	electrode-4
1	UPBPI (close to ID-2 entrance)	-3.43	-3.4	-3.42	-3.39
2	UPBPI (close to ID-2 exit)	-4.04	-4	-4.01	-3.95
3	UPBPI (straight section)	-3.4	-3.42	-3.37	-3.37
4	Old BPM (straight section)	-4.49	-4.47	-4.47	-4.51
5	IDBPI (at ID-2 entrance)	-4.28	-4.28	-4.24	-4.33
6	IDBPI (at ID-2 exit)	-4.38	-4.3	-4.26	-4.31

Table 4.3. Pickup powers (dBm) of UPBPI, IDBPI and old BPMs at pickup electrodes after subtracting effect of cable loss.

Sr. No.	BPM type	Signal power (dBm)				DC beam current 'I_{dc}' (mA)
		electrode-1	electrode-2	electrode-3	electrode-4	
1	UPBPI (close to ID-2 entrance)	-12.77	-12	-11.78	-12.91	68
2	UPBPI (close to ID-2 exit)	-12.66	-12.8	-12.09	-12.15	68
3	UPBPI (straight section)	-12.9	-11.88	-13.03	-13.93	63.4

4	Old BPM (straight section)	-15.81	-15.43	-14.43	-15.09	68
5	IDBPI (at ID-2 entrance)	-11.82	-11.62	-9.86	-9.87	68
6	IDBPI (at ID-2 exit)	-10.32	-9.7	-10.44	-11.09	68

Table 4.4. Pickup voltage (volt) of UPBPI, IDBPI and old BPMs at pickup electrodes.

Sr. No.	BPM type	Pickup voltage (mV)				DC beam current 'I_{dc}' (mA)
		electrode-1	electrode-2	electrode-3	electrode-4	
1	UPBPI (close to ID-2 entrance)	72.6	79.4	81.5	71.5	68
2	UPBPI (close to ID-2 exit)	73.6	72.4	78.6	78.1	68
3	UPBPI (straight section)	71.6	80.5	70.6	63.6	63.4
4	Old BPM (straight section)	51.2	53.5	60.1	55.6	68
5	IDBPI (at ID-2 entrance)	81.1	82.9	101.6	101.51	68
6	IDBPI (at ID-2 exit)	96.3	103.5	95.1	88.2	68

Table 4.5. Voltage signal and transfer impedance (at 505.81 MHz) of UPBPI, IDBPI and old BPMs measured using actual beam during operation of Indus-2.

Sr. No.	BPM type	Average Pickup signal (mV)	DC beam current (mA)	Transfer impedance (Ω)
1	UPBPI (close to ID-2 entrance)	76.3	68	0.56
2	UPBPI (close to ID-2 exit)	75.7	68	0.56
3	UPBPI (straight section)	71.6	63.4	0.56
4	Old BPM (straight section)	55.1	68	0.40
5	IDBPI (at ID-2 entrance)	91.8	68	0.675
6	IDBPI (at ID-2 exit)	95.8	68	0.7

4.4.2 Test bench measurement

Bench measurement of transfer impedance of UPBPI and IDBPI has also been carried out using coaxial wire method. For this a modified setup of coaxial wire method is developed which is presented in next chapter.

4.5 Summary

The bench and in-situ measurements performed on UPBPI, IDBPI and old BPMs show that there is significant improvement in signal quality, transfer impedance and vertical position sensitivity of UPBPI and IDBPI as compared to old BPMs. Simulation of UPBPI and IDBPI also matches closely with the measurements.

The old BPMs (individual type) of Indus-2 are being replaced by UPBPIs in phased manner. So far 21 old BPMs have been replaced in Indus-2 storage ring. Presently there are three undulators installed in Indus-2. The IDBPIs have been deployed at entry and exit of each undulator. The UPBPI and IDBPI are essential part of beam position monitoring system for various applications (like tune measurement, closed orbit measurement, various feedback system, undulator interlock system etc.) in Indus-2.

CHAPTER-5

MODIFIED COAXIAL WIRE METHOD FOR MEASUREMENT OF TRANSFER IMPEDANCE OF BEAM POSITION MONITORS OF INDUS-2

A modified set up of coaxial wire method is conceptualized, designed and implemented to measure transfer impedance of capacitive BPMs (IDBPI and UPBPI) of Indus-2. This chapter presents concept, theory and experimental implementation of the modified coaxial wire method to measure transfer impedance of capacitive BPMs. The present chapter can broadly be divided into two parts. Fist part presents introduction to modified setup of coaxial wire method, derivation of modified expressions for transfer impedance of capacitive pickups and its validation through simulation. Second part presents measurement of transfer impedance of beam position monitors (UPBPI and IDBPI) of Indus-2 using modified setup of coaxial wire method and comparison of measured results with simulation.

5.1 Modified coaxial wire method and its validation

5.1.1 Conventional coaxial wire method

The coaxial wire method was proposed in early seventies by Sands and Rees to measure energy loss of a stored beam in a cavity [79]. Since then a large number of people have used coaxial wire method, in different forms, to measure beam coupling impedance of various components [51-58]. In coaxial wire method, a thin wire is stretched along the axis of the device under test (DUT) to form coaxial transmission line like structure. The current flowing through wire generates electromagnetic field inside the DUT similar to that generated by the beam. Generally, the characteristic impedance of the coaxial structure formed by wire and the DUT is much higher than the impedance of the external circuit (generator and cables). In order to simulate particle beam realistically and avoid trapped modes, the impedance of the external circuit should be matched to the characteristic impedance of coaxial structure. Fig. 5.1 shows schematic of conventional coaxial wire method using impedance matching elements. The most common method of impedance matching between external circuit (VNA and cables) and DUT is use of electrical network or tapered structures.

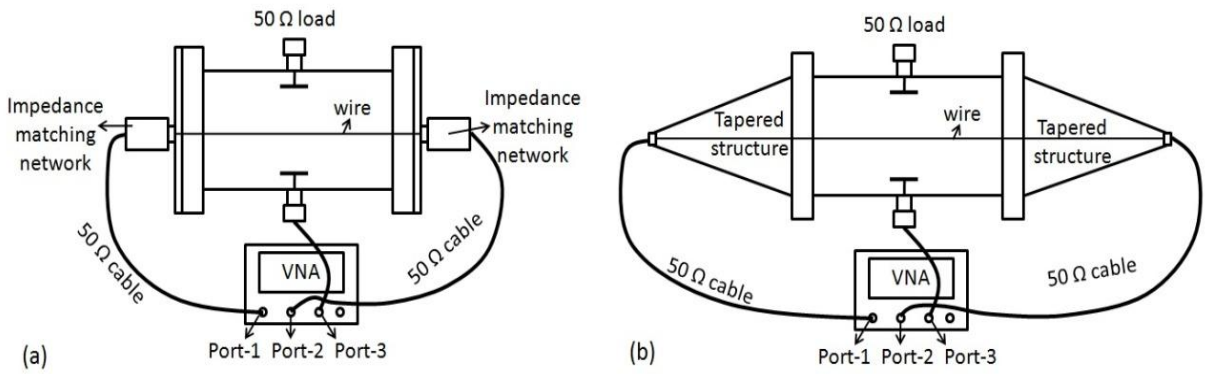

Fig. 5.1 Schematic setup of conventional wire method. Impedance matching using electrical network (a) and tapered mechanical structure (b).

Coaxial wire method is mainly used for measurement of beam coupling impedance but this technique has also been used to measure transfer impedance of button electrode BPM [59-61]. For transfer impedance measurement, the coaxial structure is connected to the vector network analyser (VNA) as shown in Fig.5.1and transfer impedance 'Z_T' is calculated using equation (5.1).

$$Z_T(\omega) = \frac{S_{31}(\omega)}{S_{21}(\omega)}\sqrt{Z_0 Z_w} \qquad (5.1)$$

In equation (5.1), S_{31} and S_{21} are S-parameters from port-1 to port-3 and port-2 respectively, Z_0 is the characteristic impedance of the cables between VNA and BPM, and Z_w is characteristic impedance of the coaxial structure.

5.1.2 Modified coaxial wire method

The implementation of impedance matching between DUT and external electronic demands extra efforts which is practically a tedious task. Moreover, if characteristic impedance of the coaxial structure changes, one has to redesign/replace existing impedance matching elements accordingly. Therefore, to simplify the setup of coaxial wire method a modified coaxial wire method is conceived. In this method impedance matching elements have been eliminated and DUT is directly (without impedance matching) connected to the external electronics (cables, VNA , load etc). The schematic setup of modified coaxial wire method is shown in Fig. 5.2**.** The detail of the setup is as follows.

Two metallic plates hold electrical feedthroughs at the entry and exit of the DUT. A wire is stretched between central pins of the electrical feedthroughs to form coaxial structure with DUT. The VNA is directly connected to one end of the wire using signal cable. The other end of the wire is either terminated with a load (50 Ω) or electrically shorted at the center of the metallic plate. In second case (shorted end of the wire) no electrical feedthrough is required at the second plate, thus, practical implementation of the setup is quite simplified.

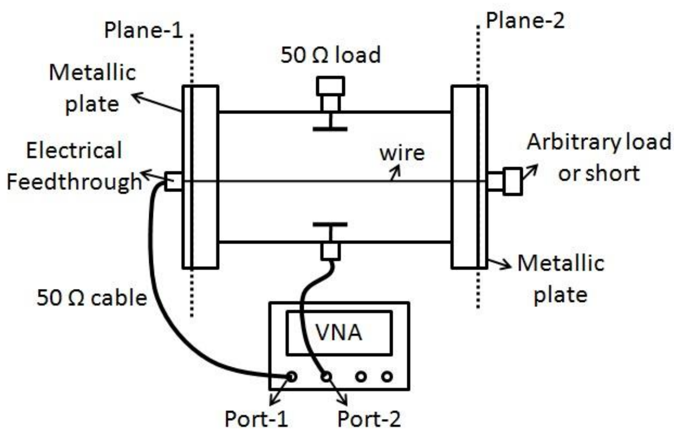

Fig. 5.2 Schematic of general setup of modified coaxial wire method.

5.1.2.1 Expression for transfer impedance in modified setup

In modified coaxial wire setup, the impedance matching elements have been eliminated. The elimination of impedance matching elements results in multiple (infinite) reflections inside the coaxial structure making conventional expression (equation (5.1)) of transfer impedance invalid for modified setup of coaxial wire method. Using principle of superposition of signal induced on pickup electrode due to infinite reflections of wire current inside DUT, the modified expression of transfer impedance (Z_T) of pickup electrode in modified setup is derived. The derivation is presented in appendix-D. The modified expression of transfer impedance is given by

$$|Z_T(\omega)| = \frac{|S_{pick,1}(\omega)|(Z_0 + Z_w)\sqrt{1 + (|\rho_1||\rho_2|)^2 - 2|\rho_1||\rho_2|\cos(\beta)}}{2\sqrt{1 + |\rho_2|^2 + 2|\rho_2|\cos(\gamma)}} \tag{5.2}$$

Here $|\rho_1|$ and $|\rho_2|$ are reflection coefficients at plane-1 and plane-2 respectively (Fig. 5.2). Other parameters (γ, β, Z_0 and Z_w) are explained in appendix-D. Equation (5.2) gives transfer impedance of the pickup electrode in terms of S-parameter ($S_{pick,1}$) from wire to pickup electrode. Equation (5.2) is valid for any arbitrary load at downstream port of coaxial wire. Two special cases in which downstream port is terminated with 50 Ω and electrically shorted are given below.

Case-1. Downstream port of the coaxial wire is terminated with 50 Ω load

When downstream port of coaxial wire structure is terminated with 50 Ω load (equal to the impedance of VNA and cables) we get $|\rho_1|=|\rho_2|$ and $\varphi_1=\varphi_2$. Using $|\rho_1|=|\rho_2| =|\rho|$, the equation (5.2) can be written as

$$\left|Z_T(\omega)\right| = \frac{\left|S_{pick,1}(\omega)\right|\left(Z_0 + Z_w\right)\sqrt{1+|\rho|^4 - 2|\rho|^2\cos(\beta)}}{2\sqrt{1+|\rho|^2 + 2|\rho|\cos(\gamma)}} \tag{5.3}$$

Generally, the characteristic impedance of the coaxial structure formed by wire and the BPM is greater than the impedance of VNA. Therefore, using $\varphi_1 = \varphi_2 = \pi$ we get $\beta = 2\omega L/c + 2\pi$ and $\gamma = \omega(L+2\Delta L)/c + \pi$. Thus, equation (5.3) becomes

$$\left|Z_T(\omega)\right| = \frac{\left|S_{pick,1}(\omega)\right|\left(Z_0 + Z_w\right)\sqrt{1+|\rho|^4 - 2|\rho|^2\cos\left(2\omega L/c\right)}}{2\sqrt{1+|\rho|^2 - 2|\rho|\cos\left(\omega(L+2\Delta L)/c\right)}} \tag{5.4}$$

Case-2. Downstream port of the coaxial wire is shorted with metallic plate

When downstream port of coaxial wire is shorted we get $|\rho_2|=1$. Using $|\rho_2|=1$, $|\rho_1|=|\rho|$ and $\varphi_1 = \varphi_2 = \pi$, the equation (5.2) can be written as

$$\left|Z_T(\omega)\right| = \frac{\left|S_{pick,1}(\omega)\right|\left(Z_0 + Z_w\right)\sqrt{1+(|\rho|)^2 - 2|\rho|\cos\left(2\omega L/c\right)}}{4\sin\left(\omega(L+2\Delta L)/2c\right)} \tag{5.5}$$

Equations (5.4) and (5.5) give transfer impedance for special cases of 50 Ω and shorted termination of coaxial wire respectively.

5.1.3 Validation of modified coaxial wire method

A general button electrode BPM (Fig. 5.3) is considered as a test BPM to establish the modified coaxial wire method and test the validity of associated expressions. Important geometric parameters of the test BPM are given in table 5.1.The transfer impedance of the test BPM is calculated through simulation of the BPM with particle beam, conventional wire method and modified coaxial wire method using CST Studio Suite [75]. The results obtained through these methods are compared with each other to test the validity of the modified coaxial wire method.

Table 5.1. Geometric parameters of the test BPM.

Sr. No.	Parameter	Value
1	Radius of button electrode	5 mm
2	Radius of beam pipe	10 mm
3	Annular gap between button and beam pipe	0.5 mm
4	Thickness of button electrode	3 mm
5	Length of the BPM	100 mm

5.1.3.1 Simulation of test BPM with particle beam

The wakefield solver of the CST Particle Studio simulates interaction of electromagnetic field of a beam of charge particles with its surroundings like pickup electrode and vacuum chamber etc.. The interaction of electromagnetic field with pickup electrodes generates pickup signal (button voltage) for a given (defined) beam current.

To simulate button voltage, the test BPM is modeled in CST Particle Studio and an electron beam having Gaussian longitudinal distribution is defined to travel along the axis of the BPM (Fig. 5.3). Fourier transform of the button voltage and beam current is shown in Figs. 5.4 and 5.5 respectively. The transfer impedance is calculated as the ratio of button signal to the beam current and it is shown in Fig. 5.6.

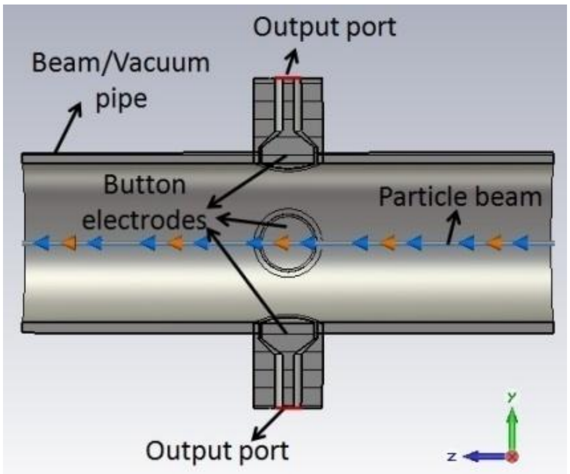

Fig. 5.3. CST model for the simulation of test BPM with particle beam.

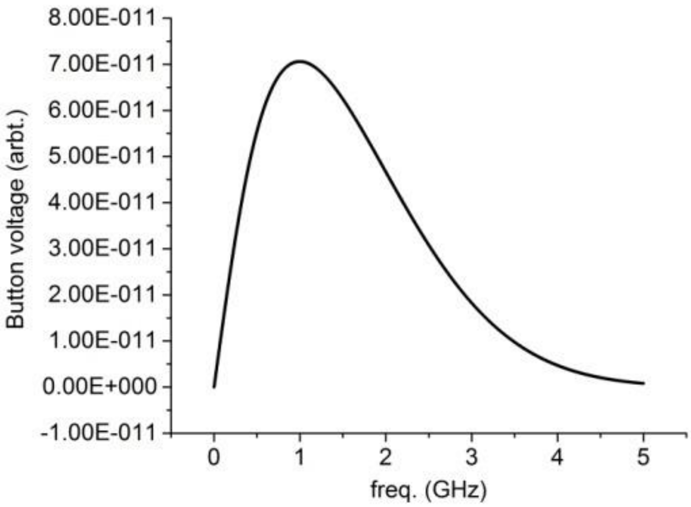

Fig. 5.4. Fourier transform of voltage signal induced at the button electrode of the test BPM obtained through simulation with particle beam.

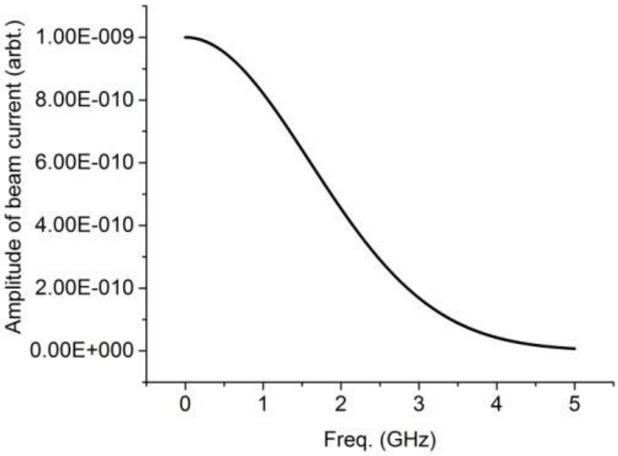

Fig. 5.5. Fourier transform of beam current used for the simulation of test BPM with particle beam.

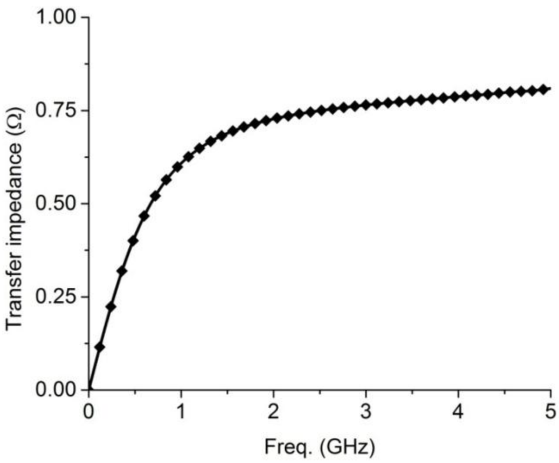

Fig. 5.6 Transfer impedance of test BPM obtained using simulation with particle beam.

5.1.3.2 Simulation of test BPM using conventional coaxial wire method

The transfer impedance of test BPM is also calculated by simulating it through conventional coaxial wire method as explained in reference [60]. Simulation model of the conventional coaxial wire method for the test BPM is shown in Fig. 5.7. The test BPM and a thin metallic cylinder along the BPM axis are modeled in CST Microwave Studio to simulate coaxial wire method. The radius of the wire is taken to be 0.5 mm. Two waveguide ports (port-1 and port-2) are defined at the entry and exit of the coaxial structure. These ports act as matched source and load at the upstream and downstream of the coaxial structure respectively. Four waveguide ports (port-3 to port-6) are also defined at the output of the pickup electrodes to simulate 50 Ω load.

The S-parameter (S_{21} and S_{i1}; i=3 to 6) obtained through transient solver of the CST Microwave Studio is shown in Fig. 5.8. The transfer impedance is calculated using equation (5.1) and shown in Fig. 5.9.

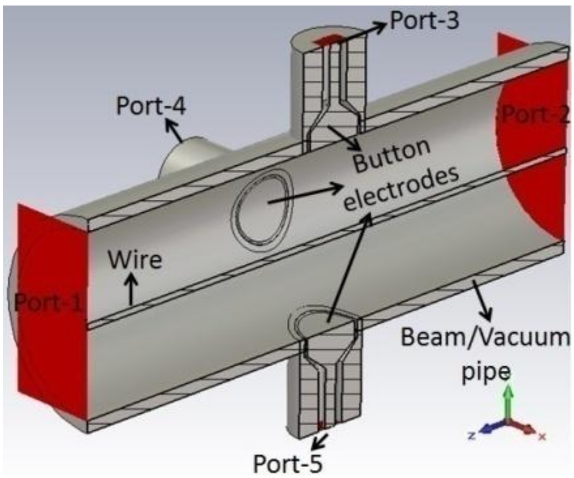

Fig. 5.7 CST model for the simulation of conventional coaxial wire method used for the calculation of transfer impedance of test BPM.

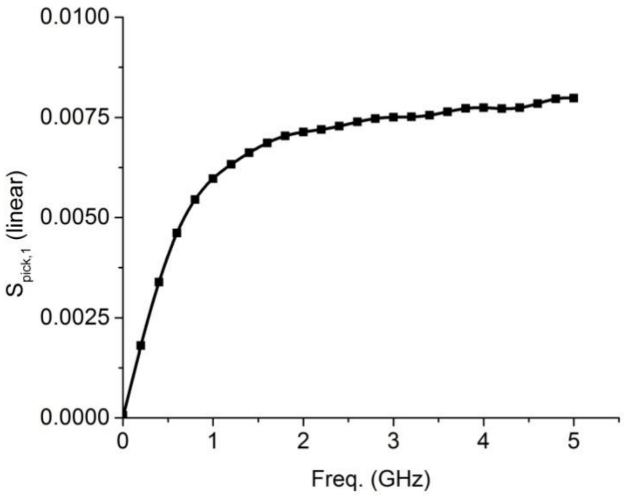

Fig. 5.8 S-parameters for simulation of conventional coaxial wire method for test BPM.

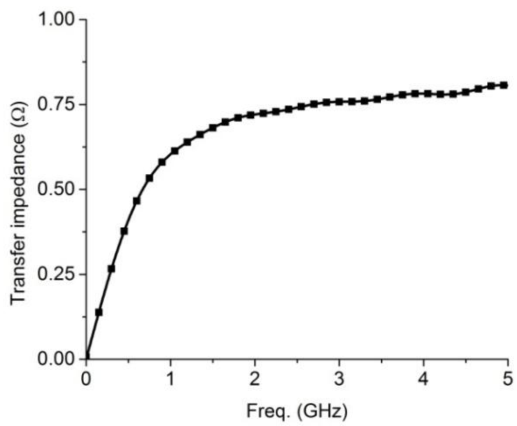

Fig. 5.9 Transfer impedance of test BPM obtained using simulation of conventional coaxial wire method.

5.1.3.3 Simulation of test BPM using modified coaxial wire method

Simulation model of modified coaxial wire method, used to calculate transfer impedance of test BPM, is shown in Fig. 5.10. The only difference between simulation model of modified and conventional coaxial wire method lies in modeling of port-1 and port-2. For the case of 50 Ω downstream port, port-1 and port-2 are modeled such that they act as 50 Ω waveguide ports. For the case of shorted downstream port, only port-1 is modeled.

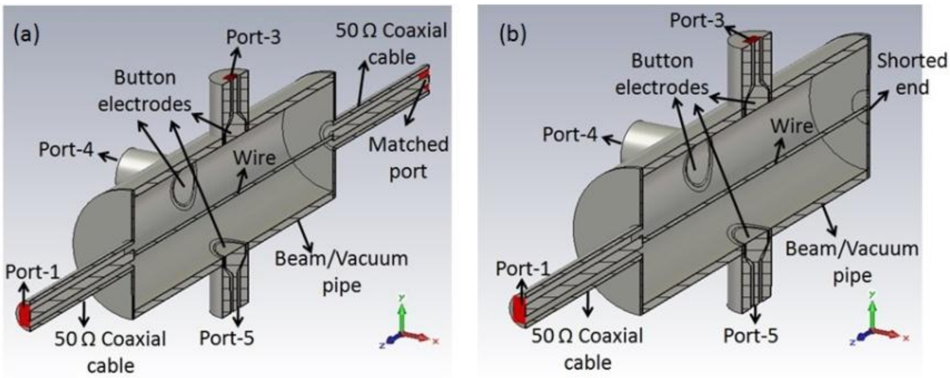

Fig. 5.10 CST model for the simulation of modified coaxial wire method used for the calculation of transfer impedance of test BPM. (a) 50 Ω downstream port and (b) shorted downstream port.

The S-parameters obtained through transient solver of the CST Microwave Studio are shown in Fig. 5.11. Transfer impedance calculated using equations (5.4) and (5.5) for 50 Ω termination and shorted configuration is shown Fig. 5.12.

Simulated S-parameters (Fig. 5.11) have resonances at 1.5 GHz and 4.5 GHz. These resonances are due to the fact that the coaxial structure forms a cavity of length L=100 mm. Thus, the structure have discrete resonances (trapped modes) at L=(2n-1)λ/2 (n=1,2,3...) with λ being wavelength at resonance. The electromagnetic fields corresponding to these resonances (trapped modes) decay through the coaxial wire. The rate of decay of electromagnetic field depends on the mismatch between DUT and the external circuit, and it decreases with increasing impedance mismatch. Since, the equations (5.4) and (5.5) have been derived by superposition of infinite number of reflections. Therefore, mathematically, these resonances (at 1.5 GHz and 4.5 GHz) have no effect on the accuracy of transfer impedance calculated using equations (5.4) and (5.5) as indicated in Fig 5.12.

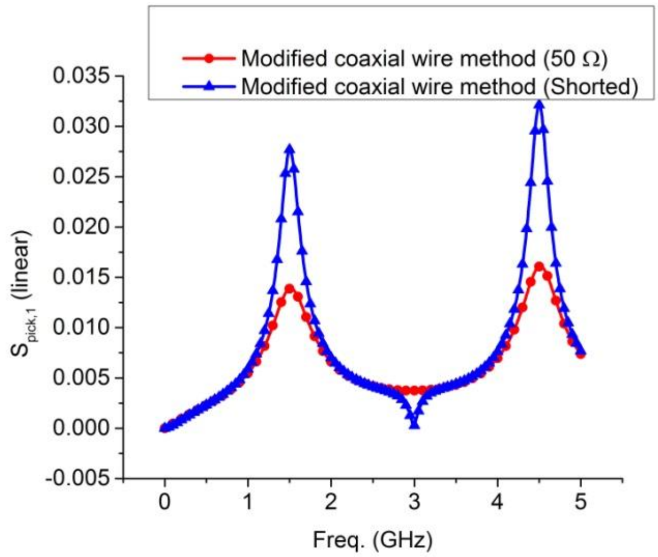

Fig. 5.11 S-parameters for simulation of modified coaxial wire method for test BPM.

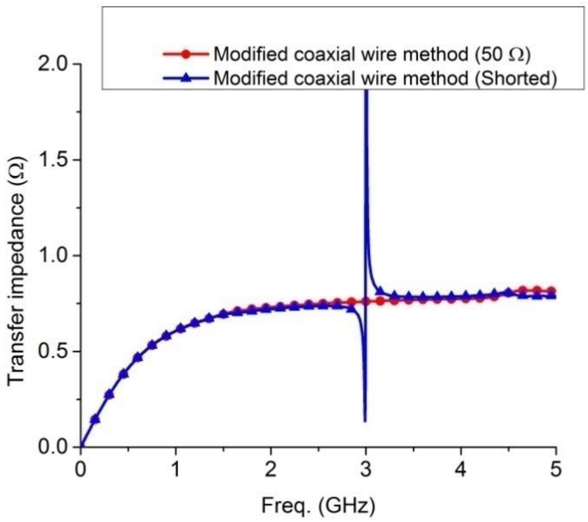

Fig. 5.12 Transfer impedance of test BPM obtained using simulation of Modified coaxial wire method.

5.1.3.4 Comparison of results (test BPM)

Comparison of transfer impedance of test BPM obtained through three methods (presented in previous sections) is shown in Fig. 5.13. The simulations results show that the transfer impedance obtained through direct simulations of test BPM using particle beam and conventional wire method matches closely with the transfer impedance obtained by simulation of modified coaxial wire setup terminated with 50 Ω at downstream stream port. For setup with shorted downstream end, the results are also matching closely except discontinuity at 3.0 GHz. This is because, the denominator of equation (5.5) becomes zero at 3.0 GHz giving discontinuity at this frequency.

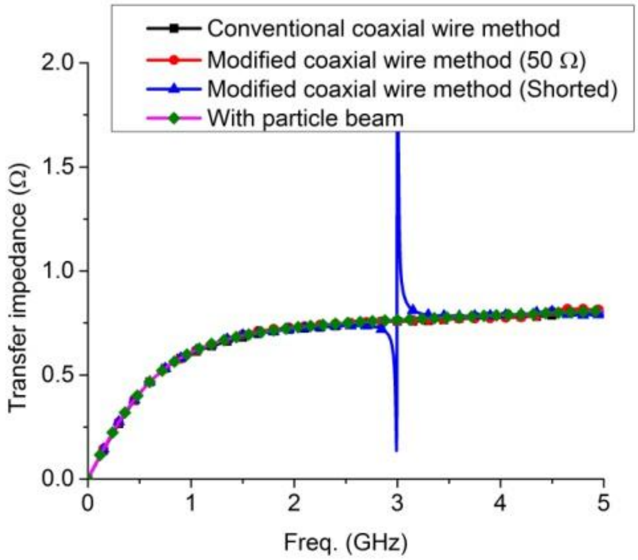

Fig. 5.13 Transfer impedance of the test BPM obtained through simulation (using CST Studio Suite) of the BPM.

5.2 Measurement of transfer impedance of beam position monitors of Indus-2

5.2.1 Measurement and calculation

Practical implementation of modified coaxial wire setup is relatively easy for shorted downstream end as compared to 50 Ω termination. Therefore, modified coaxial wire method with shorted downstream port has been implemented to measure transfer impedance of button electrode BPMs (IDBPI and UPBPI) of Indus-2. The detail of the BPMs is given in Chapter-4. Measurement setup for IDBPI is shown in Fig. 5.14. Two aluminum plates each having thickness 2 mm are mounted at the end of the BPM body. An SMA type electrical feedthrough is mounted at the centre of one aluminum plate such that central pin of the SMA feedthrough protrudes inside and its connector part lies outside of the BPM. A copper wire (having diameter 1.5 mm) is stretched from the pin of the electrical feedthrough and fixed (electrically shorted) at the center of the other aluminum plate.

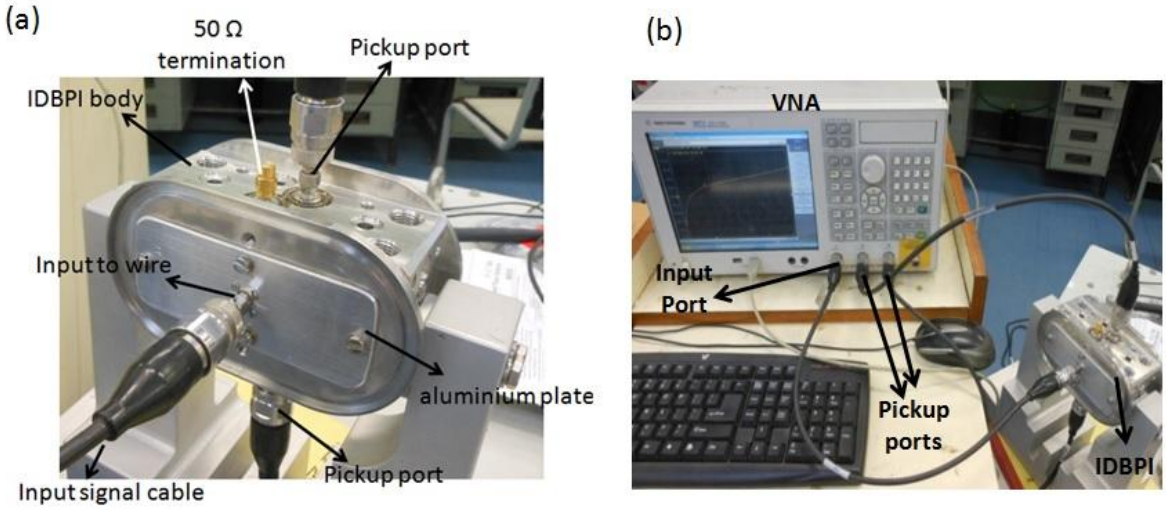

Fig. 5.14 Modified coaxial wire setup for the measurement of transfer impedance of IDBPI.

(a) Coaxial structure only; (b) Coaxial structure with VNA.

Port-1 of the VNA is connected to the coaxial wire and S-parameters ($S_{pick,1}$) from the coaxial wire to different pickup electrodes are measured one by one using port-2 of the VNA. While measuring S-parameter for a given electrode, the other pickup electrodes are terminated with load of 50 Ω each. Similar setup is used for UPBPI. The measured S-parameters for different pickup electrodes are shown in Fig. 5.15 and Fig. 5.16 for IDBPI and UPBPI respectively.

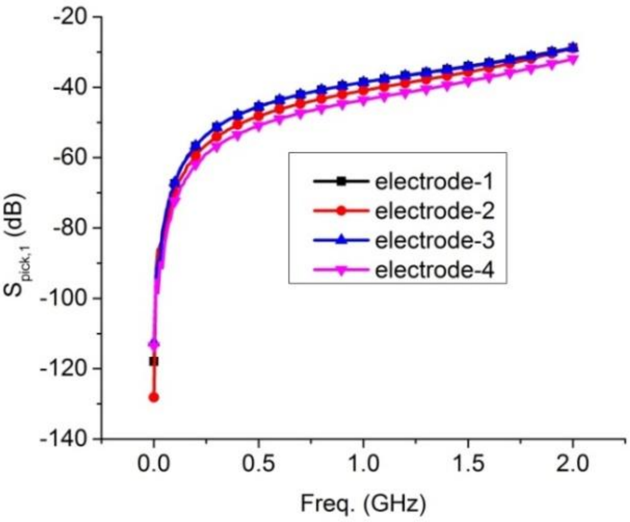

Fig. 5.15 S-parameter of IDBPI measured using modified wire method.

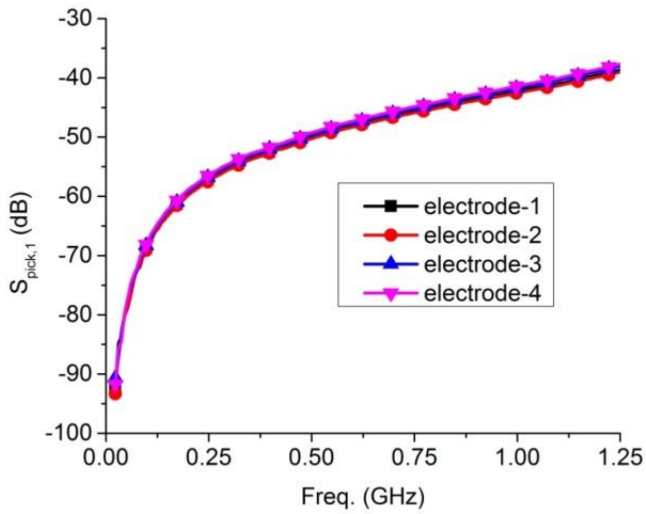

Fig. 5.16 S-parameter of UPBPI measured using modified wire method.

For racetrack geometry, having vertical aperture much smaller than horizontal aperture, the characteristic impedance of coaxial structure is given by [61]

$$Z_w \approx 60ln\left(1.27\frac{H}{D_w}\right) \tag{5.6}$$

In equation (5.6), D_w is wire diameter and H is vertical aperture.

The reflection coefficient '$|\rho|$' at plane-1 is given by

$$|\rho| = \frac{|Z_w - Z_0|}{|Z_w + Z_0|} \tag{5.7}$$

For IDBPI (vertical aperture 17 mm) the characteristic impedance (Z_w) and reflection coefficient (ρ), calculated using equations (5.6) and (5.7), come out to be ~160 Ω and ~0.524 respectively. For UPBPI (vertical aperture 36 mm) characteristic impedance and reflection coefficient come out to be ~208 Ω and ~0.612 respectively. The transfer impedance of different electrodes of IDBPI and UPBPI is calculated using equation (5.5). The results are shown in Fig. 5.17 and Fig. 5.18.

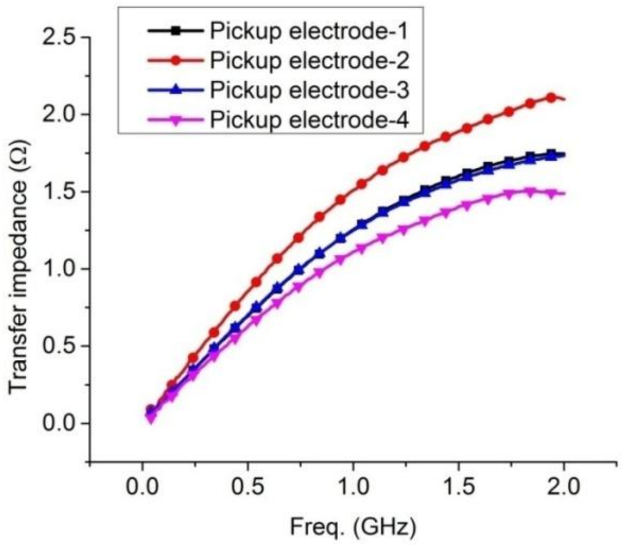

Fig. 5.17 Transfer impedance of different pickup electrodes of IDBPI measured using modified wire method.

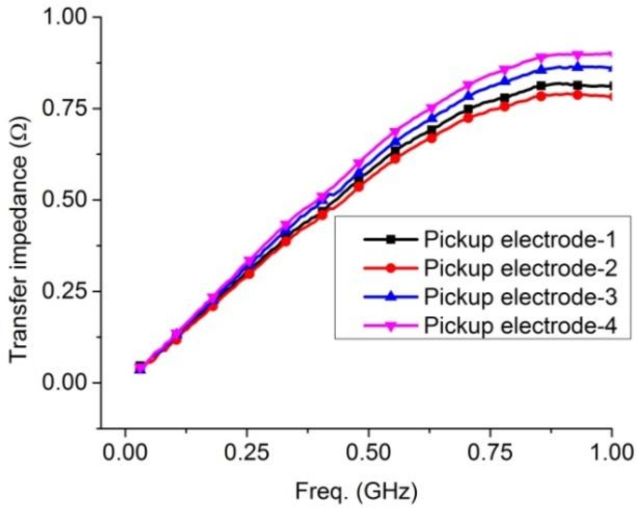

Fig. 5.18 Transfer impedance of different pickup electrodes of UPBPI measured using modified wire method.

As observed in Figs. 5.17 and 5.18, the transfer impedance calculated experimentally for different pickup electrodes vary from each other. The possible reason for this could be that the wire may have slight offset or angle with respect to the axis of the IDBPI. The transfer impedance corresponding to the axis of the IDBPI is calculated by averaging the transfer impedance of all pick up electrodes of a given BPM.

5.2.2 Measurement versus simulation

Comparison of transfer impedance of UPBPI and IDBPI measured using modified coaxial wire method with simulation (presented in Chapter-4) is presented in Figs. 5.19 and 5.20. The measured transfer impedance matches closely with designed (simulated) value up to frequencies well above signal processing frequency (505.8 MHz). For IDBPI, there is good agreement between transfer impedance obtained through bench measurement and simulations up to ~1.8 GHz. For UPBPI, the measured and simulated result matches closely up to ~900 MHz.

Above 1.8 GHz (for IDBPI) and 900 MHz (for UPBPI), the measured results start showing deviation from the simulation. This deviation is due to the resonance in coaxial structure occurring at L=λ/2 with λ being wavelength and L, the length of DUT. For IDBPI the resonance occurs at ~ 2.4 GHz (for L=62.5 mm) and for UPBPI the resonance occurs at ~1.5 GHz (for L=100 mm). Theoretically, these resonances should not have any effect on accuracy of calculated transfer impedance as shown earlier through simulation of test BPM. In practical case, as one approaches these resonances, the measured results become quite sensitive to the length of DUT (L) and offset (ΔL) of the electrodes from the center of the DUT. Therefore, even small error in measured value like S-parameters, length of DUT etc. can cause significant error (deviation) in measured transfer impedance. Overall, the measured transfer impedance shows very good accuracy around signal processing frequency (505.8 MHz) of Indus-2.

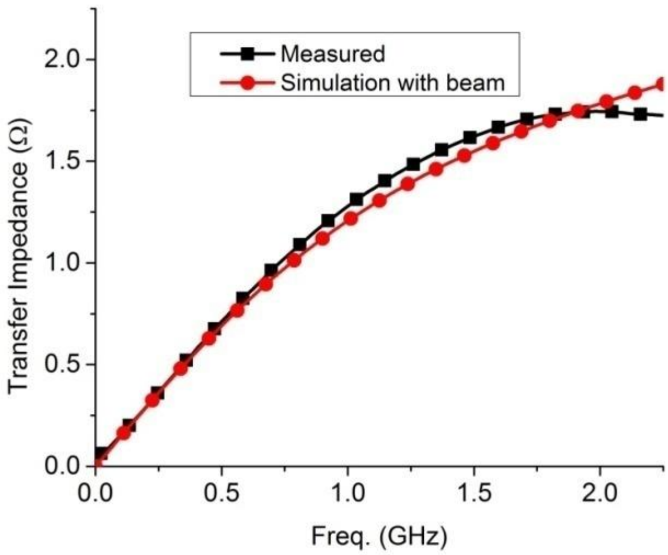

Fig. 5.19. Comparison of the transfer impedance of IDBPI obtained experimentally with simulations.

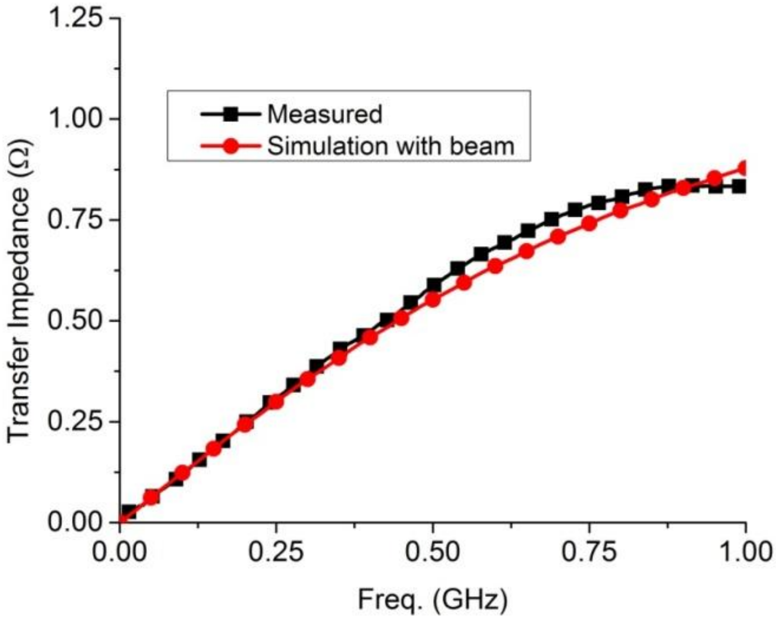

Fig. 5.20 Comparison of the transfer impedance of UPBPI obtained experimentally with simulations.

5.3 Summary

The concept, theory, validation and practical implementation of modified coaxial wire method for measurement of transfer impedance of button electrode BPM are presented in this chapter. The transfer impedances of button electrodes BPMs of Indus-2 are measured using modified coaxial wire method. The transfer impedance, at 505.8 MHz, of IDBPI and UPBPI measured using modified coaxial wire method is 0.71 Ω and 0.59 Ω respectively which is quite close to the transfer impedance measured in-situ with real electron beam during operation of Indus-2.

The modified setup of coaxial wire method does not require impedance matching elements between device under test (DUT) and external electronics thus the practical implementation of the setup is relatively easy as compared to the conventional setup. The concept of modified setup of coaxial wire method presented in this chapter may also be used to measure shunt impedance using relation between pickup and kickers properties.

CHAPTER-6

CONCLUSION AND FUTURE PROSPECTS

Pickups and kickers have wide applications in different accelerator facilities like electron accelerator, proton accelerator, heavy ions accelerator, circular accelerator, linear accelerators or transport lines. The work presented in this thesis mainly deals with capacitive pickups (button electrode and shoe box BPMs) and stripline which are commonly used as pickups and kickers in various types of accelerators and transport lines.

The major objective of the thesis work is study of pickups and kickers (button electrode BPM, stripline and shoe box) for Indus accelerators and High Intensity Proton linear Accelerator (HIPA) for Indian Spallation Neutron Source (ISNS), and design of new/upgraded button electrode BPMs for Indus-2.

Thesis starts with fundamental and important properties of pickup and kicker with their functional details. Fundamentals and applications of general capacitive pickup and specific devices like shoe box BPM, button electrode BPM and stripline are also described in chapter 1.

In chapters 2 and 3, study of fringe field in stripline and effect of inter-electrode cross talk in shoe box BPM is presented. Modified expressions of various parameters like normalized difference signal in a two electrodes BPM, position sensitivity of shoe box BPM, effective width of strip in stripline, characteristic impedance of stripline etc. are derived and presented. The results obtained through modified expressions are more close to the simulation results as compared to the conventional expressions being used widely in the literature.

Chapters 4 and 5 focus on design and characterization of new button electrode BPMs for Indus-2. New BPMs (UPBPI and IDBPI) having improved qualities like higher transfer impedance, similar response (equal position sensitivity) in both of the transverse planes, resonance free structure over wide frequency range and fast decaying wake-field as compared to the old BPMs have been designed for Indus-2 storage ring. UPBPIs have been designed to replace old BPMs of Indus-2 whereas IDBPIs have been designed to provide additional beam position monitors for insertion devices installed in Indus-2. A modified setup of coaxial wire method to measure transfer impedances of capacitive BPMs is conceptualized and implemented for the test bench measurement of transfer impedances of UPBPI and IDBPI. In-situ measurement of transfer impedance and temporal response of IDBPI and UPBPI has also been carried out for the performance analysis of these BPMs.

The UPBPI and IDBPI are essential part of beam position monitoring system of Indus-2 and they are playing very important role in various applications like closed orbit measurement, orbit correction, slow and fast orbit control feedback system, multibunch instability control feedback system, undulator interlock system etc..

6.1 Future perspectives and Outlook

The old BPMs of Indus-2 are being replaced by UPBPIs in phased manner. In the first phase, 21 old BPMs have been replaced in Indus-2 storage ring. Presently there are three undulators in Indus-2. The IDBPIs have been deployed at entry and exit of each undulator.

For further up-gradation of beam position monitors in Indus-2, integrated button electrode beam position monitors (BPM integrated with dipole magnet chamber) for Indus-2 would also be replaced with new integrated BPMs. Design of upgraded version of integrated beam position monitor, its development, calibration, characterization and installation would be done in coming time.

Study of fringe field effect in stripline and effect of inter-electrode cross talk on position sensitivity of BPM would be very helpful in designing of pickups and kickers (striplines/ shoe box monitors) for up-gradation of beam diagnostics in Indus accelerators (Indus-1 &2) and future projects like high intensity linear accelerator for ISNS. A high brightness synchrotron radiation source (HBSRS) is also being planned to be developed at RRCAT. The planned HBSRS has sub nm-rad beam emittance, high average beam current, very short bunch length, small transverse size etc. Therefore, a large number of button electrode beam position monitors would be required to provide beam position for various activities like closed orbit measurement and correction, fast orbit feedback system, slow orbit feedback system, coupled bunch instability feedback system etc. To utilize advantage of very small transverse bunch size and beam emittance the BPM should have sub micron level resolution. The study and development done for design and characterization of button electrode BPMs for Indus-2 would also be very helpful for such projects.

APPENDIX-A

This appendix presents derivation of the relation between transverse and longitudinal effects of the kicker using Panofsky Wenzel theorem.

The force experienced by charge particle passing through electromagnetic field with velocity v_b is given by

$$\boldsymbol{F} = e[\boldsymbol{E} + \boldsymbol{v_b} \times \boldsymbol{B}] \tag{A.1}$$

The change in momentum of the particle passing through kicker is

$$\Delta\boldsymbol{p} = \int_{t_a}^{t_b} \boldsymbol{F} dt = e\int_{t_a}^{t_b} [\boldsymbol{E} + \boldsymbol{v_b} \times \boldsymbol{B}] dt \tag{A.2}$$

Here t_a and t_b are time coordinates when particle enters and exits kicker respectively. The rate of change of $\boldsymbol{\Delta p}$ with respect to time 't' in going from kicker entrance to kicker exit is given by

$$\frac{\partial\Delta\boldsymbol{p}}{\partial t} = e\int_{t_a}^{t_b} \left[\frac{\partial\boldsymbol{E}}{\partial t} + \boldsymbol{v_b} \times \frac{\partial\boldsymbol{B}}{\partial t}\right] dt \tag{A.3}$$

For $v_b\, dt = ds$, equation (A.3) gives

$$\frac{\partial\Delta\boldsymbol{p}}{\partial t} = e\left[\int_{t_a}^{t_a} \frac{\partial\boldsymbol{E}}{\partial t} dt + \int_a^b d\boldsymbol{s} \times \frac{\partial\boldsymbol{B}}{\partial t}\right] \tag{A.4}$$

Using $\frac{\partial\boldsymbol{B}}{\partial t} = -\boldsymbol{\nabla} \times \boldsymbol{E}$ and $\mathrm{d}\boldsymbol{s} \times \boldsymbol{\nabla} \times \boldsymbol{E} = \boldsymbol{\nabla}(d\boldsymbol{s} \cdot \boldsymbol{E}) - (d\boldsymbol{s} \cdot \boldsymbol{\nabla})\boldsymbol{E} = \boldsymbol{\nabla}(d\boldsymbol{s} \cdot \boldsymbol{E}) - \frac{\partial\boldsymbol{E}}{\partial s} ds$ in equation (A.4), we get

$$\frac{\partial \Delta \boldsymbol{p}}{\partial t} = e\left[\int_{t_a}^{t_b} \frac{\partial \boldsymbol{E}}{\partial t} dt - \int_a^b \left(\nabla(d\boldsymbol{s}\cdot\boldsymbol{E}) + \frac{\partial \boldsymbol{E}}{\partial s} ds\right)\right] \tag{A.5}$$

$$\Rightarrow \frac{\partial \Delta \boldsymbol{p}}{\partial t} = e\left[\int_{t_a}^{t_b} \frac{\partial \boldsymbol{E}}{\partial t} dt + \int_a^b \frac{\partial \boldsymbol{E}}{\partial s} ds - \int_a^b \boldsymbol{\nabla}(d\boldsymbol{s}\cdot\boldsymbol{E})\right] \tag{A.6}$$

$$\Rightarrow \frac{\partial \Delta \boldsymbol{p}}{\partial t} = e\left[\int_a^b d\boldsymbol{E} - \int_a^b \boldsymbol{\nabla}(d\boldsymbol{s}\cdot\boldsymbol{E})\right] \tag{A.7}$$

Using $e\int_a^b d\boldsymbol{s}\cdot\boldsymbol{E} = \Delta\mathcal{E}$ (energy change) in equation (A.7) we get

$$\frac{\partial \Delta \boldsymbol{p}}{\partial t} = -\boldsymbol{\nabla}(\Delta\mathcal{E}) + e[\boldsymbol{E}(b) - \boldsymbol{E}(a)] \tag{A.8}$$

Considering only transverse component of momentum we get

$$\frac{\partial \Delta \boldsymbol{p}_\perp}{\partial t} = -\boldsymbol{\nabla}_\perp(\Delta\mathcal{E}) + e[\boldsymbol{E}_\perp(b) - \boldsymbol{E}_\perp(a)] \tag{A.9}$$

Here $\Delta p_\perp$= momentum change in direction perpendicular to particle velocity and $E_\perp(a)$ and $E_\perp(b)$ are transverse component of electric field at kicker's entry and exit respectively.

If we choose entry and exit of kicker so that the kicker field vanishes at these points (in most cases the kickers fields attenuates rapidly in beam pipe) we get

$$\frac{\partial \Delta \boldsymbol{p}_\perp}{\partial t} = -\boldsymbol{\nabla}_\perp(\Delta\mathcal{E}) \tag{A.10}$$

If the time variation in E and B and hence in Δp is sinusoidal then equation (A.10) gives

$$j\omega\Delta\boldsymbol{p}_{\perp} = -\boldsymbol{\nabla}_{\perp}(\Delta\mathcal{E}) \tag{A.11}$$

Equation (A.11) represents transverse momentum change in terms of energy change of a relativistic particle moving under electromagnetic field.

For horizontal plane equation (A.11) gives

$$j\omega\Delta p_x = -\frac{\partial(\Delta\mathcal{E})}{\partial \mathrm{x}} = -\frac{\partial eV_k K_{//}}{\partial \mathrm{x}} \tag{A.12}$$

$$\Rightarrow \frac{\partial K_{//}}{\partial \mathrm{x}} = -\frac{1}{eV_k} j\omega\Delta p_x \tag{A.13}$$

Using $\frac{\Delta p_x v_b / e}{V_k} = K_x$ we get

$$\frac{\partial K_{//}}{\partial \mathrm{x}} = -j\frac{\omega}{v_b} K_x \tag{A.14}$$

Similarly for vertical plane we have

$$\frac{\partial K_{//}}{\partial \mathrm{y}} = -j\frac{\omega}{v_b} K_y \tag{A.15}$$

Equations (A.11), (A.14) and (A.15) give relation between transverse and longitudinal characteristics of a kicker.

APPENDIX-B

Pickup and kicker are two different functions of the same device. This appendix presents derivation of the relation between pickup and kicker function/action of a general pickup/kicker.

B.1 Lorentz reciprocity theorem

Let we have two independent sources of electromagnetic excitation in a volume V bounded by surface S (Fig. B.1). The source-1 is associated with current density $\mathbf{J_1}$ electric field $\mathbf{E_1}$ and a magnetic field $\mathbf{H_1}$. The source-2 is associated with current $\mathbf{J_2}$, electric field fields $\mathbf{E_2}$ and magnetic field $\mathbf{H_2}$. For all the fields and current densities periodic functions of time with angular frequency ω, the Lorentz reciprocity theorem states that the relation between current densities and fields of given sources can be written as

$$\int_V [\boldsymbol{E_2} \cdot \boldsymbol{J_1} - \boldsymbol{E_1} \cdot \boldsymbol{J_2}] dV = \int_S [\boldsymbol{E_1} \times \boldsymbol{H_2} - \boldsymbol{E_2} \times \boldsymbol{H_1}] \cdot d\boldsymbol{S} \qquad \text{(B.1)}$$

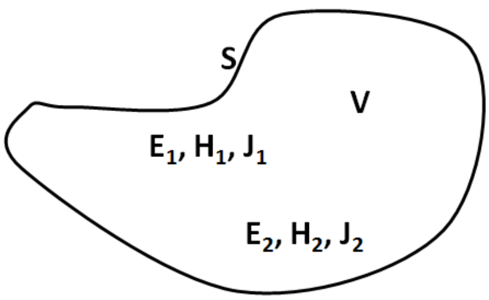

Fig. B.1 Volume containing two source of electromagnetic field excitation.

B.2 Relation between pick-up and kicker characteristics

Let, we have a pickup electrode placed inside the pickup chamber as shown in Fig. B.2. In first case (kicker mode), a voltage V_k is applied to the pickup which generates electric field $\mathbf{E_k}$, magnetic field $\mathbf{H_k}$ inside the pickup chamber and current density $\mathbf{J_k}$ in resistive medium. In second case (pickup mode), a beam of current density $\mathbf{J_b}$ passes through the pickup chamber and induced electric field $\mathbf{E_b}$ and magnetic field $\mathbf{H_b}$ inside the chamber. The outgoing signal, due to beam current $\mathbf{J_b}$, produces voltage V_0 at pickup port.

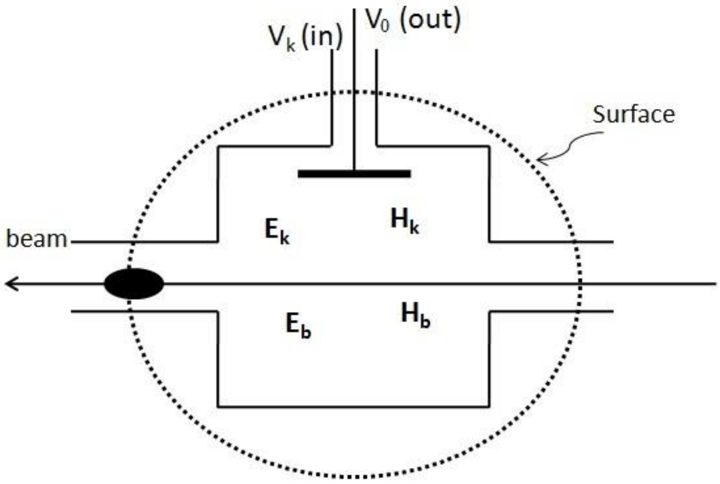

Fig. B.2 Schematic of pickup/kicker electrode for application of reciprocity theorem to pickup/kicker.

Applying Lorentz reciprocity theorem to the volume shown by dotted boundary in Fig. B2 we get

$$\int_V \, [\boldsymbol{J_k} \cdot \boldsymbol{E_b} - \boldsymbol{J_b} \cdot \boldsymbol{E_k}] \, dV = \int_S \, [\boldsymbol{E_k} \times \boldsymbol{H_b} - \boldsymbol{E_b} \times \boldsymbol{H_k}] \cdot d\boldsymbol{S} \qquad \text{(B.2)}$$

Since, $\mathbf{J_k}$ and $\mathbf{E_b}$ are perpendicular to each other we get

$$-\int_V [\boldsymbol{J_b} \cdot \boldsymbol{E_k}]\, dV = \int_S [\boldsymbol{E_k} \times \boldsymbol{H_b} - \boldsymbol{E_b} \times \boldsymbol{H_k}] \cdot d\boldsymbol{S} \tag{B.3}$$

The surface integral of two signal travelling at pickup port (ingoing and outgoing TEM waves) is equal to $\frac{2V_k V_0}{Z_0}$. Here Z_0 is output impedance. The contribution of surface integration for rest of the surface vanishes as no electric and magnetic field exists outside the chamber. Thus, equation (B.3) can be written as

$$2\frac{V_k V_0}{Z_0} = -\int_V [\boldsymbol{J_b} \cdot \boldsymbol{E_k}]\, dV \tag{B.4}$$

$$\Rightarrow V_0 = -\frac{Z_0}{2V_k}\int_V [\boldsymbol{J_b} \cdot \boldsymbol{E_k}]\, dV \tag{B.5}$$

Equation (B.5) gives signal induced by a beam in terms of the electric field generated in the chamber when the same pickup is excited by a voltage (V_k). In other word, equation (B.5) represents a mathematical relation between pickup and kicker characteristics of a pickup/kicker.

The important point to be noted here is that equation (B.5) has to be evaluated at a fixed time and spatial variation of $\mathbf{J_b}$ at that time must be considered while evaluating volume integral. Spatial variation of $\mathbf{J_b}$ along z is represented as $e^{j\frac{\omega}{v_b}z}$. Also, if we assume that the variation of electric field over the transverse cross section of the beam is negligible then volume integral in equation (B.5) reduces to line integral along longitudinal axis. Thus equation (B.5) can be written as

$$V_0 = -\frac{Z_0}{2V_k}\int_z \; I_b e^{j\frac{\omega}{v_b}z} \, (E_k)_z dz \tag{B.6}$$

Here $(E_k)_z$ represents z component of electric field $\boldsymbol{E_k}$.

Using $\frac{1}{V_k}\int_z \; e^{j\frac{\omega}{v_b}z} \, (E_k)_z dz = k_{//}$ (longitudinal kicker constant) and $Z_T = \frac{V_0}{I_b}$ (transfer impedance) in equation (B.6)

$$Z_T = \frac{Z_0 k_{//}}{2} \tag{B.7}$$

Equation (B.7) states that that if the behavior of a device is known as a pickup then its behavior as a kicker can be understood/analyzed and vice versa.

Differentiating equation (B.7) with x

$$\frac{\partial Z_T}{\partial x} = \frac{Z_0}{2}\frac{\partial k_{//}}{\partial x} \tag{B.8}$$

Using $\frac{\partial K_{//}}{\partial \mathrm{x}} = -\frac{1}{v_b} j\omega K_x$ (see equation A.14, appendix A) we get

$$Z_T{}' = \frac{\partial Z_T}{\partial x} = -j\frac{Z_0}{2}\frac{\omega}{v_b}K_x \tag{B.9}$$

Now

$$\frac{\partial Z_T}{\partial x} = \frac{1}{I_b}\frac{\partial V_0}{\partial x}\left(\frac{V_0}{V_0}\right) = Z_T S_x \tag{B.10}$$

Here $S_x = \frac{1}{V_0}\frac{\partial V_0}{\partial x}$ is position sensitivity of pickup in horizontal plane.

From equations (B.9) and (B.10) we have

$$K_x = j\frac{2v_{b}z_T S_x}{\omega Z_0} \tag{B.11}$$

Similarly, for vertical plane, we can write

$$K_y = j\frac{2v_{b}z_T S_y}{\omega Z_0} \tag{B.12}$$

Using

$$(R_{sh})_x T^2 = Z_0|\boldsymbol{K_x}|^2 = Z_0 {K_x}^2 \qquad \text{(for horizontal)} \tag{B.13}$$

and

$$(R_{sh})_y T^2 = Z_0\left|\boldsymbol{K_y}\right|^2 = Z_0 {K_y}^2 \qquad \text{(for vertical)} \tag{B.14}$$

in equations (B.11) and B.12) we get

$$(R_{sh})_x T^2 = 4\left(\frac{v_b}{\omega}\right)^2 \frac{{z_T}^2 {S_x}^2}{Z_0} \quad \text{(for horizontal)} \tag{B.15}$$

$$(R_{sh})_y T^2 = 4\left(\frac{v_b}{\omega}\right)^2 \frac{{z_T}^2 {S_y}^2}{Z_0} \quad \text{(for vertical)} \tag{B.16}$$

APPENDIX-C

In this appendix normalized derivation of difference signal for two electrodes BPM having inter-electrode cross talk is presented [43] . The equivalent circuit of two electrodes BPM is shown in Fig. C.1.

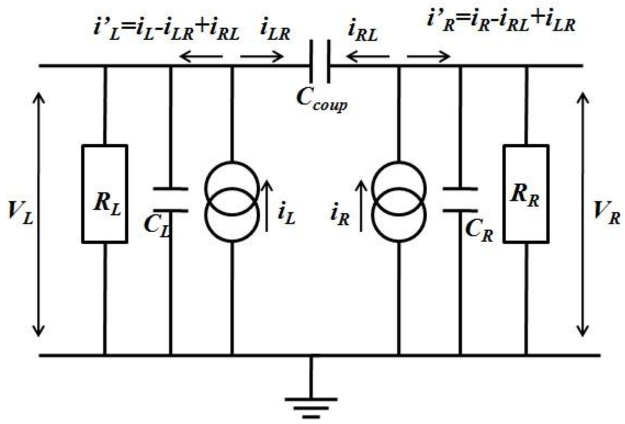

Fig. C.1. Equivalent circuit of two electrodes BPM.

Using superposition principle, i'_L and i'_R (see Fig. C.1) can be written as

$$i'_L = i_L - i_{LR} + i_{RL} \tag{C.1}$$

$$i'_R = i_R - i_{RL} + i_{LR} \tag{C.2}$$

The normalized difference signal is given by

$$\frac{\Delta V}{\Sigma V} = \frac{|V_R| - |V_L|}{|V_R| + |V_L|} = \frac{\left|i'_R\left(\frac{R_R}{1 + j\omega C_R R_R}\right)\right| - \left|i'_L\left(\frac{R_L}{1 + j\omega C_L R_L}\right)\right|}{\left|i'_R\left(\frac{R_R}{1 + j\omega C_R R_R}\right)\right| + \left|i'_L\left(\frac{R_L}{1 + j\omega C_L R_L}\right)\right|} \tag{C.3}$$

For identical electrodes (C_R= C_L= C) and R_R=R_L=R, the equation (C.3) can be written as

$$\frac{\Delta V}{\Sigma V} = \frac{|i'_R| - |i'_L|}{|i'_R| + |i'_L|} \qquad \text{(C4.)}$$

Using

$$i_{RL} = f_{RL} i_R \qquad \text{(C.5)}$$

$$i_{LR} = f_{LR} i_L \qquad \text{(C.6)}$$

we get

$$\frac{\Delta V}{\Sigma V} = \frac{|i_R - f_{RL} i_R + f_{LR} i_L| - |i_L - f_{LR} i_L + f_{RL} i_R|}{|i_R - f_{RL} i_R + f_{LR} i_L| + |i_L - f_{LR} i_L + f_{RL} i_R|} \qquad \text{(C.7)}$$

Here f_{LR} and f_{RL} are inter-electrode coupling factors.

The inter-electrode coupling factor (f_{LR} or f_{RL}) can be calculated by considering current induced on one electrode only and different paths through which this current can flow to reach ground potential. For example, the current (i_L) induced on left electrode sees two different (parallel) paths to reach to the ground. First path is parallel combination of C_L and R_L of left hand side branch in Fig. C.1. Second path is via C_{coup} and parallel combination of C_R and R_L of right hand side branch. To calculate f_{LR}, the equivalent circuit given in Fig. C.1 can be represented as shown in Fig. C.2.

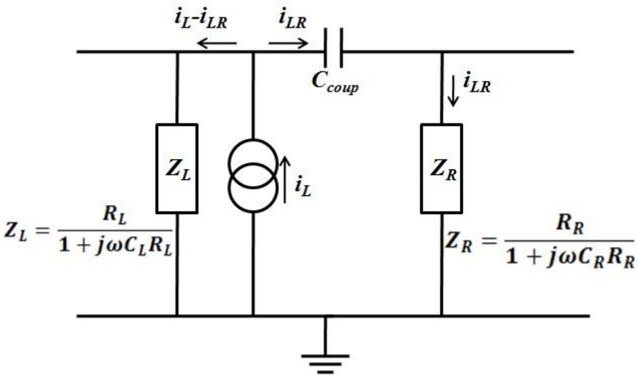

Fig. C.2 Simplified equivalent circuit of capacitive BPM used to calculate inter-electrode coupling factor from left electrode to the right electrode (f_{LR}).

In Fig. C.2, the current source due to charge induced on right hand side electrode has been removed (as ideal current source has infinite internal impedance) and parallel combination of C_L and R_L is replaced with Z_L and parallel combination of C_R and R_R has been replaced with Z_R.

From Fig. C.2, using current division formula, we get

$$i_{LR}(\omega) = i_L(\omega)\left[\frac{Z_L(\omega)}{Z_L + \left(Z_R + \frac{1}{j\omega C_{coup}}\right)}\right] \tag{C.8}$$

From equations (A.6) and (A.8) we have

$$f_{LR} = \frac{Z_L(\omega)}{Z_L(\omega) + \left(Z_R(\omega) + \frac{1}{j\omega C_{coup}}\right)} \tag{C.9}$$

Following similar steps for f_{RL} we get

$$f_{RL} = \frac{Z_R(\omega)}{Z_R(\omega) + \left(Z_L(\omega) + \frac{1}{j\omega C_{coup}}\right)} \qquad \text{(C.10)}$$

For $C_R=C_L$ and $R_R=R_L$ we have $Z_R=Z_L$ which gives $f_{LR} = f_{RL}$. Thus using $f_{LR} = f_{RL}=f$ in equation (C.7) we get

$$\frac{\Delta V}{\Sigma V} = \frac{|i_R - f(i_R - i_L)| - |i_L - f(i_L - i_R)|}{|i_R - f(i_R - i_L)| + |i_L - f(i_L - i_R)|} \qquad \text{(C.11)}$$

Again, using $Z_L = Z_R = Z$ in equations (C.9) and (C. 10) we get

$$f = \frac{Z(\omega)}{Z(\omega) + \left(Z(\omega) + \frac{1}{j\omega C_{coup}}\right)} \qquad \text{(C.12)}$$

For $R_R=R_L=R$ we have

$$Z(\omega) = \frac{R}{1 + j\omega CR} \qquad \text{(C.13)}$$

This gives

$$f = \frac{j\omega R C_{coup}}{1 + 2j\omega R C_{coup} + j\omega RC} \qquad \text{(C.14)}$$

From equations (C.11) and (C.14) we get

$$\frac{\Delta V}{\Sigma V} = \frac{(i_R + i_L)(i_R - i_L)[1 - 2\alpha]}{[|i'_R| + |i'_L|]^2} \qquad \text{(C.15)}$$

Here α is real part of inter-electrode coupling factor (*f*) given by

$$\alpha = \frac{\omega^2 R^2 C_{coup}\left(2C_{coup} + C\right)}{1 + \omega^2 R^2 \left(2C_{coup} + C\right)^2} \qquad \text{(C.16)}$$

APPENDIX-D

In this appendix, derivation of expression of transfer impedance applicable in modified setup of coaxial wire method is presented [62]. For easy to refer, the setup of modified coaxial wire method as explained in chapter 5 is again shown as Fig. D.1.

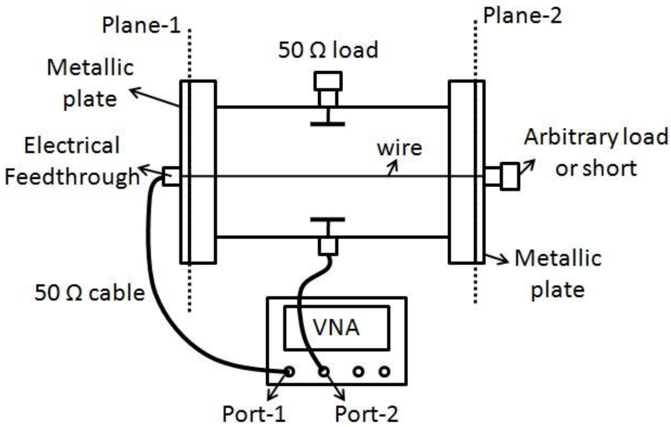

Fig. D.1 Schematic of general setup of modified coaxial wire method.

Let the forward voltage 'V_{in}' generated at port-1 of the VNA is

$$V_{in}(\omega,t)=V_0 e^{i\omega t} \tag{D.1}$$

The voltage signal 'V_{in}' is carried to the coaxial wire using cables having characteristic impedance Z_0. Therefore the forward current 'I_{in}' generated at port-1 is

$$I_{in}(\omega,t)=\frac{V_0 e^{i\omega t}}{Z_0} \tag{D.2}$$

This current (equation (D.2)) travels up to the coaxial wire and undergoes partial transmission and reflection at plane-1 (Fig. D.1). The current transmitted into to the coaxial structure is given by equation (D.3).

$$I_1(\omega,t)=\frac{V_0 e^{i(\omega t+\varphi_0)}}{Z_0}\left[\frac{2Z_w}{Z_0+Z_w}\right]\left[\frac{Z_0}{Z_w}\right] \tag{D.3}$$

Here I_1 is current entering the coaxial structure, φ_0 is phase difference between I_{in} and I_1 at plane-1, Z_w is characteristic impedance of the coaxial structure formed by wire and the device. Writing

$$\left[\frac{2V_0}{Z_0+Z_w}\right]=I_0 \tag{D.4}$$

the equation (D.3) can be written as

$$I_1(\omega,t)=I_0 e^{i(\omega t+\varphi_0)} \tag{D.5}$$

Inside the coaxial structure, the current I_1 undergoes multiple reflections at plane-1 and plane-2 (Fig. D.1). Each reflected component of the current flowing through the wire generates voltage at the pickup electrodes. If $Z_T(\omega)=|Z_T(\omega)|e^{i\Delta\varphi}$ is transfer impedance of the pickup electrode, the net voltage 'V_{pick}' induced at the pickup electrode can be written as.

$$\begin{aligned}
V_{pick}(\omega,t) &= I_0 e^{i(\omega t+\varphi_0)}|Z_T(\omega)|e^{i\Delta\varphi} \\
&+ I_0 e^{i(\omega t+\varphi_0)}|\rho_2|e^{i\varphi_2}e^{i\frac{\omega(L+2\Delta L)}{c}}|Z_T(\omega)|e^{i\Delta\varphi} \\
&+ I_0 e^{i(\omega t+\varphi_0)}|\rho_2|e^{i\varphi_2}|\rho_1|e^{i\varphi_1}e^{i\frac{\omega(2L)}{c}}|Z_T(\omega)|e^{i\Delta\varphi} \\
&+ I_0 e^{i(\omega t+\varphi_0)}\left[|\rho_2|e^{i\varphi_2}\right]^2|\rho_1|e^{i\varphi_1}e^{i\frac{\omega(2L)}{c}}e^{i\frac{\omega(L+2\Delta L)}{c}}|Z_T(\omega)|e^{i\Delta\varphi} \\
&+ I_0 e^{i(\omega t+\varphi_0)}\left[|\rho_2|e^{i\varphi_2}\right]^2\left[|\rho_1|e^{i\varphi_1}\right]^2\left[e^{i\frac{\omega(2L)}{c}}\right]^2|Z_T(\omega)|e^{i\Delta\varphi}\ldots\ldots\ldots\ldots+\inf
\end{aligned} \tag{D.6}$$

In equation (D.6)

$|\rho_2|e^{i\varphi_2}$ is reflection coefficient at plane-2.

$|\rho_1|e^{i\varphi_1}$ is reflection coefficient at plane-1.

L is length of DUT and ΔL is distance of pickup electrode from the centre of DUT towards plane-1.

$\frac{\omega(L+2\Delta L)}{c}$ = phase difference occurring due to distance ($L+2\Delta L$) travelled by the current/wave from pick-up electrode to plane-2 and back to pickup electrode.

$\frac{\omega(2L)}{c}$ = phase difference occurring due to distance [($L+2\Delta L$)+($L-2\Delta L)=2L$] travelled by the current/wave in one complete reflection between plane-1 and plane-2.

$\Delta\varphi$ is phase difference between pickup voltage and beam current.

Taking/adding alternate terms we get

$$\begin{aligned} V_{pick}(\omega,t) &= I_0|Z_T(\omega)|e^{i(\omega t+\varphi_0)}e^{i\Delta\varphi}\sum_{k=0}^{\infty}\left[|\rho_2|e^{i\varphi_2}|\rho_1|e^{i\varphi_1}e^{i\frac{\omega(2L)}{c}}\right]^k \\ &+ I_0|Z_T(\omega)|e^{i(\omega t+\varphi_0)}e^{i\Delta\varphi}\sum_{k=0}^{\infty}\left[|\rho_2|e^{i\varphi_2}\right]^{k+1}\left[|\rho_1|e^{i\varphi_1}e^{i(\frac{\omega(2L)}{c}}\right]^k e^{i\frac{\omega(L+2\Delta L)}{c}} \end{aligned} \tag{D.7}$$

$$\Rightarrow V_{pick}(\omega,t) = I_0|Z_T(\omega)|e^{i(\omega t+\varphi_0+i\Delta\varphi)}\left[\frac{1}{1-|\rho_1||\rho_2|e^{i\left(2\omega L/c+\varphi_1+\varphi_2\right)}}+\frac{|\rho_2|e^{i\left(\omega(L+2\Delta L)/c+\varphi_2\right)}}{1-|\rho_1||\rho_2|e^{i\left(2\omega L/c+\varphi_1+\varphi_2\right)}}\right] \tag{D.8}$$

Let

$\omega t+\varphi_0+\Delta\varphi=\alpha$

$2\omega L/c+\varphi_1+\varphi_2=\beta$

$\omega(L+2\Delta L)/c+\varphi_2=\gamma$

The equation (D.8) can be rewritten as

$$V_{pick}(\omega,t)=I_0|Z_T(\omega)|\left[\frac{e^{i(\alpha)}}{1-|\rho_1||\rho_2|e^{i(\beta)}}+\frac{|\rho_2|e^{i(\alpha+\gamma)}}{1-|\rho_1||\rho_2|e^{i(\beta)}}\right] \tag{D.9}$$

$$\Rightarrow |V_{pick}(\omega,t)|=\frac{I_0|Z_T(\omega)|\sqrt{1+|\rho_2|^2+2|\rho_2|\cos(\gamma)}}{\sqrt{1+(|\rho_1||\rho_2|)^2-2|\rho_1||\rho_2|\cos(\beta)}} \tag{D.10}$$

Using equation (D.4) in equation (D.10) we get

$$\frac{|V_{pick}(\omega,t)|}{V_0}=\frac{2|Z_T(\omega)|\sqrt{1+|\rho_2|^2+2|\rho_2|\cos(\gamma)}}{(Z_0+Z_w)\sqrt{1+(|\rho_1||\rho_2|)^2-2|\rho_1||\rho_2|\cos(\beta)}} \tag{D.11}$$

Using

$$\frac{|V_{pick}(\omega,t)|}{V_0}=|S_{pick,1}(\omega)| \tag{D.12}$$

we get

$$|S_{pick,1}(\omega)|=\frac{2|Z_T(\omega)|\sqrt{1+|\rho_2|^2+2|\rho_2|\cos(\gamma)}}{(Z_0+Z_w)\sqrt{1+(|\rho_1||\rho_2|)^2-2|\rho_1||\rho_2|\cos(\beta)}} \tag{D.13}$$

It gives

$$|Z_T(\omega)|=\frac{|S_{pick,1}(\omega)|(Z_0+Z_w)\sqrt{1+(|\rho_1||\rho_2|)^2-2|\rho_1||\rho_2|\cos(\beta)}}{2\sqrt{1+|\rho_2|^2+2|\rho_2|\cos(\gamma)}} \tag{D.14}$$

Here $S_{pick,1}$ is S-parameter from wire to pickup electrode.

REFERENCES

[1] G. R. Lambertson, Dynamic devices-Pickup and Kickers, Report, Lawrence Berkeley Laboratory, LBL-22085 (1986).

[2] D. A. Goldberg and G. R. Lambertson, Dynamic Devices: A Primer On Pickups and Kickers, Report, Lawrence Berkeley Laboratory, LBL-31664 (1991).

[3] Peter Strehl, Beam Instrumentation and diagnostics, Springer (2006).

[4] Peter Forck, Lecture notes on beam instrumentation and diagnostics, Joint University Accelerator School (JUAS), January-March (2011).

[5] H. Koziol, Beam Diagnostics for accelerators, CERN/PS-2001-012(DR) (2001).

[6] M. Gasior, R. Jones, T. Lefevre, H. Schmickler and K. Wittenburg, Introduction to beam instrumentation and diagnostics, Proceedings of the CAS–CERN Accelerator School: Advanced Accelerator Physics; DOI: http://dx.doi.org/10.5170/CERN-2014-009 (2014).

[7] M. Lonza, Multi-Bunch feedback system, Proceedings of the CAS–CERN Accelerator School: Advanced Accelerator Physics; DOI: http://dx.doi.org/10.5170/CERN-2014-009 (2014).

[8] P. Wesolowski, I. Birkel, E. Huttel, A.-S. Müller, F. Pérez and M. Pont, A vertical multi-bunch feedback system for ANKA, Proceedings of 2005 Particle Accelerator Conference, Knoxville, Tennessee, pp.761-63 (2005).

[9] David Olsson, Lars Malmgren, and Anders Karlsson, The Bunch-by-Bunch Feedback System in the MAX IV 3 GeV Ring, Technical Report LUTEDX/(TEAT-7253)/1-48/(2017); **Vol. 7253**, MAX-lab, Lund University, Sweden (2017).

[10] Y. K. Wu† , J. Li, P. Wang and V. Litvinenko, BPM and orbit correction systems at the Duke storage ring, Proceedings of the 2003 Particle Accelerator Conference, pp. 2479-81 (2003).

[11] D. D. Bhawalkar, G. Singh, R. V. Nandedkar, Synchrotron Radiation Source Indus-1 and Indus-2, PRAMANA - journal of Phys. **50** (1998).

[12] P. R. Hannurkar, S. K. Deb, A. C. Thakurta, T. A. Puntambekar, S. R. Tiwari, M. R. Lad, P. Fatnani, R. S. Shinde, A. D. Ghodke, R. Sridhar, P. Shrivastava, R. K. Sahu, R. M. Pandey, J. Dwivedi, G. Singh and P. D. Gupta, Indus Synchrotron Radiation Sources: A national Facility, Indian Nuclear Society News **Vol. 10(3-4)** (2013).

[13] http://www.cat.gov.in/technology/accel/indus/indus2.html

[14] G. Singh, G.K. Sahoo, D. Angal, B. Singh, A.D. Ghodke and P. Kant, Synchrotron radiation source Indus-2, Indian Journal of Pure and Applied Physics **35(3),183** (1997).

[15] A. D. Ghodke, Riyasat Husain, G. Singh and Indus-2 commissioning team, Progress in Commissioning of Indus-2, ICFA, Beam Dynamics Newsletter No.-41 (2006).

[16] S.K. Deb, Gurnam singh and P.D. Gupta, Indus-2 Synchrotron Radiation Source: Current Status and Utilization, Journal of Physics: Conference series 425, 072009 (2013).

[17] http://www.rrcat.gov.in/technology/accel/isrf_index.html#

[18] Amalendu Sharma et. al. Reference Physics Design for 1 GeV Injector Linac and Accumulator Ring for Indian Spallation Neutron Source , https://arxiv.org/abs/1609.04518.

[19] V. K. Senecha, Physics Design Studies of Proton Accelerator and Target for SNS applications, National Symposium on Radiation Physics (NSRP-21), RRCAT Indore (2018).

[20] T. J. Shea, S. Assadi, R. Witkover, L. Doolittle, D. Oshatz, M. Plum, M. Stettler, J. O'Hara, J. Power, R. Shafer, P. Cameron, R. Connolly, D. Gassner and M. Kesselman, SNS accelerator diagnostics: Progress and challenges, Proceedings of the 2001 Particle Accelerator Conference, Chicago, USA (2001).

[21] J. Powert, J. O'Hara, S. Kurennoy, M. Plum and M. Stettler, Beam position monitors for the SNS linac, Proceedings of the 2001 Particle Accelerator Conference, Chicago, USA (2001).

[22] S. Sato, A. Miura, T. Tomisawa, H. Sako, T. Morishita, A. Ueno, K. Hasegawa, H. Yoshikawa,Z. Igarashi and M. Ikegami, Study of J-PARC linac beam position monitor as phase monitor, Proceedings of PAC09, Vancouver, BC, Canada (2009).

[23] S.Lee , Z. Igarashi , M. Tanaka , S. Sato , H. Akikawa , F. Hiroki , T. Tomisawa , H. Yoshikawa , J. Kishiro and T. Toyama, The beam diagnostics system in the J-PARC linac, Proceedings of LINAC 2004, Lübeck, Germany, pp. 441-443 (2004).

[24] C.C. Wilcox, J.C. Medland, S.J. Payne, A. Pertica and M. Probert, Optimisation of a split plate position monitor for the ISIS proton synchrotron, Proceedings of IBIC2013, Oxford, UK, pp. 739-41 (2013).

[25] T. Toyama, D. Arakawa, Y. Hashimoto, S. Lee, T. Miura, S. Muto, N. Hayashi, R. Toyokawa, and J. Kishiro, Beam diagnostics for the J-PARC main ring synchrotron, Proceedings of 2005 Particle Accelerator Conference, Knoxville, Tennessee, pp. 958-60 (2005).

[26] T. Toyama, D. Arakawa, Y. Hashimoto, S. Lee, T. Miura, H. Nakagawa, N. Hayashi and R. Toyokawa, Beam position monitor for the J-PARC main ring synchrotron, Proceedings of DIPAC 2005, Lyon, France, pp. 270-72 (2005).

[27] N. Hayashi M. Kawase, S. Hatakeyama, S. Hiroki, R. Saeki, H. Takahashi, Y. Teruyama, R. Toyokawa , D. Arakawa, S. Hiramatsu, S. Lee, K. Satou, M. Tejima, and T. Toyama, Beam

position monitor system of J-PARC RCS, Nuclear Instruments and Methods in Physics Research A **677**, 94–106 (2012).

[28] N. Hayash, S. Hiroki, K. Satou, R. Toyokawa, Tokai-Mura, Naka-Gun, D. Arakawa, S. Lee, Y. Hashimoto, T. Miura and T. Toyama, The beam diagnostics system for J-PARC synchrotrons Proceedings of HB2006, Tsukuba, Japan, pp. 128-30 (2006).

[29] R.E. Shafer, Beam position monitoring, AIP Conference Proc. **212**, pp. 26 (1990).

[30] F. Marcellini, M. Serio and M. Zobov, DAϕNE Broad band Button electrodes, DAϕNE tech. Note:CD-6 (1996).

[31] F. Marcellini, M. Serio, A. Stella and M Zobov, DAϕNE broad-band button electrodes, Nuclear Instruments and Methods in Physics Research A **402**, 27-35 (1998).

[32] S. R. Marques, J. B. Gonzalez, P. F. Tavares, O. R. Bagnato, M. J. Ferreira, R. H. A. Farias and C. Rodrigues, Design of button beam position monitor for the Brazilian Synchrotron Light Source, Proceedings of PAC07, Albuquerque, New Mexico, USA, pp. 3871-73 (2007).

[33] Zhichu Chen, Yongbin Leng, Kairong Ye, Guobi Zhao and Renxian Yuan, Beam position monitor design for a third generation light source, Physical Review Special Topics - Accelerators and Beams **17**, 112801 (2014).

[34] A. Molaee, M. Samadfam, M. Mohammadzadeh and Mehdi Shafiee, General consideration for Button-BPM, Proceedings of IPAC2014, Dresden, Germany, pp. 3537-40 (2014).

[35] N. Kurita, D. Martin, S. Smith, C. Ng, M. Nordby and C. Perkins, Design of the button beam position monitor for PEP-II, SLAC-PUB-95-6991 (1995).

[36] J-P. Papis and L. Vos, CERN report, CERN SL/91-6, LHC note 140, appendix B (1991).

[37] Mukesh Kumar, New expression for the current induced in a strip for the fringe field effect in a circular cross-section stripline, Journal of Korean physical Society **Vol. 60**, Issue 9, pp. 1469-1472 (2012).

[38] P. Kowina, W. Kaufmann, J. Scholles and M. Schwickert, Optimisation of 'Shoe-Box Type' Beam Position Monitors Using the Finite Element Methods, DIPAC 05 Proc., Lyon, France, 114-116 (2005).

[39] P. Kowina, W. Kaufmann, J. Scholles and A Galatis, Numerical calculations of position sensitivity for linear cut beam position monitors, EPAC 2006 Proc., Edingburg Scotland, 1022-1024 (2006).

[40] P. Kowina, W. Kaufmann and J. Scholles, Optimization of the linear cut beam position monitors based on finite element method, DIPAC 2007 Proc., Venice Italy, 96-98 (2007).

[41] J. Harasimowicz and C.P. Welsch, Optimisation studies of a resonant capacitive pick-up for beam position monitoring of low intensity, low velocity antiproton beams at FLAIR, DIPAC 09 Proc., Basel Switzerland, 300-302 (2009).

[42] Ji-Gwang Hwang, Tae-Keun Yang, Seon Yeong Noh, Peter Fork and Changbum Kim, Development of capacitive linear cut beam position monitor for heavy ion synchrotron of KHIMA project, IBIC 2015 Proc., Melbourne, Australia,405-409 (2015).

[43] Mukesh Kumar, A. Ojha, A.D. Garg , T.A. Puntambekar and V.K. Senecha, Analytical expression for position sensitivity of linear response beam position monitor having inter-electrode cross talk, Nuclear Instruments and Methods in Physics Research A, **844**, pp. 90-95 (2017).

[44] A.C. Thakurta, Indus Upgrade activities, InPAC 2018, RRCAT, Indore, India (2018).

[45] T.A. Puntambekar, Upgradation of beam diagnostics system of Indus-2, InPAC 2018, RRCAT, Indore, India (2018).

[46] R.P. Yadav and P. Fatnani, Global fast orbit feedback control system for Indus-2, RRCAT Newsletters, **vol 27, Issue 2** (2014).

[47] Surendra Yadav et. Al., Operational Experience of Transverse Bunch by Bunch Feedback System of Indus-2, InPAC-2018, RRCAT, Indore, India (2018).

[48] Riyasat Husain, A D Ghodke, Surendra Yadav, A C Holikatti, R P Yadav, P Fatnani, T. A. Puntambekar and P R Hannurkar, Measurement, analysis and correction of the closed orbit distortion in Indus-2 synchrotron radiation source, Pramana February 2013, Volume **80,** Issue **2**, pp. 263-275 (2013).

[49] Mukesh Kumar, L.K. Babbar, A.C. Holikatti, S. Yadav, Y. Tyagi, T.A. Puntambekar and V.K. Senecha, Improved design and in-situ measurements of new beam position monitors for Indus-2,Journal of Instrumentation **13(01)**, P01003 (2018).

[50] Mukesh Kumar, L.K. Babbar, S. Yadav, T. A. Puntambekar and C. P. Navathe, Physics design of beam position indicator for insertion device section in Indus-2, Proceedings of InPAC-2013, VECC, Kolkata, India (2013).

[51] F. Caspers, Beam impedance measurements using the coaxial wire method, CERN PS/88-59 (AR/OP) (1988).

[52] Giuseppe Di Massa and Maria Rosaria Masullo, Beam impedance measurement coaxial wire method, Conference record of the IEEE particle accelerator conference, San Francisco, USA (1991).

[53] J. J. Song, Experimental study of beam coupling impedance Part-1 longitudinal impedance measurement techniques, LS Note-201, APS-ANL (1991).

[54] L. S. Walling, D. E. McMurry, D. V. Neuffer and H. A. Thiessen, Transmission line impedance measurements for an advanced hadron facility, Nuclear Instruments and Methods in Physics Research A **281**, 433-447 (1989).

[55] Liu Yu Dong, Huang Liang Sheng and Wang Sheng, Coupling impedance measurements of the extractor kicker in CSNS/RCS, Proceedings of symposium on accelerator physics, Lanzhou, China, pp. 102-105 (2014).

[56] H. Hahn and F. Pedersen, On coaxial wire measurements of the longitudinal coupling impedance, BNL 50870 (1978).

[57] M. J. barnes, F. Caspers, T. Kroyer, E. Mitral, F. Roncarolo and B. Salvant, Measurement of transverse impedance of licker magnets using the coaxial wire method, Proceedings of particle accelerator conference, Vancouver, BC, Canada, pp. 1726-1728 (2009).

[58] M.R. Masullo, V.G. Vaccaro and M. Panniello, The stretched wire method: A comparative analysis performed by means of the mode matching technique, Proceedings of LINAC-2010, Tsukuba, Japan (2010).

[59] J.N. Corlett, Coaxial wire impedance measurement of BPM buttons for the PEP-II B-FACTORY, International workshop for B-factories, Tsukuba, Japan (1995).

[60] F. Marcellini, M. Serio, A. Stella and M Zobov, DAϕNE broad-band button electrodes, Nuclear Instruments and Methods in Physics Research A **402**, pp. 27-35 (1998).

[61] T. Kroyer, F. Caspers, E. Gaxiola, Longitudinal and Transverse Wire Measurements for the Evaluation of Impedance Reduction Measures on the MKE Extraction Kickers, CERN-AB-Note-2007-028 (2007).

[62] Mukesh Kumar, L.K. Babbar, R.K.Deo, T.A. Puntambekar and V.K. Senecha, Modified coaxial wire method for measurement of transfer impedance of beam position monitors, Physical Review Accelerators and Beams **21**, 052801 (2018).

[63] Helmut Wiedmann, Particle Accelerator Physics, Springer (2007).

[64] Shaukat Khan, Collective Phenomenon in Synchrotron Radiation Source, Springer (2006).

[65] Bruno W. Zotter and Semyon A. Kheifets, Impedances and Wakes in High-Energy Particle Accelerators, World Scientific (1998).

[66] David M. Pozar, Microwave Engineering, John Wiley and Sons, **3rd Ed** (2009).

[67] Donald E. Kerr, Propagation of Short Radio Waves, IET (1987).

[68] Peter Russer, Electromagnetics, Microwave Circuit and Antenna Design for Communication Engineering, Artech House (2003).

[69] D.A. Edward, M.J. Syphers, In Introduction to the Physics of High Energy Accelerators John Wiley and sons (2004).

[70] Mario Conte, William W. Mackey, An Introduction to the Physics of Particle Accelerators World Scientific pub, **2nd Ed** (2008).

[71] G. Rumolo, Beam Instabilities, Proceedings of the CAS–CERN Accelerator School: Advanced Accelerator Physics; DOI: http://dx.doi.org/10.5170/CERN-2014-009 (2014).

[72] M. Ferrario et. al , Wakefields and Instabilities in Linear Accelerators, Proceedings of the CAS–CERN Accelerator School: Advanced Accelerator Physics; DOI:http://dx.doi.org/10.5170/CERN-2014-009 (2014).

[73] Robert E. Collin, Foundations for Microwave Engineering, John Wiley and Sons, **2nd Ed 2007**.

[74] M. Kumar, Modification in fraction of beam current intercepted by strip and output signal of stripline with circular cross-section, Nuclear Instruments and Methods in Physics Research A **602**, 315 (2009).

[75] CST STUDIO SUITE website : http://www.cst.com/

[76] http://www.rrcat.gov.in/technology/accel/indus/psd/bdml/beamdiagi2.html

[77] T. A. Puntambekar and et al., Experience of beam diagnostic systems in commissioning stage of Indus-2, APAC-2007, RRCAT, Indore, India (2007).

[78] A. Stella, Analysis of the DAϕNE beam position monitor with a boundary element method, DAϕNE tech. Note:CD-10 (1997).

[79] H.O.C. Duarte, L. Sanfelici and S.R. Marques, Design and Impedance optimization of the SIRIUS BPM button, Proceedings of IBIC-2013 (2013).